1-20-2006

Sediment Transport and Pathogen Indicator Modeling in Lake Pontchartrain

Chandra Sekhar Chilmakui
University of New Orleans

SEDIMENT TRANSPORT AND PATHOGEN INDICATOR MODELING IN LAKE PONTCHARTRAIN

A Dissertation

Submitted to the Graduate Faculty of the
University of New Orleans
in partial fulfillment of the
requirements for the degree of

Doctor of Philosophy
in
Engineering and Applied Science

by

Chandra Sekhar Chilmakuri

B. Tech. Jawaharlal Nehru Technological University, 2000
M.S. University of New Orleans, 2002

December 2005

ACKNOWLEDGEMENT

I express my sincere heartfelt gratitude to my major professor, Dr. Alex McCorquodale, the most knowledgeable, humble and noble human I have ever met, for giving me an opportunity to work with him. There aren't enough words to express my appreciation for his continuous encouragement and guidance over the period of this dissertation.

The dissertation would not have been completed without the support of my dissertation committee member and friend, Dr. Ioannis Georgiou. I am especially thankful for the countless hours he spent discussing and explaining various issues during this research.

I extend my deepest appreciation to the other committee members, Dr. Donald Barbé, Dr. Gianna Cothren, Dr. Martin Guillot and Dr. Curtis Outlaw for their constructive advice and their help in fulfilling the requirements during the hardest of times due to Hurricane Katrina.

I express my sincere thanks to the following people and agencies for helping me acquire the very important data required for the research.

- Dr. Richard Signell, USGS, for sharing wave and current data.
- Dr. Richard Miller, NASA Stennis Space Center, for sharing MODIS reflectance data.
- Dr. Katy Haralampedes, University of New Brunswick, for sharing sediment data.
- Mr. David Walters, USGS, for providing stage data.
- Lake Pontchartrain Basin Foundation, for sharing fecal coliform data.
- Ms. Jeimmy Leal and Ms. Maria Martinez for their help in acquiring field data.

- Mr. Rick Wilke, Ronald Everest and Members of the Northshore Chapter of the Power Squadron for their assistance with the boat during field sampling.
- Jefferson Parish pumps operators, engineers and officials for providing the pumping data.

I extend special thanks to Dr. Alan Blumberg and Hydroqual, Inc. for making the ECOMSED code available.

I am indebted to my beloved wife, Sirisha Nemani, for her love, patience and support. I thank my family for their care and encouragement all my life.

Last but not least, this research was made possible by the funding from National Oceanic and Atmospheric Administration through the co-operative support of Lake Pontchartrain Basin Foundation.

TABLE OF CONTENTS

LIST OF FIGURES

LIST OF TABLES

ABSTRACT

A nested three dimensional numerical modeling application was developed to determine the fate of pathogen indicators in Lake Pontchartrain discharged from its tributaries. To accomplish this, Estuarine, coastal and ocean model with sediment (ECOMSED) was implemented to simulate various processes that would determine the fate and transport of fecal coliform bacteria in the lake. The processes included hydrodynamics, waves, sediment transport, and the decay and transport of the fecal coliforms. Wind and tidal effects were accounted along with the freshwater inflows. All the components of the modeling application were calibrated and validated using measured data sets. Field measurements of the conventional water quality parameters and fecal coliform levels were used to calibrate and validate the pathogen indicator transport. The decay of the fecal coliforms was based on the literature and laboratory tests. The sediment transport module was calibrated based on the satellite reflectance data in the lake. The north shore near-field model indicated that the fecal coliform plume can be highly dynamic and sporadic depending on the wind and tide conditions. It also showed that the period of impact due to a storm event on the fecal coliform levels in the lake can be anywhere from 1.5 days for a typical summer event to 4 days for an extreme winter event. The model studies showed that the zone of impact of the stormwater from the river was limited to a few hundred meters from the river mouth. Finally, the modeling framework developed for the north shore was successfully applied to the south shore of Lake Pontchartrain to simulate fate and transport of fecal coliforms discharged through the urban stormwater outfalls.

1. INTRODUCTION

1.1 Background

Lake Pontchartrain is a shallow brackish estuarine lake located in southeastern Louisiana to the north of New Orleans. It is connected to Lake Maurepas at its western end and with the Gulf of Mexico at its eastern end through Lake Borgne. Together, Lakes Maurepas, Borgne and Pontchartrain form one of the largest estuaries in the United States.

Lake Pontchartrain has an area of 630 sq mi (1,630 sq km) approximately. It has an average depth of 3.7 m. Figure 1.1 shows the bathymetry and features of the lake. It is 41 mi (66 km) long in east-west direction and 25 mi (40 km) wide in north-south direction. Typical east to west salinities in the lake range from 1 ppt to 4 ppt. Tidal exchange occurs through two passes and a man-made channel namely Rigolets, Chef Menteur, and Inner Harbor Navigational Canal (IHNC). Tchefuncte River, Tangipahoa River, the Lake Maurepas basin, and the storm water outfalls in the south shore and direct rainfall on the lake surface constitute the major sources of fresh water into the lake. Also, occasionally, the lake receives fresh water input from the diversion of Mississippi River water through Bonnet Carré spillway. The average annual precipitation in the Lake is approximately 1.6 m. Since the lake is wide and shallow, the evaporation is high and is nearly equal to the average annual precipitation and is about 1.4 m (McCorquodale et al., 2001).

The proximity of the Pontchartrain estuary to the Gulf of Mexico results in a humid, subtropical climate. Seasonal variation exists in the precipitation and evapotranspiration

mechanisms and the resulting runoff. In summer the southerly winds provide abundant moisture from the Gulf of Mexico causing favorable conditions for intense isolated afternoon storms. In winter, the cold fronts moving over the area cause strong, area-wide precipitation. The period May through October has been designated as the summer season and November through April as the winter (Cruise and Arora, 1990). The average temperature in New Orleans is 77.6 ^{o}F (25.33 ^{o}C) in summer and 58.6 ^{o}F (14.78 ^{o}C) in winter. The average precipitation is 31.2 inches (792.5 mm) in summer and 30.6 inches (777.2 mm) in winter.

The summer season is generally characterized by high recreational use and by summer storm activity. Historically, Lake Pontchartrain has been popular for swimming, fishing, boating, and other recreational activities, especially in the summer season. Over the past several decades, the water quality of the lake has deteriorated. In mid 80's, Louisiana Department of Health and Hospitals (LDHH) issued an advisory discouraging swimming and other primary contact recreation (PCR) activities on the south shore of the lake as the concentration of fecal coliform exceeded the state water quality standards. The rivers in the north shore frequently exceeded the federal and state limits on the concentration of total coliform for PCR. US Environmental Protection Agency (EPA) and other regional environmental agencies such as Louisiana Department of Environmental Quality (LDEQ) have been using total coliform levels as the indicator for pathogen concentrations.

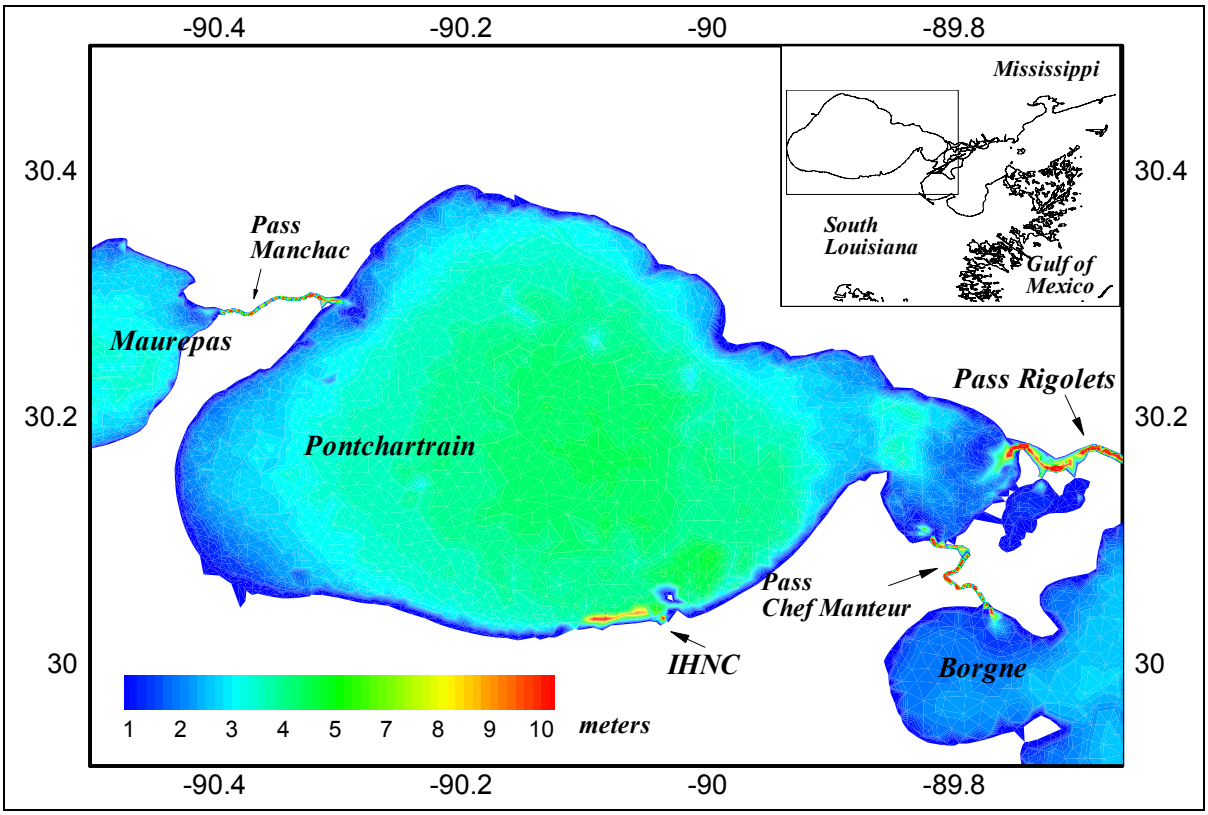

Figure 1.1 Location and bathymetry of Lake Pontchartrain

The degradation of the water quality of Lake Pontchartrain can be attributed to the anthropogenic alterations to the environment. The watersheds in the north shore of Lake Pontchartrain have diverse land use. Not all the runoff from these agricultural lands, pastures, dairy farms, forests, wetlands, camping grounds, and constructed urban areas is treated before it drains into the lake (Barbé et al. 1999). In addition to that, in the recent past, there has been a rapid development along the north shore of the lake.

Unlike the north shore, contamination in the south shore is a result of stormwater runoff from the Greater New Orleans area. Since the average elevation in New Orleans is several feet below sea level, levees have been constructed to protect the City from flooding. Most stormwater runoff must be pumped to Lake Pontchartrain via drainage canals. Although the sanitary and

stormwater sewer systems in New Orleans are separate, age and high subsidence rates in the area result in damaged pipes that allow cross-flow and contamination of the storm runoff. There is evidence of cross-contamination between the sanitary sewers and storm drains caused because of sanitary sewer overflows during a storm event (Georgiou and Tittlebaum, 2001).

All the rivers in the north shore of the lake, Bogue Falaya, Tchefuncta, Tangipahoa, and the drainage canals discharging into the Lake Pontchartrain in Jefferson and Orleans Parishes were listed in the revised 2004 303(d) list of impaired waters released by the LDEQ for non-attainment of the Total Fecal Coliform for PCR. In addition, many bayous and creeks draining into the lake such as Bayou Bonfouca, Bayou Lacombe, Salt Bayou, and Bayou Cane etc. were reported for non-attainment because of high fecal coliform levels (LDEQ, 2004).

In the recent past, there is evidence that overall water quality of the lake has improved significantly. The weekly sampling conducted by the Lake Pontchartrain Basin Foundation (LPBF) in the lake and its surroundings indicated fewer violations of the fecal coliform limits in the recent months (Bourgeois-Calvin and Dufrechou, 2003). As a result, some beaches along the south shore were opened to public in 2004.

1.2 Problem Statement

The recreational use of Lake Pontchartrain is currently limited due to elevated fecal coliform counts. In the recent past there has been an upsurge in the number of people returning to the lake. However, the public needs to be advised about the suitability of the lake water for safe recreational activities without any health risk. Currently fecal coliform levels in the lake are

estimated by collecting samples and performing laboratory analysis. Since the laboratory analysis to measure indicators is a 48-hour process it provides only a two-day old "snapshot" of the water quality. Since the indicator bacteria levels deteriorate with time, these "snapshots" are rarely representative of the environment when the data are reported. There is a need for a reliable tool to predict the bacteria levels in the recreational waters, promptly and precisely, in addition to the conventional methods.

The concentration of the pathogen indicators at any given location depends on the strength of the sources, hydrodynamics of the receiving water, dilution, and the decay of the indicator organisms between the source and the receiving waters. Previous studies have shown that resuspended bed sediments can be a source of the fecal coliform (Van Donsel and Geldreich 1971, Grimes 1975, Gary and Adams 1985).

Quick and accurate prediction of the areas with potential health risks can be achieved by developing a numerical model that can account for hydrodynamics, transport, waves, sediment dynamics and the fate of the pathogens in the lake.

1.3 Objectives

The specific objectives of this study are as follows:

- Develop a Lake-wide model to simulate the hydrodynamics and wave dynamics based on the wind and tide.
- Develop a sediment transport model for Lake Pontchartrain.

- Develop a Near-field model to simulate sediment dynamics, transport and the fate of fecal coliform in the north shore of Lake Pontchartrain.
- Apply the Near-field model to the south shore of Lake Pontchartrain.
- Study the residence times and shoreline impact of the fecal coliform plumes.

1.4 General Methodology

A brief outline of the procedure followed to meet the objectives is as follows:

1. The literature related to the problem in the study area was reviewed.
2. Water and sediment samples were collected to measure the fecal coliform levels and other conventional water quality parameters in the vicinity of the Tchefuncte River and the stormwater outfalls in Jefferson Parish during wet weather and dry weather.
3. Fecal coliform loading from the rivers and the stormwater canals was estimated using the field data and the data collected by Lake Pontchartrain Basin Foundation (LPBF).
4. A 3-D numerical model capable of simulating hydrodynamics, sediment dynamics, fate and transport of the fecal coliform was selected and customized for Lake Pontchartrain to simulate hydrodynamics and wave dynamics due to wind and tide.
5. The water levels in the Lake-wide model were calibrated using the information from the stage gages in the Lake Pontchartrain. The tracer transport was calibrated using the reflectance images of the 1997 Bonnet Carré spillway opening event.
6. The same 3-D model was used to set up Near-field models to simulate sediment resuspension and deposition, and transport and fate of the fecal coliform in the study areas on high resolution grids.

7. The sediment model was calibrated using the reflectance imagery from NASA Terra/Aqua satellites.
8. The Near-field model for the north shore of Lake Pontchartrain was calibrated and validated based on the measured water quality data.
9. Various scenarios were simulated to study the residence times and shoreline impact of the fecal coliform plumes.
10. The Near-field model was applied to the south shore of Lake Pontchartrain and was calibrated and validated based on the measured water quality data.

2. LITERATURE REVIEW

2.1 Hydrodynamic and Transport Modeling in Lake Pontchartrain

A two-dimensional, depth-averaged model used by Gael (1980) to study the water circulation patterns was the first modeling effort in Lake Pontchartrain. Hamilton et al. (1982) used a two-dimensional, depth-averaged model to simulate the wind and tide effects on the circulation patterns in Lake Pontchartrain. Both studies indicated that the dominant circulation in the lake is largely dependent on wind shear. A double gyre pattern was observed in the lake circulation when wind stresses were applied. This trend was also reported by Stone et al. (1972) by studying the surface currents using dye tests in the Lake Pontchartrain. It was identified that the tidal effects are dominant when the wind speeds are less than 2 m/s, when the speeds are greater than 3 m/s wind controls the circulation, while wind and tide have equal effects on circulation for wind speeds between 2 to 3 m/s.

McAnally and Berger (1996) developed the first 3-dimensional hydrodynamic model (RMA10 - WES) for the Lake Pontchartrain system to simulate the salinity changes that might occur in Biloxi marshes due to the proposed diversion of fresh water from the Mississippi River through the Bonnet Carré spillway. The model showed that the Mississippi River Gulf Outlet (MRGO) contributes significantly to the salinity regime in Lake Pontchartrain. The model also indicated long response times for the changes in the lake due to freshwater inputs.

In a U.S. Geological Survey (USGS) study, Signell (1996, 1997) configured a 3-dimensional model to study the physical processes in Lake Pontchartrain. A modified version of

the Estuary, Coastal and Ocean Model (ECOM) as described in Blumberg and Mellor (1987), ECOM-si was used to simulate wind driven circulation processes in the lake. It was concluded that water levels in Mississippi Sound influence the circulation patterns in the eastern part of the lake, while wind forcing dominates in the western end (Signell and List, 1997). Figure 2.1 shows the depth-averaged circulation in Lake Pontchartrain for a southeasterly wind of 5 m/s.

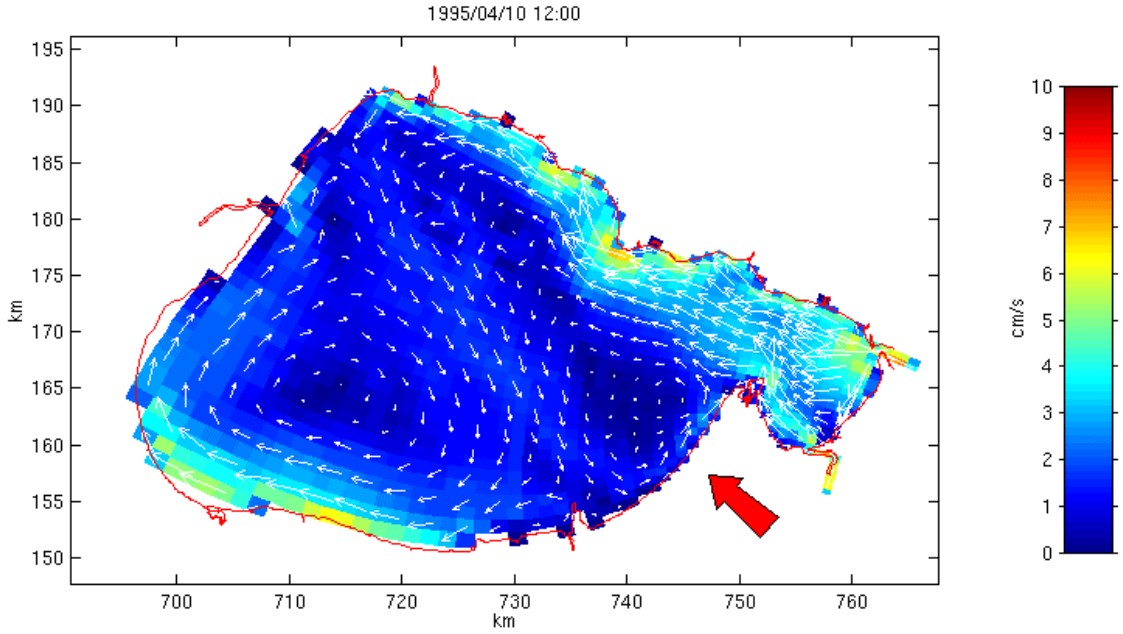

Figure 2.1 Depth-averaged circulation in Lake Pontchartrain due to a southeasterly wind of 5m/s (Signell and List, 1996)

A two-dimensional depth-averaged finite element hydrodynamic and transport model (RMA2/RMA4) was used by Haralampides (2000) to study the response of freshwater inputs from the tributaries, diversion from Bonnet Carré spillway, and saltwater inputs from the Inner Harbor Navigational Canal (IHNC)/MRGO in the Lake Pontchartrain system. The model simulated the 1997 Bonnet Carré spillway opening event accurately and predicted double gyre circulation pattern in both Lake Pontchartrain and Lake Maurepas (Figure 2.2). The field

measurements showed that drought-like conditions can increase the salinities in the lake and indicated a slow return to normal salinities after the diversion.

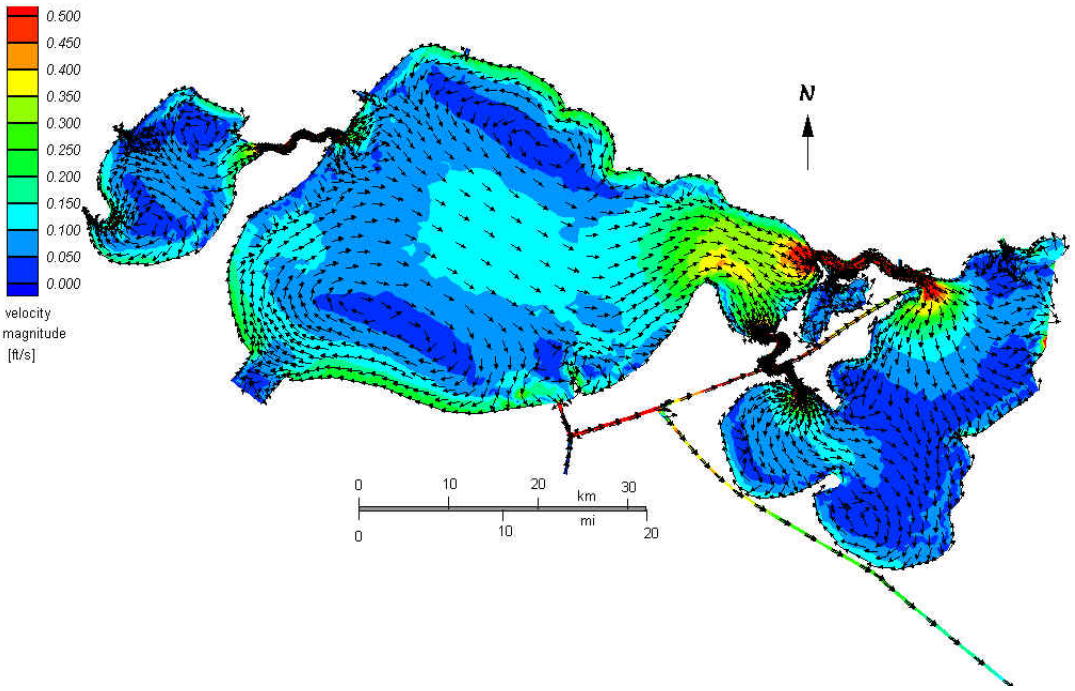

Figure 2.2 Depth-averaged circulation due to southeasterly wind at 6 ms-1 (Haralampides, 2000)

Georgiou (2002) developed a three-dimensional hydrodynamic and transport model for Lake Pontchartrain based on the Princeton Ocean Model (Blumberg and Mellor, 1987) to simulate the circulation patterns and saltwater intrusion into Lake Pontchartrain (Figure 2.3). Salinity stratification in Lake Pontchartrain near the IHNC was studied and it was observed that the density gradients caused the saltwater wedge to propagate large distances into the lake developing favorable conditions for hypoxia (Figure 2.4). It was also identified that relatively small diversions from the Mississippi River into the lake would result in a stable and acceptable salinity gradient from west to east and would suppress the intrusion at IHNC. In addition, the

model showed that the freshwater plume from the west trapped inside an eddy and has high residence times due to limited transport and mixing.

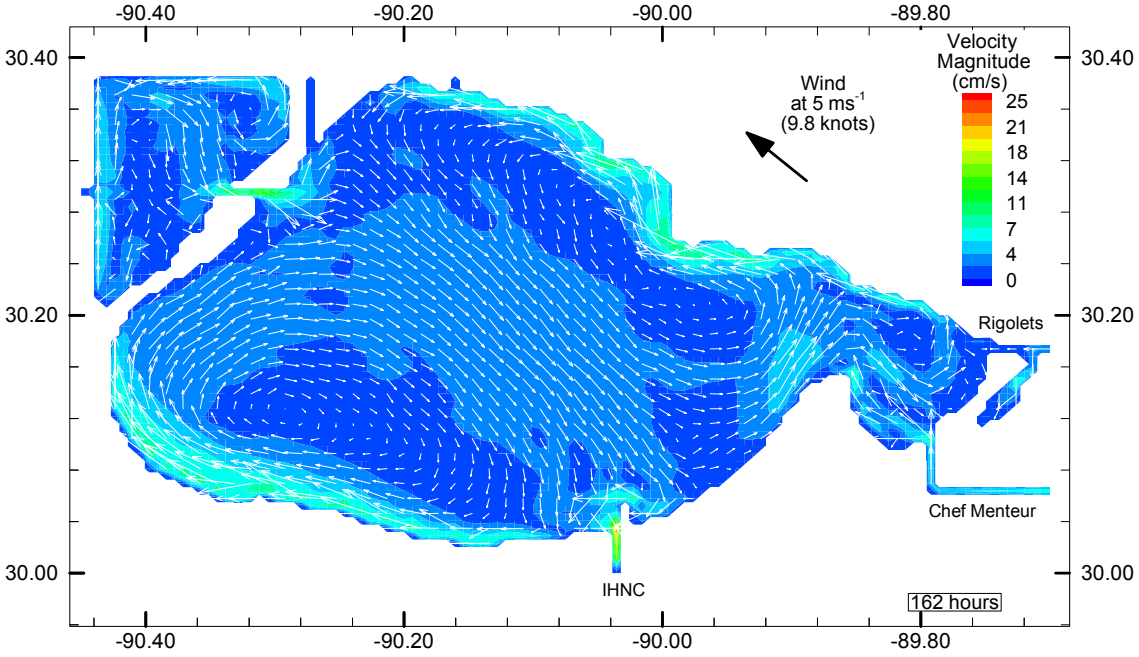

Figure 2.3 Depth-averaged circulation from a southeasterly wind at 5 m s-1 (Georgiou, 2002)

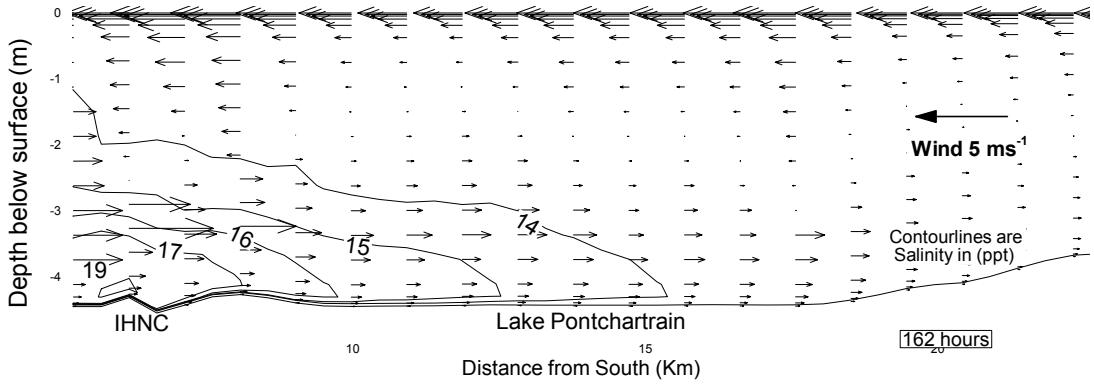

Figure 2.4 A side view of the velocity profile and salinity distribution at the IHNC due to a northerly wind at 5ms-1 (Georgiou, 2002)

2.2 Studies Related to Fecal Coliform Levels in Water Column and Bottom Sediments

Barbé and Francis (1992) developed a statistical model to estimate fecal coliform concentrations in the lower Tchefuncte River as a function of the river discharge. The study identified that the fecal coliform counts are significantly different between summer and winter seasons. Later, Barbé et al. (1999) developed a statistical model to estimate fecal coliform concentrations in the Bogue Falaya and Tchefuncte Rivers as a function of basin average precipitation. The study found that fecal coliform counts in the Bogue Falaya River were independent of the season whereas, in the Tchefuncte, they were seasonally dependent. Also, the analysis of precipitation data over 104 years showed that the amount of precipitation in southeast Louisiana is not strongly seasonal.

Barbé et al. (2001) tested for correlation between fecal coliform and parameters such as rainfall up to four days prior to the fecal coliform measurement, salinity, water temperature and average daily wind speed in a shoreline study on the south shore of Lake Pontchartrain. Fecal coliform concentrations were found to be wet weather dependent. The study identified an active continuous source of fecal coliform near the IHNC. For the remaining area fecal coliform levels were found to increase only after a pumping event. It was also found that the fecal coliform levels were a function of both rainfall amounts and salinity levels; a direct relationship exists between fecal coliform levels and precipitation while an inverse relationship exists between fecal coliform and salinity.

In environments similar to Lake Pontchartrain there is significant evidence to verify the presence of fecal coliform in the bottom sediments (McCorquodale et al. 2004, Englande et al. 2002, Goyal et al. 1977). The data collected by LaBelle and Gerba (1979) indicated that the degree of adsorption of enteric viruses to marine sediments was very high. LaBelle et al. (1980) showed that the number of viruses found in sediment was strongly correlated to the number of fecal coliform found in sediment.

Several studies showed that the survival rates were significantly higher in sediments with predominantly clay-sized particles than in coarser sediments (Howell et al. 1996, Burton et al. 1987). Davies et al. (2000) compared the effectiveness of constructed wetlands and water pollution control ponds to remove the stormwater associated bacteria. It was concluded that wetlands were far more effective than pollution control ponds in bacteria removal. The reason attributed to this was the inability of the pond system to retain the fine clay particles (<2microns) to which the bacteria were largely adsorbed. Adsorption of bacteria to particles allows them to persist in aquatic environments as they are: 1) protected from factors like solar radiation, starvation and attack by bacteriophages and protozoa and 2) fed by the organic material and nutrients present in the sediment (Roper and Marshall 1974, Gerba and McLeod 1976, Gonazalez et al. 1990, Davies et al. 1995).

McCorquodale et al. (2003) observed that the mortality rates of coliform bacteria were lowest in the sandy beach sediments along the south shore of Lake Pontchartrain. The sediments collected from the stormwater canals on the south shore had 82.5% sand, and the highest organic content and nutrients among all the samples collected. It was also observed that the bacteria die-

off rate was highest in the canal sediments. It was concluded that the relative organic and nutrient content of the sediment may not play an important role in the survival of the organisms adsorbed to the sediment in the south shore of Lake Pontchartrain.

There is sufficient evidence in the literature to safely assume that bacteria-adhered-sediment resuspension would release some of the adsorbed bacteria back into the water column, making it an important source of fecal coliform. Following are a few cases to illustrate this point:

Van Donsel and Geldreich (1971) observed 100 to 1000 times more fecal coliform in mud than in overlying water and found the mud-water interface to be dynamic and speculated the re-entrainment of fecal coliform by resuspension. Grimes (1975) saw a significant increase in fecal coliform concentrations in the immediate vicinity of a dredging operation in the Mississippi River. It was concluded that the disturbance and relocation of the bottom sediments by dredging released the associated fecal coliform. During a study of a stream, Gary and Adams (1985) found fecal coliform levels in water column almost doubled after disruption of the stream sediment bed. Pettibone et al. (1996) found that the concentration of fecal coliform along with total suspended solids (TSS) increased in the water column immediately after a ship passed through a channel. Crabill et al. 1998 showed that sediment agitation by recreational activities and storm surges associated with the summer storm season were responsible for the increase of fecal coliform counts. Le Fevre and Lewis (2003) suggested that wave action was the main cause of resuspension of sediment-bound enterococci in a small urban bay in New Zealand.

In a study conducted on fecal coliform levels in the Thames River sediments, Babinchak et al. (1977) identified that although the bacteria levels were high in the Thames River prior to dredging, the concentration of bacteria did not increase in the dump site sediments after the deposition of dredge materials. This indicated that bacteria were presumably present in the upper layer of the sediment.

Roper and Marshall (1974), while studying the effects of electrolyte concentration on bacterial sorption-desorption processes in sediments, found that fecal coliform desorbs under the conditions of reduced salinity.

Jamieson et al. (2005) used Escherichia coli (E. coli) bacteria to investigate the resuspension and persistence of sediment-associated bacteria in a small alluvial stream. The study was conducted in Swan Creek, located within the Grand River watershed of Ontario, Canada. The study has illustrated that the bacteria can survive in bed sediments for up to 6 weeks and that decay of the bacteria resembled typical first-order decay. The critical shear stress for E. coli resuspension in Swan Creek ranged from 1.5 to 1.7 Nm^{-2}, which was similar to the critical shear stresses for erosion of cohesive sediments. Further, it was concluded that the bacteria resuspension was primarily limited to the rising limb of storm hydrographs implying that a finite supply of sediment-associated bacteria were available for resuspension during individual storm events.

2.3 Fecal Coliform Modeling in Lake Pontchartrain

Carnelos (2003) used the modified Princeton Ocean Model to develop a forecasting model to predict the pathogen indicator levels in the recreational waters receiving contaminated stormwater from multiple outfalls (McCorquodale et al., 2004) in the south shore of Lake Pontchartrain. The framework consisted of a nested lake wide hydrodynamic model (Georgiou, 2002) and a high resolution near field bacteria fate – transport sub-model. The model was calibrated based on the field studies on the south shore of the lake. The model verified the observed two to three day impact period associated with stormwater discharges and highly variable wind-driven plume migration patterns often characterized by shore attachment (Figure 2.5). The study illustrated a potential risk pertaining to the entrainment of the high bacteria levels in the bottom sediments of the lake by resuspension.

Jin et al. (2003) in a study to assess the impact of rainfall events on Lake Pontchartrain water quality found that the drainage canals constitute a significant microbial loading to lake waters. The concentration of the indicator microbes in water column was observed to decrease significantly in two to three days after storm pumping events into the lake. A simple two-dimensional mathematical model incorporating the advection and dispersion processes was developed. The hydrodynamics were derived from the field data. The model results underestimated the concentration of the fecal coliform. The authors suggested that resuspension of sediment and re-introduction of indicator organisms that attached to the sediment back into the water column could be the reason. Jin et al. (2004) indicated that the attachment of microbial indicators to suspended matter and subsequent sedimentation as a significant fate mechanism in Lake Pontchartrain. It was also noted that, with a slower decay rate of indicator organisms in the

bottom sediment, there is a potential threat of recontamination of overlaying waters due to resuspension.

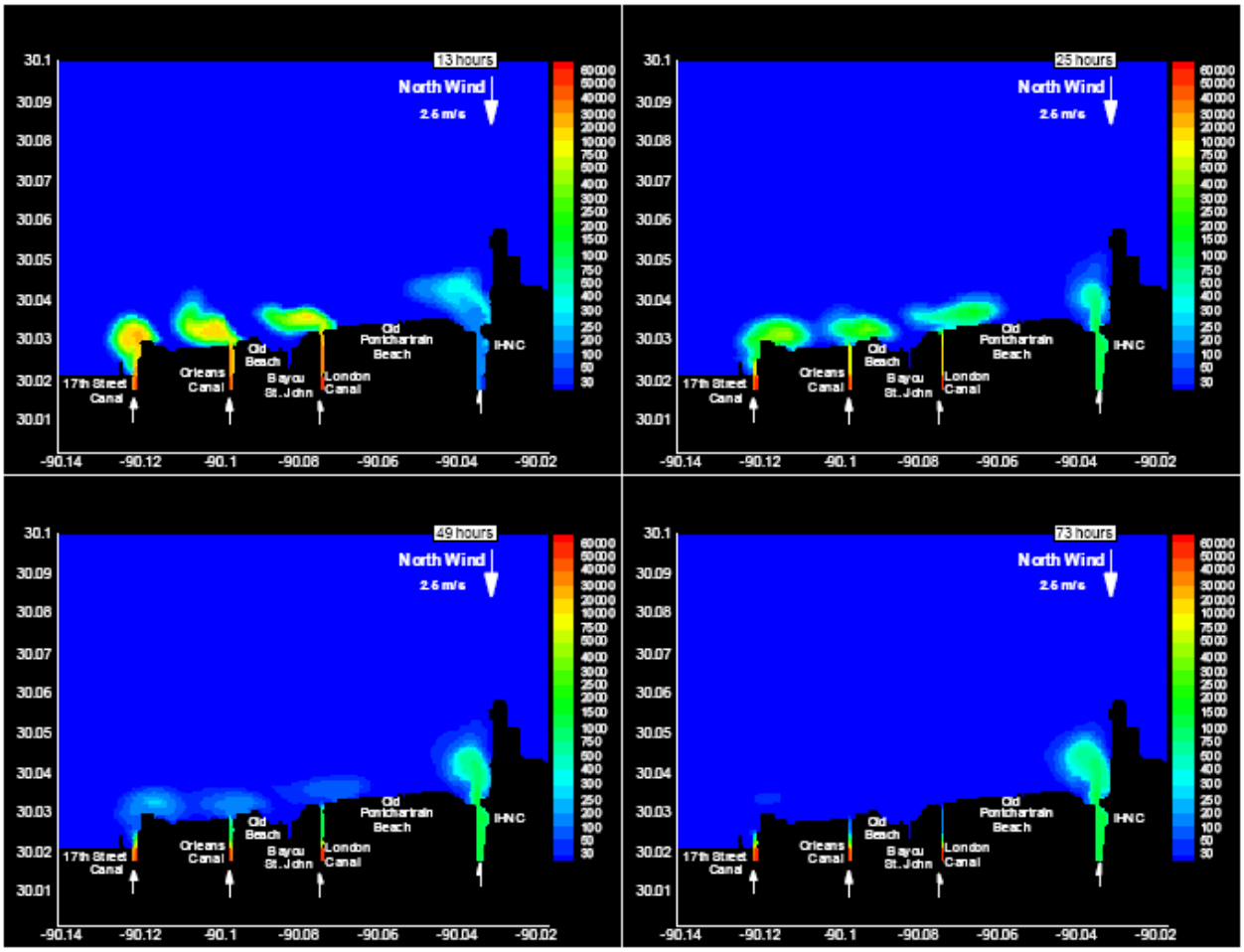

Figure 2.5 Three-day simulation of fecal coliform plumes for an average pump event with north winds of 2.5 m/s (Carnelos, 2003)

2.4 Wave and Sediment Transport Studies in Lake Pontchartrain

USGS conducted a study to understand sediment resuspension and transport processes in Lake Pontchartrain during 1995 – 1998. The study included synoptic measurement of velocities, water levels, waves, and turbidity at two locations in the lake. In addition to the circulation

model mentioned earlier, a wave prediction model was developed to study the potential sediment resuspension (Signell et al. 2001, List and Signell 2001). A steady-state wave model Hindcasting Shallow Water Waves (HISWA) was employed to compute wave heights and corresponding orbital velocities. Wave climates in 128 simulations (eight wind speeds and sixteen wind directions) were executed. Figure 2.6 shows the comparison of model predicted significant wave heights and periods with the observed values in Lake Pontchartrain. There was an excellent match between the modeled wave climate and the field data with a correlation of 80 %. It was observed that waves lag the wind by approximately two hours. The field measurements indicated strong correlation between turbidity and bottom currents.

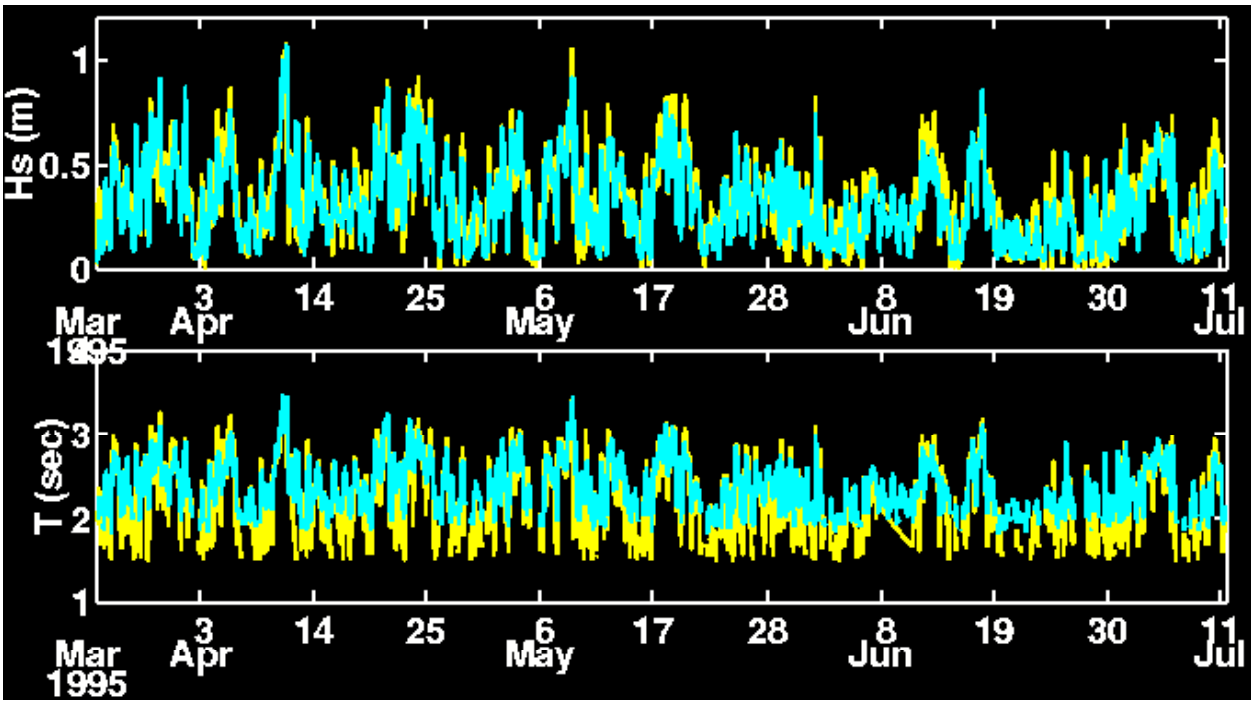

Figure 2.6 Comparison of observed and modeled significant wave heights and wave periods in Lake Pontchartrain. The predicted values are shown in yellow and the observed values in cyan (List and Signell, 2001)

2.5 Review of Numerical Models

Several numerical models were considered prior to selecting the suitable one for the present study. A brief review of the available models and their feasibility in current scenario is presented below.

2.5.1 RMA2/RMA4/RMA10

RMA2 and RMA4 (Resource Management Associates) are US Army Corps of Engineers' two-dimensional depth-averaged finite element hydrodynamic and contaminant transport models and RMA10 is a three dimensional hydrodynamic and transport model (USACE – WES, 1997). The package was successfully employed to simulate the two-dimensional hydrodynamics and transport processes in Lake Pontchartrain (Haralampides, 2000). The model's ability to use unstructured grids is offset by the excessive computational run times required. The model's inherent numerical diffusion in the region of advancing front can induce errors in the prediction of contaminant concentrations (Haralampides, 2000) and can be problematic for the nature of the current study. Also the RMA2 and RMA4 are not fully public domain models and RMA10 is only available through a cooperative agreement with US Army Engineer Research and Development Center (USACE-ERDC).

2.5.2 A Coupled and Hydrodynamical-Ecological Model for Regional and Shelf Seas (COHERENS)

COHERENS is a three-dimensional hydrodynamic and transport multi-purpose model for coastal and shelf seas and is coupled to biological, resuspension and contaminant models (Luyten et al. 1998, 1996). The modular structure of the model is convenient to enable only the necessary

process modules. COHERENS offers a wide variety of turbulence schemes ranging from simple algebraic formulas to one- or two-equation turbulence energy models, such as the Mellor-Yamada (1982) and the k-ε turbulence energy schemes (Rodi, 1984, Luyten et al., 1996). The biological and sediment modules work together to simulate internal non-conservative biological or chemical processes and photosynthesis by the absorption of PAR (photosynthetically active radiation) and transported by advection and diffusion. Deposition and erosion processes occur via a "fluff" layer. Although the model has necessary biological, resuspension and transport capabilities, it would not serve the given purpose due to its inability to simulate the crucial non-conservative contaminants in its current version.

2.5.3 TELEMAC

TELEMAC modeling system is an integrated tool to simulate free surface flows. It contains finite element based two- and three-dimensional hydrodynamic and transport models. It also includes two-dimensional water quality and sediment transport model. The three-dimensional model was observed to have relatively long run times and moreover, it is not a public domain model, thus not serving the research objectives of this project (Galland 1991, Janin et al. 1997).

2.5.4 H3D

H3D is a three-dimensional Cartesian finite-difference hydrodynamic and transport model based on a model called GF8 (Stronach et al. 1993). The model has capabilities to simulate sediment and pollution transport. The model's external gravity wave computation is implicit allowing large time steps. The model is better suited for the processes whose time scale

is similar to or longer than tidal periods. The horizontal eddy coefficient is taken as constant and the vertical eddy viscosity is assumed to depend on vertical shear and the Richardson number. Although the model is suitable for the present study, it is subject to limited distribution and has not been tested as extensively as some of the other models.

2.5.5 Princeton Ocean Model (POM)

Princeton Ocean Model (Blumberg and Mellor, 1987) is a three-dimensional, sigma coordinate, free surface ocean model with an embedded turbulence closure sub model. It has been used extensively in modeling of lakes, estuaries, coasts, and oceans. It has been used to study hydrodynamic and transport processes in Lake Pontchartrain (Georgiou 2002). Although POM was successfully implemented to simulate fate of pathogens in Lake Pontchartrain (Carnelos, 2003), the need for modeling sediment processes in the current study prevented its use since it does not have a sediment transport model.

2.5.6 Estuarine, Coastal and Ocean Modeling System with Sediments (ECOMSED)

ECOMSED is a three-dimensional hydrodynamic and sediment transport model with an ability to transport both conservative and non-conservative contaminants (Blumberg and Mellor 1987) based on POM. It includes separate modules for the computation of hydrodynamics, wind induced waves, sediment transport, transport of salinity, temperature, conservative and non-conservative tracer, heat flux calculations, and particle tracking. ECOMSED allows the use of orthogonal curvilinear grids in the horizontal direction and is based on the sigma coordinate system in the vertical, making it suitable for coastal applications. However, the standard release version of ECOMSED does not allow simulating the wetting and drying of the grid cells in

intertidal marshes and tidal flats. The model formulation uses the finite control volume principle. The model has a two time step solution scheme. The horizontal (external) free surface mode solves the depth-average surface wave equation using a small time step. The internal mode solves the three-dimensional part using a much larger time step of the order of 40 times the external time step. It is a three time level model and time stepping is accomplished by the leap frog scheme.

Sediment module of ECOMSED allows to model cohesive and non-cohesive sediment transport including the combined effect of currents and waves. This makes ECOMSED ideal to model fate and transport of pathogens including the contribution of fecal coliform from the sediment.

2.5.7 Finite-Volume Coastal Ocean Model (FVCOM)

FVCOM is a prognostic, unstructured grid, finite-volume, free-surface, three-dimensional primitive equations ocean model developed by Chen et al. (2003a). FVCOM combines the best attributes such as simple computational efficiency of finite-difference methods and geometric flexibility in finite element methods. It allows the use of unstructured grids in horizontal direction and has an improved sigma level model for the vertical. It includes multiple turbulence closure schemes from simple Richardson number parameterization to Mellor Yamada 2.5 level (Mellor and Yamada 1982) to k-ε turbulent model (Rodi 1980), for parameterization of vertical eddy viscosity. FVCOM discretizes the integral form of the governing equations. It has a wetting-drying option which is important to accurately simulate the hydrodynamics in estuarine environments with intertidal marshes and tidal flats. FVCOM includes biological and water

quality sub-models. A simple three-dimensional sediment suspension and tracer tracking model with settling, sedimentation, and resuspension processes is included. FVCOM is advantageous over ECOMSED because of unstructured grids and multiple turbulence closure schemes. Other than that most of the physics are similar in both the models. FVCOM was available only recently as a public domain model. This allows it to be the ideal choice for future modeling efforts in Lake Pontchartrain system and surrounding coastal basins.

2.6 ECOM/ECOMSED Applications

Signell and Harris (1999) used ECOMSED to test the hypothesis that tidally-averaged residual fields lead to the formation of sandbanks in the vicinity of coastal headlands. An idealized symmetrical coastline geometry and tidal forcing that represents conditions similar to regions where these tidal sandbanks were known to occur was chosen for the model simulations. Symmetric sandbanks were observed to form in both suspended and bedload simulations. The patterns of shear stress and sediment flux that occur over the course of tidal cycle and the sediment supply available were found to be the important factors in controlling the nature of the resulting sandbanks.

ECOMSED have been used in a number of sediment transport studies, including: Pawtuxet River in Rhode Island (Ziegler and Nisbet, 1994), Watts Bar Reservoir in Tennessee (Ziegler and Nisbet, 1995), Green Bay in Wisconsin (Shrestha et al., 2000) , Lower Fox River in Wisconsin (Gailani et al. 1991), Buffalo River in New York (Gailani et al. 1996) etc. Lick et al. (1994) used ECOMSED to simulate the resuspension and transport of fine-grained sediments in Lake Erie for a variety of wind conditions. The study found that major storms, despite their

infrequent occurrence, contribute for most of the resuspension and transport of fine-grained sediments in Lake Erie.

Blumberg et al. (1993) described the application of ECOM to Massachusetts Bay. The modeling addressed issues such as tidal and subtidal currents, the causes of the counterclockwise currents in the Bay, and outfall plume dynamics. Blumberg et al. (1996) compared ECOM predictions in the vicinity of the proposed outfall with EPA's ULINE, a near field plume dilution model. It was shown that the model comparisons for height of plume rise and initial dilution were in general agreement.

Both the near field and far field behavior of the Sand Island, Hawaii, and ocean outfall plume were modeled by Connolly et al. (1999). The three-dimensional circulation and water quality model ECOM was applied to predict the fate of pathogenic organisms in the vicinity of the outfall. Two numerical grids were generated for this application: one for the circulation model that extended around the island, and a grid for the fate and transport model that was more local in extent. The more extensive circulation model grid was needed in order to correctly simulate the observed circulation patterns in Mamala Bay. A conclusion of the study was that the Sand Island discharge was a primary contributor of observed fecal coliform levels on eastern recreational beaches. Other sources were identified as important for other beaches, and during storm events. The contribution of sediment as a fecal coliform source was neglected in this study.

Blumberg et al. (2001) described a regional scale modeling system developed and calibrated for the Northern Gulf of Mexico, that is, for the Mississippi Bight/Sound and adjoining Mobile Bay, Biloxi Bay, Bay St. Louis, and Lake Borgne using ECOMSED. The modeling system provides a reliable means to forecast littoral circulation, sediment suspension and transport, surface waves and conservative and non-conservative water quality constituents. The modeling framework adopted a high-resolution orthogonal curvilinear grid, which accurately resolved bathymetric and coastline features of the region, especially in the vicinity of the barrier islands. This modeling system was the highest horizontal resolution part of a triply nested series of three dimensional circulation models ranging from the North Atlantic Ocean to the Gulf of Mexico to the Mississippi Bight/Sound.

3. FIELD STUDIES

3.1 Objectives of the Field Study

The purpose of the field study was to quantify fecal coliform levels and the general water quality parameters in the study area; specifically, to identify the source concentrations and to obtain information on the plume migration patterns and the dilution/die-off that occurs under varying climatic conditions. The measured fecal coliform data were used to estimate decay rates in both the water column and bottom sediments which were used in the numerical models. In addition, the data were used to confirm whether the fecal coliform levels in the lake were increased by the storm water discharges in the event of wet weather in the region. And, finally the data were used to calibrate and validate the Near-field numerical models. Figure 3.1 show the locations of various stage, flow and weather gages from which the boundary conditions for the model were derived.

3.2 Methodology of the Field Study

A fixed sampling grid was designed to take the measurements along north shore of Lake Pontchartrain in the vicinity of the Tchefuncte River (Figure 3.2). Two types of field samplings were performed. A "background" survey was performed to characterize the fecal coliform levels during dry weather conditions and to identify the base conditions in the lake. A minimum period of three days of dry weather prior to sampling was required to qualify as a background survey. The other type of field sampling was a “rain event”, which was performed when there was more than 0.5 in rain in the region to characterize the wet weather effects on the levels of pathogen

indicators. The water samples were collected from the lake and the Tchefuncte River in the north shore in sterilized polyethylene bottles. Three individual estuarine sediment grab samples were collected using an Eckman dredge from the locations shown in Figure 3.2 to quantify the fecal coliform levels in the bottom sediments. All samples were preserved on ice prior to transportation to the laboratory for microbial, physical and chemical analyses. Fecal coliform, nutrients, salinity, temperature, dissolved oxygen, secchi disk, turbidity, TSS, pH were some of the parameters measured. The reader is referred to Leal (2004) for complete details of the field study.

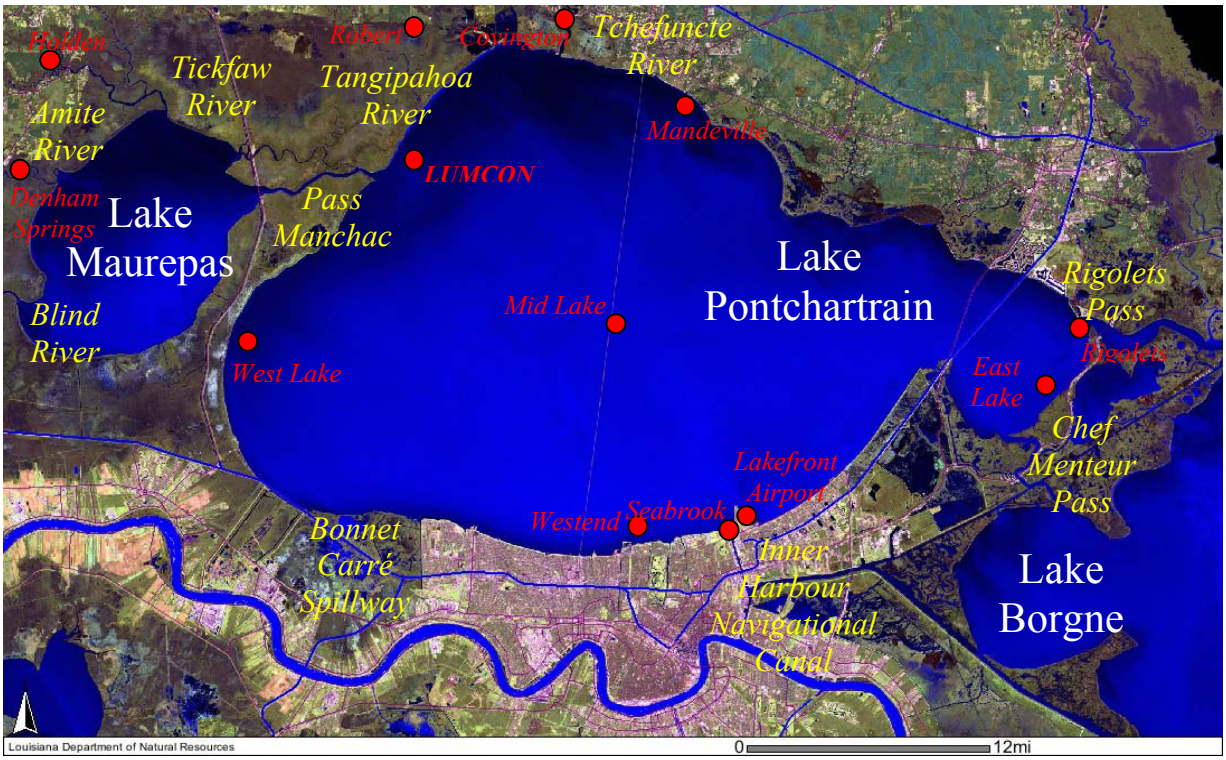

Figure 3.1 Features of Lake Pontchartrain Estuary – Lakes, Tidal passes, Rivers, and Location of Stage and Weather Gages (Filled Red Circles)

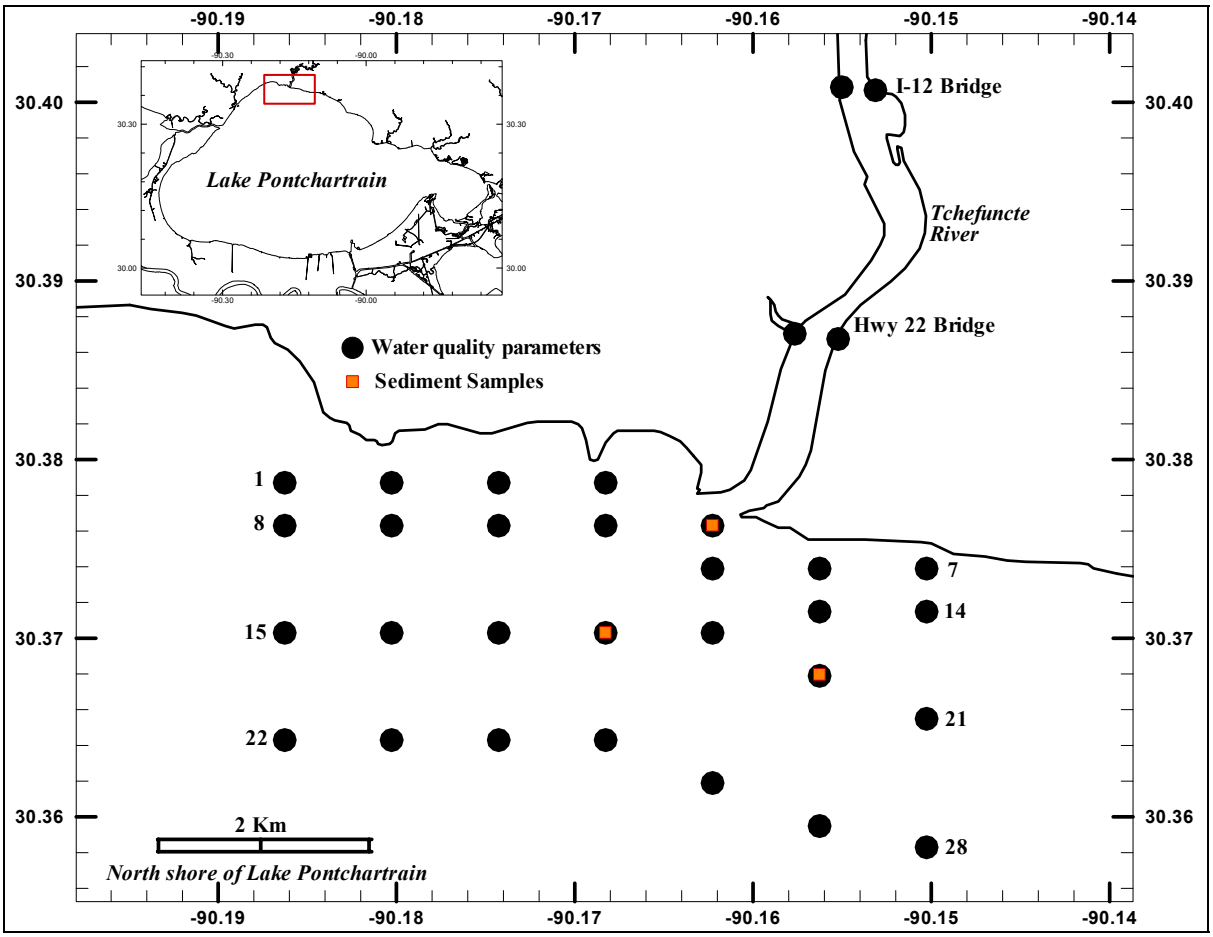

Figure 3.2 North shore Field Sampling Grid

3.3 Results from the Field Study

Figure 3.3 shows the average water quality parameters in the river, at the mouth of the river and in the lake for both wet and dry conditions. It was observed that the salinity tends to increase from the Hwy 22 Bridge to the lake. A dilution effect was apparent in the other parameters from the Hwy 22 Bridge to the lake. The statistical analysis of the data showed that there was a wet weather effect on all the parameters. However, the nutrient levels were consistently low during both dry and wet weather in the lake waters (below 0.2 mg/l). Most importantly, the wet weather effect on the fecal coliform levels was very obvious.

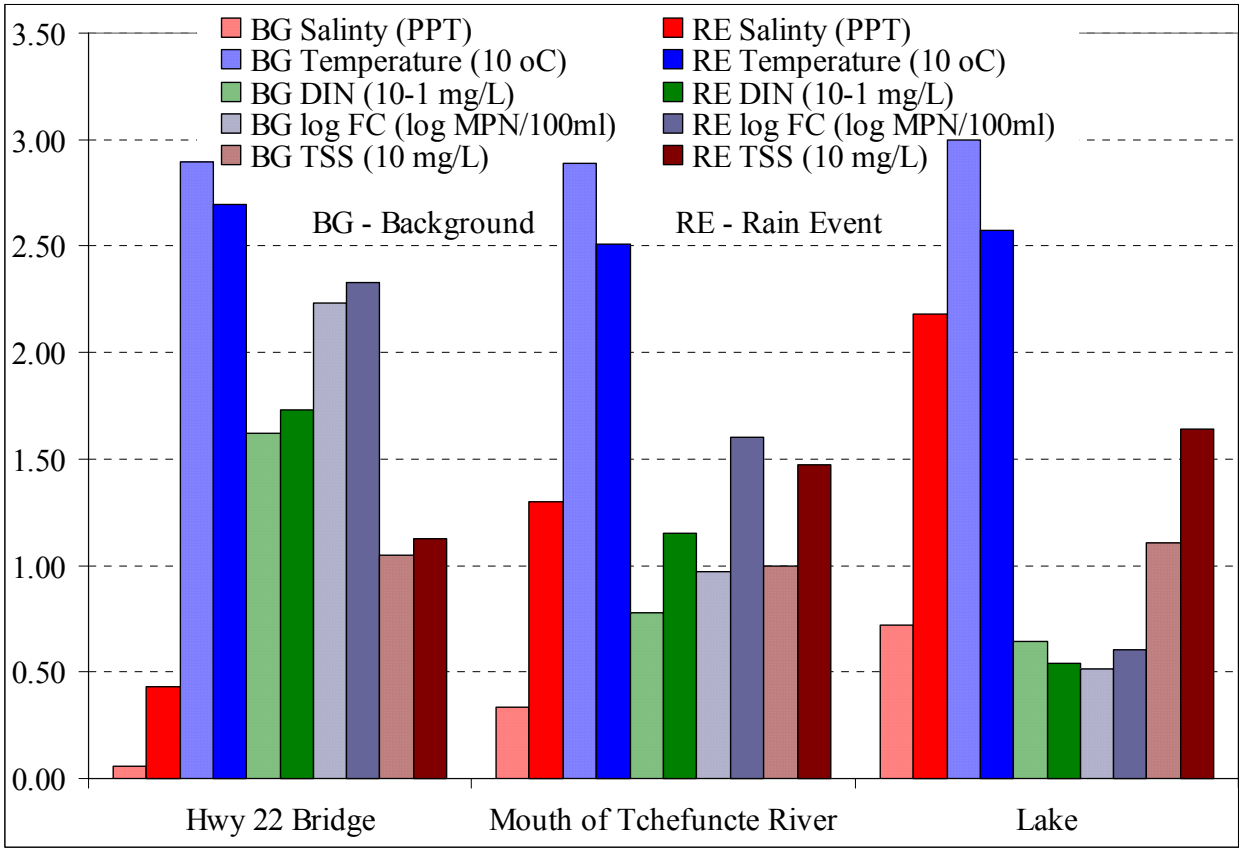

Figure 3.3 Mean water quality parameters for dry and wet weather samples from the north shore field study

Figure 3.4 shows a time series of geometric mean of fecal coliform levels observed in the lake during the two rain events: September 5th to 9th 2003, April 27th and 28th 2004. Since the storm water runoff takes approximately one day to reach the lake ("Day 1" being the first day after the storm), the initial fecal coliform levels correspond to dry weather. In general, fecal coliform levels were observed to peak during the second and third day after the rainfall event. Figure 3.5 shows a sequence of plume patterns observed during the September rain event in the north shore of Lake Pontchartrain. The first plot shows the fecal coliform levels on the first day after the storm has begun and indicates background conditions in the lake. The second plot

shows the elevated levels in both the river and the lake indicating the arrival of the storm runoff by the time the measurements were taken on the third day. The third plot shows the data collected on the fifth day after the storm has begun. It can be seen that fecal coliform levels in the lake water have returned to the background levels.

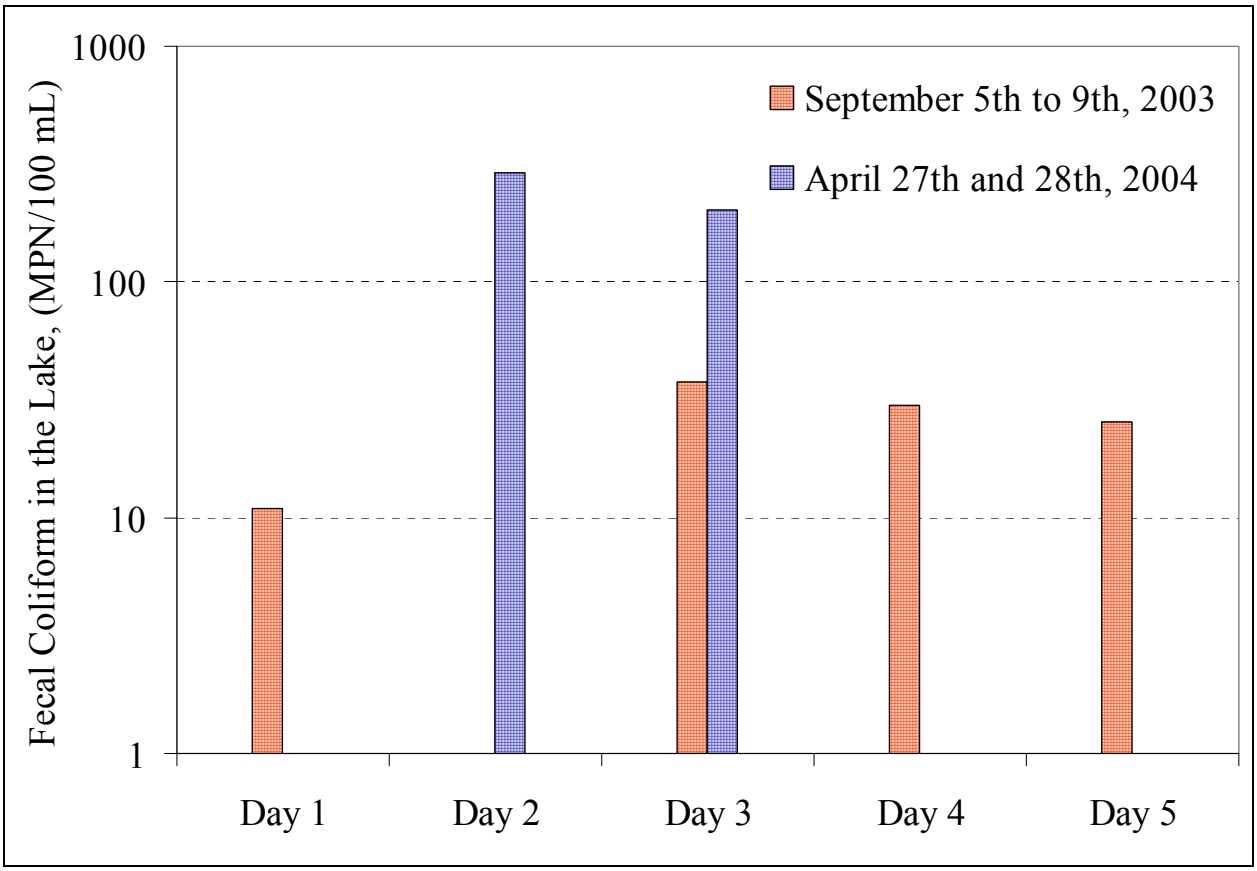

Figure 3.4 Time Series of geometric means of fecal coliform levels measured in the lake for two rain events (September data was not certified by the lab because of QA/QC concerns)

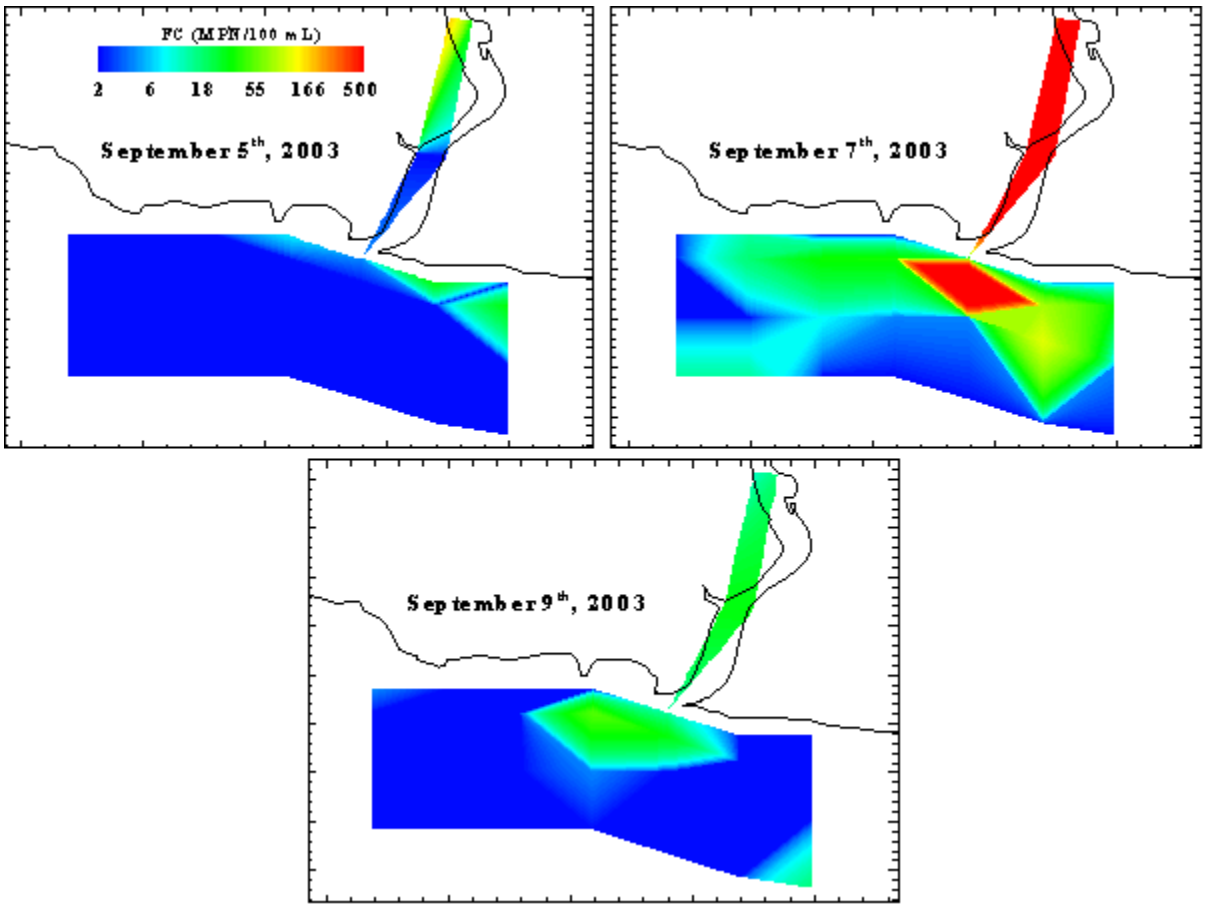

Figure 3.5 Fecal coliform levels observed during September 2003 rain event in the north shore of Lake Pontchartrain

A statistical comparison among wet and dry weather fecal coliform counts in the lake indicated a significant difference in the log weighted means 95% of the time. Even though the wet weather fecal coliform levels in the lake were generally less than 200 MPN/100mL, the fecal coliform in the river plumes were an order of magnitude higher than the dry weather counts.

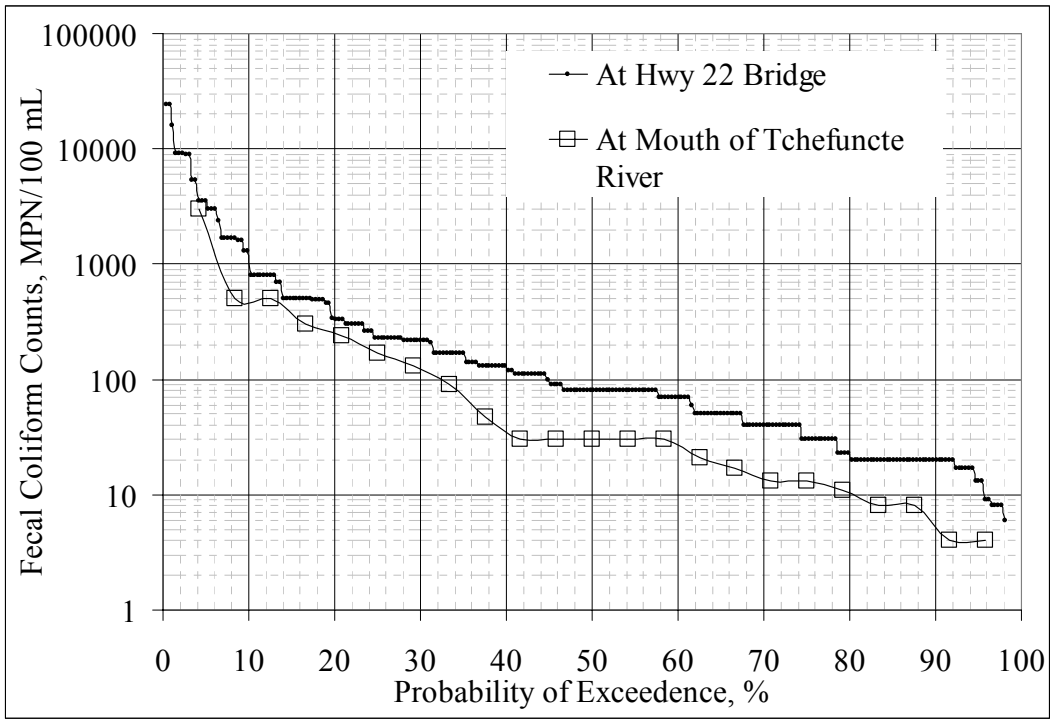

Figure 3.6 Probability of Exceedance of Fecal Coliform Levels near the Hwy 22 Bridge and at the Mouth of the Tchefuncte River for All Weather Conditions

Frequency analysis was performed on the data collected by Louisiana Department of Environmental Quality (LDEQ), Lake Pontchartrain Basin Foundation (LPBF) and the data from this field study. The probability of exceedance of the maximum allowable fecal coliform levels (200 MPN/100 ml) by the LDEQ for PCR at the Hwy 22 Bridge was found to be 31 % and 23% at the mouth of Tchefuncte River (Figure 3.6) for all weather conditions. Figure 3.7 shows the wet weather probability of exceedance of the LDEQ limit to be about 38 % at the mouth of the Tchefuncte River. The dry weather levels near the mouth of the river were found to satisfy the LDEQ criteria regularly. A more detailed discussion and the results from the field study were reported by Leal (2004).

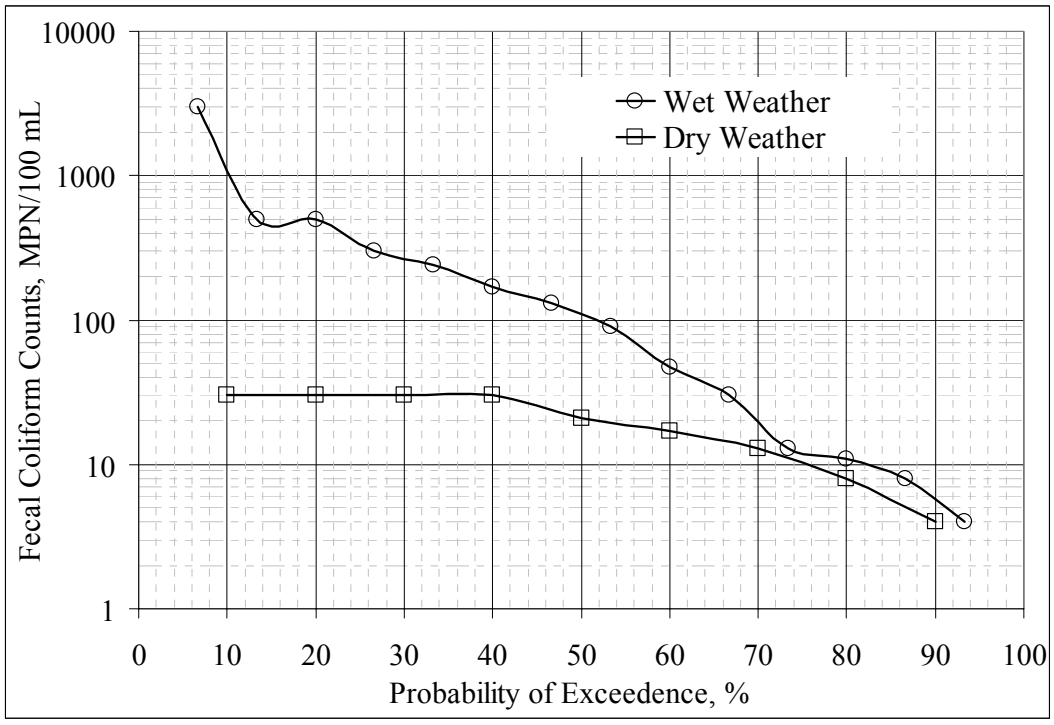

Figure 3.7 Probability of Exceedance of Fecal coliform Levels at the Mouth of the Tchefuncte River for the Wet and Dry Weather Conditions

3.4 Estimation of the Fecal Coliform Source Levels for the Tchefuncte River

Due to restricted resources, the field program was designed to obtain data for only two rain events. The amount of good quality data obtained from these two rain events was insufficient to accurately identify the fecal coliform data at the source. So the data collected by LPBF in the Tchefuncte River was used to supplement the data from this field study to estimate the source concentration. All of the available fecal coliform data were sorted based on the day of sampling relative to the start of the rising limb of the storm hydrograph. This process made sure all the data points associated with wet weather events fell into various bins corresponding to the number of days after beginning of storm runoff. The entire data were then plotted as shown in

Figure 3.8. The mean, maximum and minimum value for each bin was obtained and trend lines were plotted. The trend lines were then extrapolated to zero days, i.e. to the beginning of the storm runoff to obtain the source concentration. Thus three types of loading were defined: Mean load, High load and Low load for the Tchefuncte River. The upper envelope is used as the peak value in the pollutograph when there is a rainfall of 1 inch or more. The mean value is used when the rainfall is between 0.5 and 1 inch. The low loading is used when there is 0 to 0.5 in of rainfall.

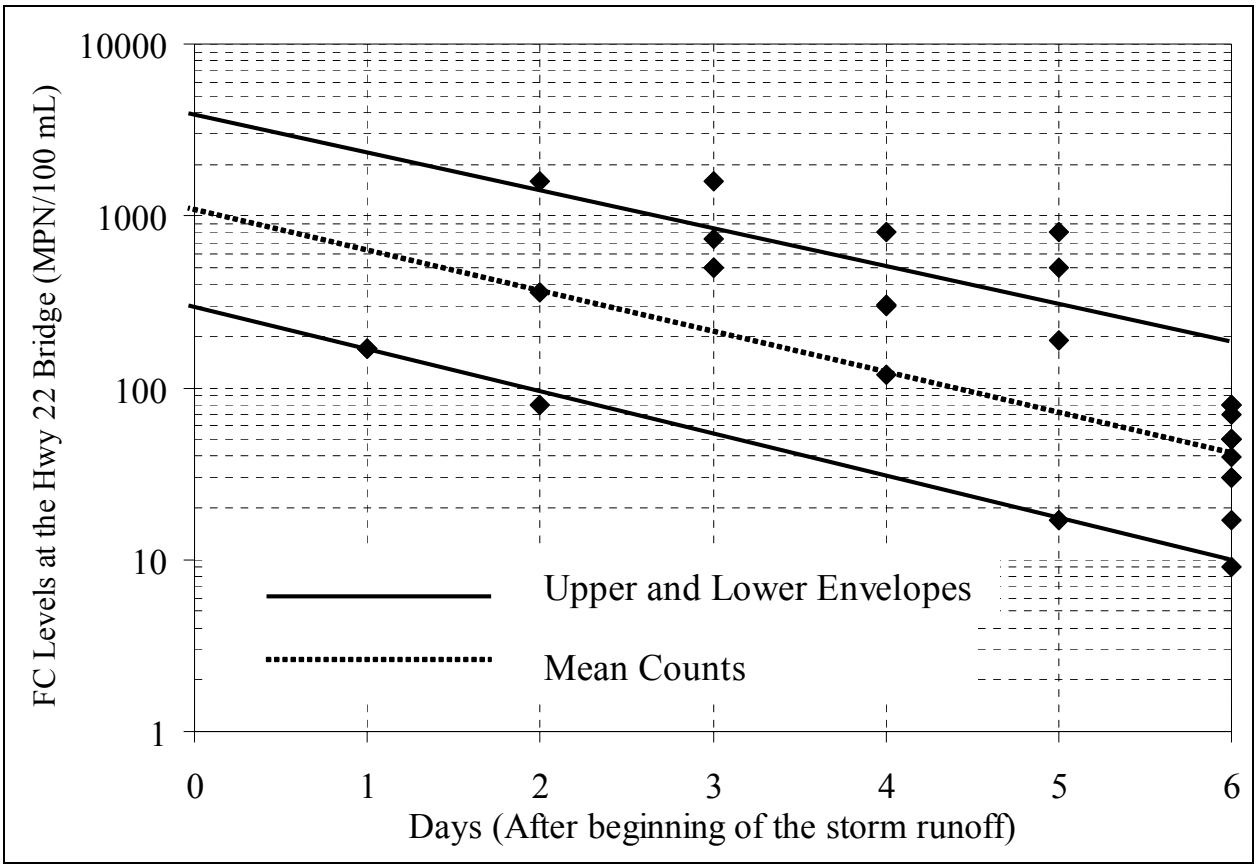

Figure 3.8 Estimation of fecal coliform source concentration near the Hwy 22 Bridge in the Tchefuncte River

4. MODEL DEVELOPMENT

4.1 Model Selection

The selection of the model that is apt for a given system is influenced by factors such as the scale and geometry of the system, the time scale of the processes, the driving forces in the system, and the physical processes occurring in the system.

A brief review of the various models considered for this study was given in Chapter 2. After the review, ECOMSED was selected based on the following criteria. ECOMSED is an improved version of the POM customized for its applicability to the estuarine environments similar to Lake Pontchartrain. As noted earlier, its predecessor POM was successfully applied by Georgiou (2002) and a semi-implicit version of the hydrodynamic module of ECOMSED, ECOM-si, was successfully implemented by Signell and List (1997) to the Lake Pontchartrain system. Moreover, ECOMSED was made available as a public domain model at the start of the study. Considering the ability of ECOMSED to simulate all the necessary processes in the present study and detailed knowledge of the physics of the model led to the selection of ECOMSED over the other models.

4.2 Description of ECOMSED

ECOMSED is a sigma coordinate, free surface model, designed to realistically simulate time-dependent distribution of waters levels, currents, temperature, salinity, tracers, cohesive and non-cohesive sediments and waves in marine and freshwater systems. It is based on the

Princeton Ocean Model developed by Alan Blumberg and George Mellor (1987) with modifications for its applicability in estuaries and coastal oceans (Blumberg 1996) and subsequent additions from many other contributors.

4.2.1 Hydrodynamic Module

The hydrodynamic module ECOM is a three-dimensional coastal ocean model, embedding a turbulence closure sub-model to provide a realistic parameterization of the vertical mixing processes. The turbulence sub-model is a 2.5 level model that uses a prognostic equation for turbulence kinetic energy and turbulence macroscale (Mellor and Yamada, 1982). The prognostic variables are the three components of velocity, temperature, salinity, turbulence kinetic energy, and turbulence macroscale. The momentum equations are nonlinear and incorporate a variable Coriolis parameter. Prognostic equations governing the thermodynamic quantities, temperature, and salinity account for water mass variations brought about by highly time-dependent coastal upwelling/downwelling processes as well as horizontal advective processes. Free surface elevation is also calculated prognostically, with only some sacrifice in computational time so that tides and storm surge events can also be simulated. Other computed variables include density, vertical eddy viscosity, and vertical eddy diffusivity. The modeling system also accommodates realistic coastline geometry and bottom topography by the use of orthogonal curvilinear grids and sigma coordinate system.

The sigma coordinate system, shown in Figure 4.1, allows for user defined logarithmic refinement of the bottom and surface boundaries while letting the vertical layers follow the bathymetry. This option is useful for the modeling of stratified flows (surface or bottom), water

elevations (surface), and boundary layers. This coordinate system is a necessary attribute in dealing with significant topographical irregularities such as those in estuaries, continental shelfs and slopes. Together with the turbulence sub-model, it produces realistic bottom boundary layers that are important to coastal waters and tidally driven estuaries (Oey et al., 1985 a, b)

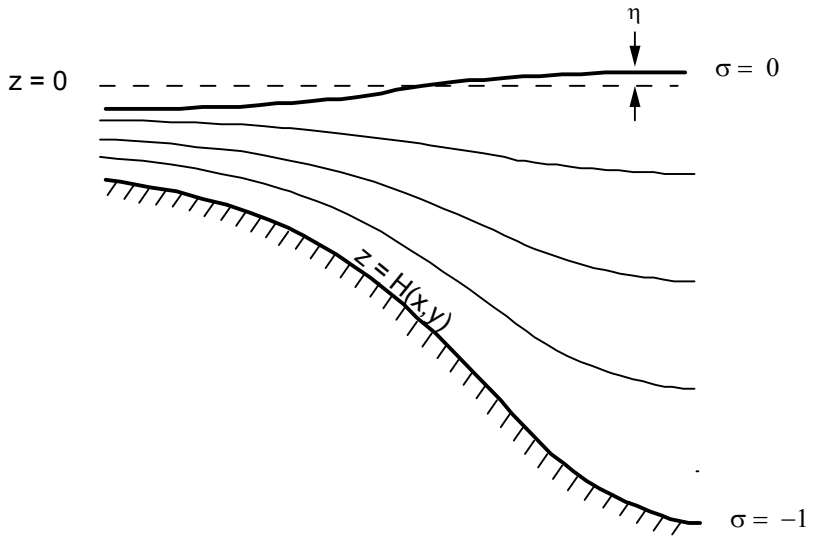

Figure 4.1 The sigma coordinate system

The governing equations of the model contain propagation of fast moving external gravity waves and slow moving internal gravity waves. For computational efficiency the vertically integrated equations of the external mode are separated from the vertical structure equations of the internal mode. The governing external and internal mode equations in (x, y, σ, t) coordinate system are shown below (Blumberg and Mellor, 1987).

The Continuity Equation:

$$\frac{\partial DU}{\partial x} + \frac{\partial DV}{\partial y} + \frac{\partial \omega}{\partial \sigma} + \frac{\partial \eta}{\partial t} = 0 \qquad (1)$$

The Reynolds Momentum Transport Equations:

$$\frac{\partial UD}{\partial t} + \frac{\partial U^2 D}{\partial x} + \frac{\partial UVD}{\partial y} + \frac{\partial U\omega}{\partial \sigma} - fVD + gD\frac{\partial \eta}{\partial x} + \frac{gD^2}{\rho_o}\int_\sigma^o \left[\frac{\partial \rho'}{\partial x} - \frac{\sigma'}{D}\frac{\partial D}{\partial x}\frac{\partial \rho'}{\partial \sigma'}\right] d\sigma' = \frac{\partial}{\partial \sigma}\left[\frac{K_M}{D}\frac{\partial U}{\partial \sigma}\right] + F_x \quad (2)$$

$$\frac{\partial VD}{\partial t} + \frac{\partial UVD}{\partial x} + \frac{\partial V^2 D}{\partial y} + \frac{\partial V\omega}{\partial \sigma} + fUD + gD\frac{\partial \eta}{\partial y} + \frac{gD^2}{\rho_o}\int_\sigma^o \left[\frac{\partial \rho'}{\partial y} - \frac{\sigma'}{D}\frac{\partial D}{\partial y}\frac{\partial \rho'}{\partial \sigma'}\right] d\sigma' = \frac{\partial}{\partial \sigma}\left[\frac{K_M}{D}\frac{\partial V}{\partial \sigma}\right] + F_y \quad (3)$$

Temperature Transport Equation:

$$\frac{\partial TD}{\partial t} + \frac{\partial TUD}{\partial x} + \frac{\partial TVD}{\partial y} + \frac{\partial T\omega}{\partial \sigma} = \frac{\partial}{\partial \sigma}\left[\frac{K_H}{D}\frac{\partial T}{\partial \sigma}\right] + F_T - \frac{\partial R}{\partial z} \quad (4)$$

Salinity Transport Equation:

$$\frac{\partial SD}{\partial t} + \frac{\partial SUD}{\partial x} + \frac{\partial SVD}{\partial y} + \frac{\partial S\omega}{\partial \sigma} = \frac{\partial}{\partial \sigma}\left[\frac{K_H}{D}\frac{\partial S}{\partial \sigma}\right] + F_S \quad (5)$$

Equation of the state for the computation of density:

$$\rho = \rho(\theta, \mathrm{S}) \quad (6)$$

$$\rho_1 = 6.76786136E-6 * S^3 - 4.8249614E-4 * S^2 + 0.814876577 * S - 0.22584586 \quad (6a)$$

$$\rho_2 = \rho_1 * \left(1.667E-8*\theta^3 - 8.164E-7*\theta^2 + 1.803E-5*\theta\right) \quad (6b)$$

$$\rho_3 = \rho_2 + 1 - 1.0843E-6*\theta^3 + 9.8185E-5*\theta^2 - 4.786E-3*\theta \quad (6c)$$

$$\rho = \rho_3 * \left(6.76786136E-6*S^3 - 4.8249614E-4*S^2 + 0.814876577*S + 3.895414E-2\right) \quad (6d)$$

Turbulent Kinetic Energy Transport Equation:

$$\frac{\partial q^2 D}{\partial t} + \frac{\partial U q^2 D}{\partial x} + \frac{\partial V q^2 D}{\partial y} + \frac{\partial \omega q^2}{\partial \sigma} = \frac{\partial}{\partial \sigma}\left[\frac{K_q}{D}\frac{\partial q^2}{\partial \sigma}\right] + \frac{2K_M}{D}\left[\left(\frac{\partial U}{\partial \sigma}\right)^2 + \left(\frac{\partial V}{\partial \sigma}\right)^2\right] + \frac{2g}{\rho_o}K_H\frac{\partial \tilde{\rho}}{\partial \sigma} - \frac{2Dq^3}{B_1 \ell} + F_q \quad (7)$$

Turbulent Macroscale Transport Equation:

$$\frac{\partial q^2 \ell D}{\partial t} + \frac{\partial U q^2 \ell D}{\partial x} + \frac{\partial V q^2 \ell D}{\partial y} + \frac{\partial \omega q^2 \ell}{\partial \sigma} = \frac{\partial}{\partial s}\left[\frac{K_q}{D}\frac{\partial q^2 \ell}{\partial \sigma}\right] + E_1 \ell\left(\frac{K_M}{D}\left[\left(\frac{\partial U}{\partial \sigma}\right)^2 + \left(\frac{\partial V}{\partial \sigma}\right)^2\right] + E_3\frac{g}{\rho_o}K_H\frac{\partial \tilde{\rho}}{\partial \sigma}\right)\tilde{W} - \frac{Dq^3}{B_1} + F_\ell \quad (8)$$

where, U is the x velocity, V the y velocity, ω the z velocity, η is the water elevation, f is the Coriolis force, D is the water depth, g is the acceleration of gravity, ρ_o is the mean density, ρ is the density, S is the salinity, T is the local temperature, θ is the potential temperature (local temperature for shallow water applications) σ is the vertical dimension (sigma levels), q^2 is the

turbulent kinetic energy, and l is the mixing length. The density ρ is computed according to an equation of state as shown in equation (6). The equations (6a) to (6d) show the actual computation steps as given by Fofonoff (1962).

The horizontal diffusion and viscosity terms are defined according to:

$$F_x \equiv \frac{\partial}{\partial x}\left(H\tau_{xx}\right)+\frac{\partial}{\partial y}\left(H\tau_{xy}\right) \tag{9}$$

$$F_y \equiv \frac{\partial}{\partial x}\left(H\tau_{xy}\right)+\frac{\partial}{\partial y}\left(H\tau_{yy}\right) \tag{10}$$

where

$$\tau_{xx} = 2A_M \frac{\partial U}{\partial x}, \quad \tau_{xy} = \tau_{yx} = A_M\left(\frac{\partial U}{\partial y} + \frac{\partial V}{\partial x}\right), \quad \tau_{yy} = 2A_M \frac{\partial V}{\partial y} \tag{11}$$

Also,

$$F_\phi \equiv \frac{\partial}{\partial x}\left(Hq_x\right)+\frac{\partial}{\partial y}\left(Hq_y\right) \tag{12}$$

where

$$q_x \equiv A_H \frac{\partial \phi}{\partial x}, \quad q_y \equiv A_H \frac{\partial \phi}{\partial y} \tag{13 a,b}$$

and where ϕ represents T, S, q^2 and $q^2 l$ (l is the mixing length).

The subgrid scale processes are parameterized by the horizontal mixing coefficients. ECOMSED uses the parameterization suggested by Smagorinsky (1963) to compute the diffusivity and has the following form:

$$A_M = \alpha \Delta x \Delta y \left[\left(\frac{\partial \mathrm{u}}{\partial \mathrm{x}}\right)^2 + \frac{1}{2}\left(\frac{\partial v}{\partial x}+\frac{\partial u}{\partial y}\right)^2 + \left(\frac{\partial v}{\partial y}\right)^2\right]^{1/2} \tag{14}$$

Recommended value of α is 0.1 and can range from 0.01 and 0.5 for various applications.

4.2.1.1 Boundary Conditions

4.2.1.1.1 Surface Boundary Conditions

The boundary conditions at the free surface include the surface wind stress, the heat flux, fresh water surface mass flux due to the net evaporation – precipitation combined with surface salinity, and the turbulent kinetic energy due to the surface wind stress. The mixing length is assumed to be zero at the surface. The vertical component of the velocity at the surface is computed using Equation (15).

$$W = U\frac{\partial \eta}{\partial x} + V\frac{\partial \eta}{\partial y} + \frac{\partial \eta}{\partial t} \qquad (15)$$

4.2.1.1.2 Bottom Boundary Conditions

The bottom frictional stress is determined by matching velocities with the logarithmic law of the wall and the turbulence kinetic energy due to the bottom stress comprise the bottom boundary conditions. In addition, the normal gradients of θ and S are set to zero on the side walls and bottom of the basin so that there are no advective and diffusive heat and salt fluxes across these boundaries. Further the mixing length is assumed to be zero at the bottom. The vertical component of the velocity is computed by Equation (16). For a more detailed description of the surface and bottom boundary conditions the reader is referred to Blumberg and Mellor (1987).

$$W = -U_b\frac{\partial H}{\partial x} - V_b\frac{\partial H}{\partial y} \qquad (16)$$

4.2.1.1.3 Open Boundary Conditions

Temperature and salinity are prescribed for inflow conditions; and for outflow boundaries, Equation (17) is solved.

$$\frac{\partial}{\partial t}(\theta, S) + U_n \frac{\partial}{\partial n}(\theta, S) = 0 \qquad (17)$$

where U is the velocity, θ is the potential temperature, S is the salinity, and subscript n is the coordinate normal to the boundary.

In case of the open lateral velocity boundary conditions, ECOMSED allows the user to specify the normal component of the velocity in terms of flow, and a free slip condition is used for the tangential component at the open boundary node.

For water levels, ECOMSED allows several types of boundary conditions. They include:

- *Clamped Boundary Condition* – the water level along the boundary grid is prescribed by the user either from observed data or tidal harmonics. However, this kind of boundary condition is considered rigid and does not allow long wave energy to radiate in or out of the model domain.
- *Reid and Bodine Boundary Condition* – To allow long wave to radiate, the model uses an open boundary condition developed by Reid and Bodine (1968) of the form,

$$\eta = \eta_0 + \frac{\lambda_t U_n}{\sqrt{g/D}} \qquad (18)$$

η is the sea level at the boundary and η_0 is the known water level. U_n is the model predicted velocity perpendicular to the open boundary, g is the acceleration due to gravity, and D is the depth of the grid cell. λ_t is Lagrange multiplier and is obtained at every time step to allow modification of sea level base on the difference between computed elevation and the forced elevation at the boundary node.

- *Optimized Clamped Boundary Condition* – It can be defined by Equation (18) and is based on work by Shulman (1995). In this, the Lagrange multiplier is computed by solving optimization problems that minimize the difference between the model computed and the forced boundary values under certain integral constraints representing energy, momentum, and mass fluxes on the open boundary.

4.2.2 Wave Module

The Wave Module in ECOMSED computes the amplitudes and periods of wind-driven surface gravity waves based on the formulations in the SMB (Sverdrup, Munk and Bretschneider) hindcasting method (USACE 1984). Surface wind waves can significantly increase bed shear stresses (van Rijn 1993) and further effect the sediment resuspension and deposition processes. Bed shear stresses due to combined effects of waves and currents can result in stresses that are two orders of magnitude higher than stresses due to currents alone. ECOMSED accounts for the increase in the bed shear stress using the Grant-Madsen wave-current model (Grant and Madsen 1979, Glenn and Grant 1987).

4.2.3 Sediment Transport Module

The SED module is a three-dimensional sediment transport model that realistically simulates resuspension, transport and deposition of both cohesive (< 75 microns) and non-cohesive (75 – 500 microns) sediments. Bed load transport which includes particle diameters greater than 500 microns is not included in this model. The cohesive sediment processes are based on the concepts developed by Lick et al. (1984) and the resuspension of non-cohesive sediments is based on van Rijn's suspended load theory (1984, 1993). The model requires experimental data in the computations of resuspension and deposition. The prognostic variables include concentrations of two fractions in water column, mass of sediment deposited/eroded, and subsequent changes in bed elevation.

The three-dimensional advection-dispersion equation for transport of sediment of size class k (cohesive: (k = 1), non-cohesive: (k=2)) is as shown in the Equation (19).

$$\frac{\partial C_k D}{\partial t} + \frac{\partial C_k UD}{\partial x} + \frac{\partial C_k VD}{\partial y} + \frac{\partial C_k \left(\omega - W_{s,k}\right)}{\partial \sigma} = \frac{\partial}{\partial \sigma}\left[\frac{K_H}{D}\frac{\partial C_k}{\partial \sigma}\right] + F_{C_k} \qquad (19)$$

Boundary Conditions:

$$K_H \frac{\partial C_k}{\partial z} = 0, z \to \eta \qquad (19a)$$

$$K_H \frac{\partial C_k}{\partial z} = E_k - D_k, z \to -H \qquad (19b)$$

where C_k is suspended sediment concentration of size class k; U, V, ω are velocities in x, y and z directions; A_H is horizontal diffusivity; K_H is vertical eddy diffusivity; D is the total depth of the water column (=H+η, H: depth, η: surface elevation) ; F_{Ck} includes the horizontal viscosity or diffusion/source-sink terms as shown in Equations (12) and (13); E_k, D_k are respectively

resuspension and deposition fluxes of size class k; η is water surface elevation above a specified datum; and H is the depth below datum.

4.2.3.1 Computation Philosophy

- To begin with, bottom shear stresses due to currents and waves are estimated since the resuspension and deposition mechanisms depend upon the shear stress induced at the sediment-water interface.
- Resuspension of cohesive sediments is modeled based on the formulation developed by Gailani et al. (1991). The amount of fine-grained sediment resuspended from a cohesive sediment bed is given as:

$$\varepsilon = \frac{a_0}{T_d^m}\left(\frac{\tau_b - \tau_c}{\tau_c}\right)^n \qquad (20)$$

  where ε is the resuspension potential (mg cm^{-2}); a_0 is a constant depending upon the bed properties; T_d is the time after deposition (days); τ_b is the applied bed shear stress (dynes cm^{-2}); τ_c is the critical shear stress for erosion (dynes cm^{-2}); and m, n are constants dependent upon the depositional environment. The parameters in the Equation (20) are determined from shaker studies (Tsai and Lick, 1987) on the bottom sediments.
- Deposition of cohesive sediments in the water column is modeled as a function of flocculation. The effect of internal shear rates and water column concentrations on flocculation is implicitly defined in the settling velocity formulation of Krone (1962). The fraction of settling sediments that are incorporated into the bed is estimated using methods proposed by either Krone (1962) or Partheniades (1992).

- To account for the consolidation of sediments with time, the bed is vertically discretized into seven layers as shown in Figure 4.2. Each layer of bed is characterized by the dry density, the deposition thickness, and the critical shear stress for erosion. The time after deposition for each layer increases linearly from one day at the surface, which has freshly deposited material, to seven days in the bottom layer. The layered bed model conserves the mass of the resuspended and deposited sediments.
- The resuspension of non-cohesive sediments is calculated using the procedure developed by van Rijn (1984). Bed armoring is accounted for by the procedure outlined by Karim and Holly (1986).
- Settling of non-cohesive sediments is assumed to be discrete, without interaction with other particles. The non-cohesive depositional sediment flux is estimated by the product of user specified settling velocity and the near-bed suspended sediment concentration.

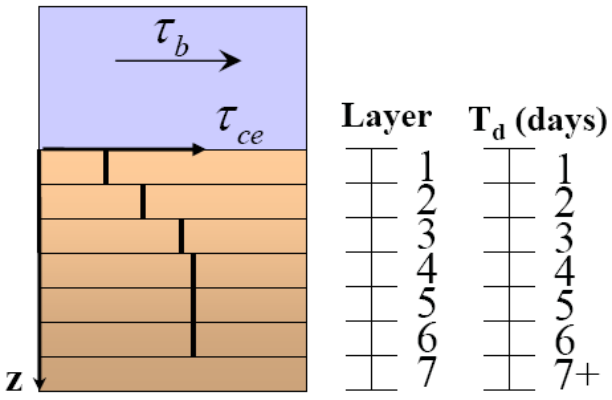

Figure 4.2 Schematic of Sediment Bed Model. (Hydroqual, Inc., 2002)

4.2.4 Pathogen Model

ECOMSED transports pathogens as a non-conservative tracer. The governing equation is shown below.

$$\frac{\partial CD}{\partial t}+\frac{\partial CUD}{\partial x}+\frac{\partial CVD}{\partial y}+\frac{\partial CW}{\partial \sigma}=\frac{\partial}{\partial \sigma}\left[\frac{K_H}{D}\frac{\partial C}{\partial \sigma}\right]+F_C+KC \qquad (21)$$

where C is the fecal coliform concentration; F_C includes the horizontal diffusivity or diffusion/source-sink terms as shown in Equations (12) and (13).

Following the transport, pathogen concentrations are decayed to determine their fate. Field data suggested that bacteria die-offs follow first-order kinetics. Laboratory data also indicated that the overall inactivation kinetic rate, K, is a function of salinity, temperature, light, turbidity, and sedimentation. The different components of the overall decay rate are calculated based on the equations given by Mancini (1978) as shown in Equation 22.

$$K = K_d + K_i + K_s \qquad (22)$$

$$K_d = \left(0.8+0.006\left(\frac{S}{S_{SEA}}\right)\right)(1.07)^{(T-20)} \qquad (22a)$$

$$K_i = \frac{\alpha I_o}{K_e Z}\left[1-e^{(-K_e Z)}\right] \qquad (22b)$$

$$K_s = \frac{V_s}{Z} \qquad (22c)$$

where K is overall decay rate of the pathogen; K_d is the decay rate for natural mortality, in dark which is a function of temperature, salinity and predation; K_i is the decay rate due to irradiance or light; K_s is the decay rate due to sedimentation; all the decay rates have day^{-1} units. S is the salinity in ppt at a given node in the modeling domain; S_{SEA} is the salinity of sea water (35 ppt);

T is the temperature in degrees Celsius at a given node in the modeling domain; K_e is the extinction coefficient and is measured in m^{-1} units; I_o is the average daily solar (surface) radiation in langleys/hr; Z is the depth at which decay is applied in m; α is proportionality constant and is generally equal to one; V_s is the net loss rate in m/day of the particulate bacterial forms. After determining the transport and fate of fecal coliform, a correction based on the field measurements of bed sediment fecal coliform counts is applied to account for the re-entrained bacteria in the water column due to resuspension.

4.2.5 Spatial and Temporal Schemes

ECOMSED formulation uses the finite control volume principle to discretize the model equations over a staggered or Arakawa C-grid. The model has three available advection discretization schemes: central difference, upwind, and the Multidimensional Positive Definite Advection Transport Algorithm (MPDATA) (Smolarkiewicz, 1984). MPDATA applies a recursive correction to the first-order truncation error after an initial upwind step by reapplying the upwind algorithm using an anti-diffusion velocity based on the local first-order truncation error. This allows in the minimizing of the numerical diffusion induced by the upwind scheme. Depending on the nature of the process to be simulated one can choose the most suitable method.

The model has a two time step solution scheme. The horizontal (external) free surface mode solves the depth-integrated three-dimensional transport equation using a small time step to compute water surface elevation and the depth-averaged velocities. The internal mode solves the three-dimensional transport equations using a much larger time step of the order of 40 times the external time step computing and updating U, V, W, T, S, the turbulence quantities and other

transport variables such as sediment and tracers concentrations. It is a three time level model and time stepping is accomplished by the leap frog scheme. A weak filter removes the time splitting fluctuations, where the solution is smoothed at each time step according to:

$$F_s^n = F^n + \frac{\alpha}{2}\left(F^{n+1} - 2F^n + F_s^{n-1}\right) \tag{23}$$

where F_s is the smoothed solution and α is a constant with a typical value of 0.05.

Momentum is always advected by central difference in the ECOMSED assuring second order accuracy. The conservation of energy, salinity, and mass is second order accurate in time and space except while the uncorrected upwinding is used which yields a first-order accurate solution in ECOMSED.

4.2.6 Stability Constraints

Finally, the computational stability condition for the vertically integrated, external mode and transport equations is the Courant-Friedrichs-Levy (CFL) condition, which limits the time step according to:

$$\Delta t_E \le \frac{1}{C_t}\left(\frac{1}{\Delta x^2} + \frac{1}{\Delta y^2}\right)^{-1/2} \tag{24}$$

where $C_t = 2(gH)^{1/2} + \overline{U}_{\max}$; $U_{\max}$ is the expected maximum average velocity.

For the internal mode the criteria is analogous to that of the external mode and is:

$$\Delta t_I \le \frac{1}{C_T}\left(\frac{1}{\Delta x^2} + \frac{1}{\Delta y^2}\right)^{-1/2} \tag{25}$$

where $C_T = 2C + U_{max}$; C is the maximum internal gravity wave speed and is of the order of 2 m/s and U_{max} is the maximum advective speed.

Another constraint based on diffusion needs to be considered for the internal time step when the grid Reynolds number is of the order 1 and is

$$\Delta t_I < \frac{1}{4A_H}\left(\frac{1}{\Delta x^2} + \frac{1}{\Delta y^2}\right)^{-1} \tag{26}$$

4.3 Description of the Sediment and Pathogen Indicator Model for Lake Pontchartrain

To accurately simulate the fate and transport of pathogen indicators near the shoreline of Lake Pontchartrain a Near-field model cannot resolve the large scale circulation due to wind and tide. On the other hand, the Lake-wide model cannot resolve the geometry around the rivers and outfall canals. Thus the current situation necessitates the use of a nested modeling system. A high resolution Near-field model to simulate local hydrodynamics, sediment transport, nutrient loading, and fecal coliform loading is required to be nested with a low resolution Lake-wide model driven by tides and wind that can simulate waves.

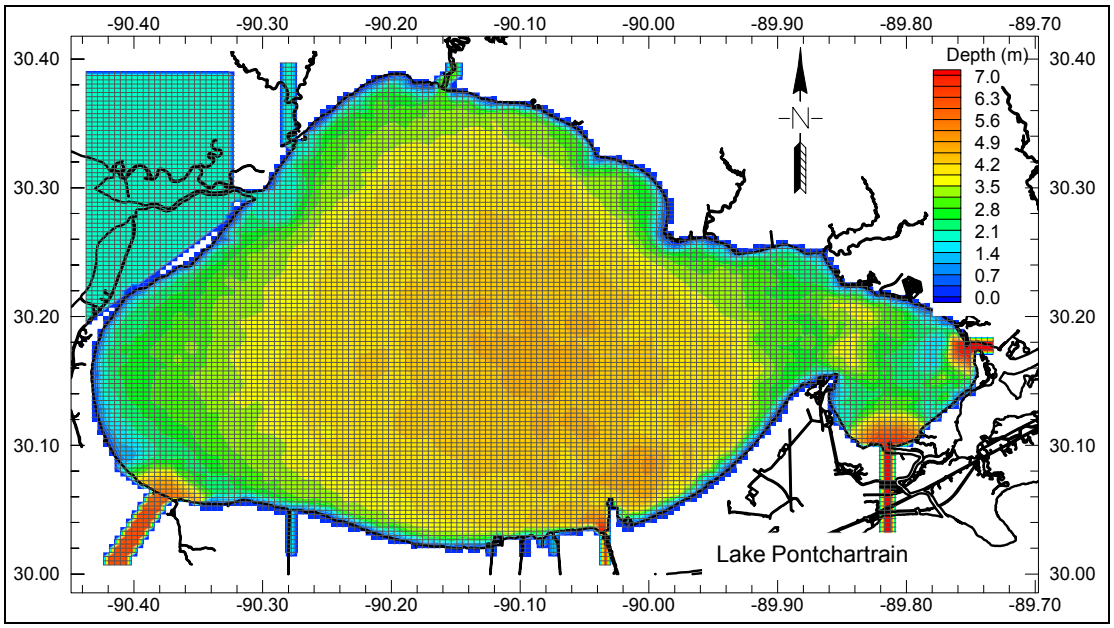

Figure 4.3 Computational grid for the Lake-wide model

4.3.1 Computational Grid Design

A Cartesian grid with a horizontal resolution of approximately 400 m (Figure 4.3), and 7 equally spaced vertical layers was used for the Lake-wide model. The Near-field grid has approximately 100 m resolution in the horizontal direction and 7 equally spaced vertical layers (Figure 4.4).

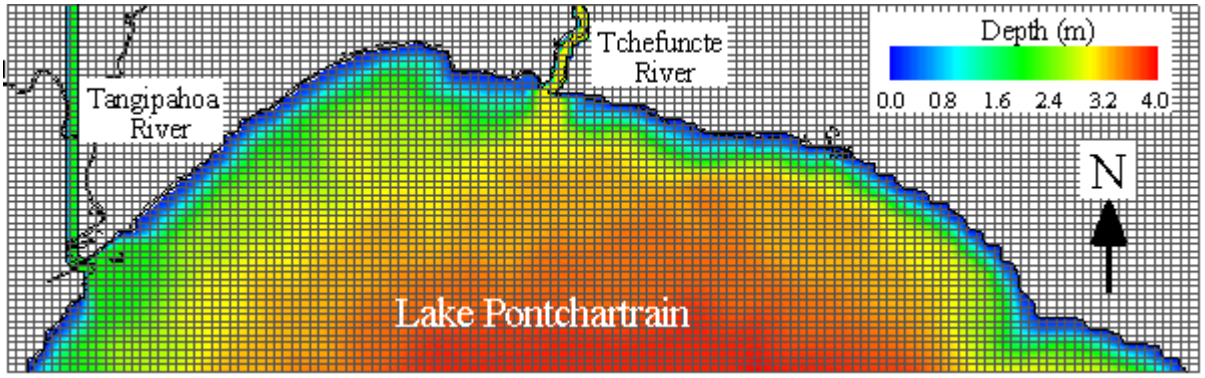

Figure 4.4 Computational grid for the north shore Near-field model (each cell represents 4 cells)

4.3.2 Modeling Methodology

The wind and tide induced hydrodynamics and circulation were simulated using the Lake-wide model. Moreover, the wind generated surface waves were simulated in the Lake-wide model since the fetch would be misrepresented in the Near-field model. Salinity, temperature, water surface elevation, depth-averaged velocities along the Near-field boundary and the wave field for the entire Near-field model domain were stored at every hour during the Lake-wide simulation. The stored data were then interpolated onto the Near-field grid.

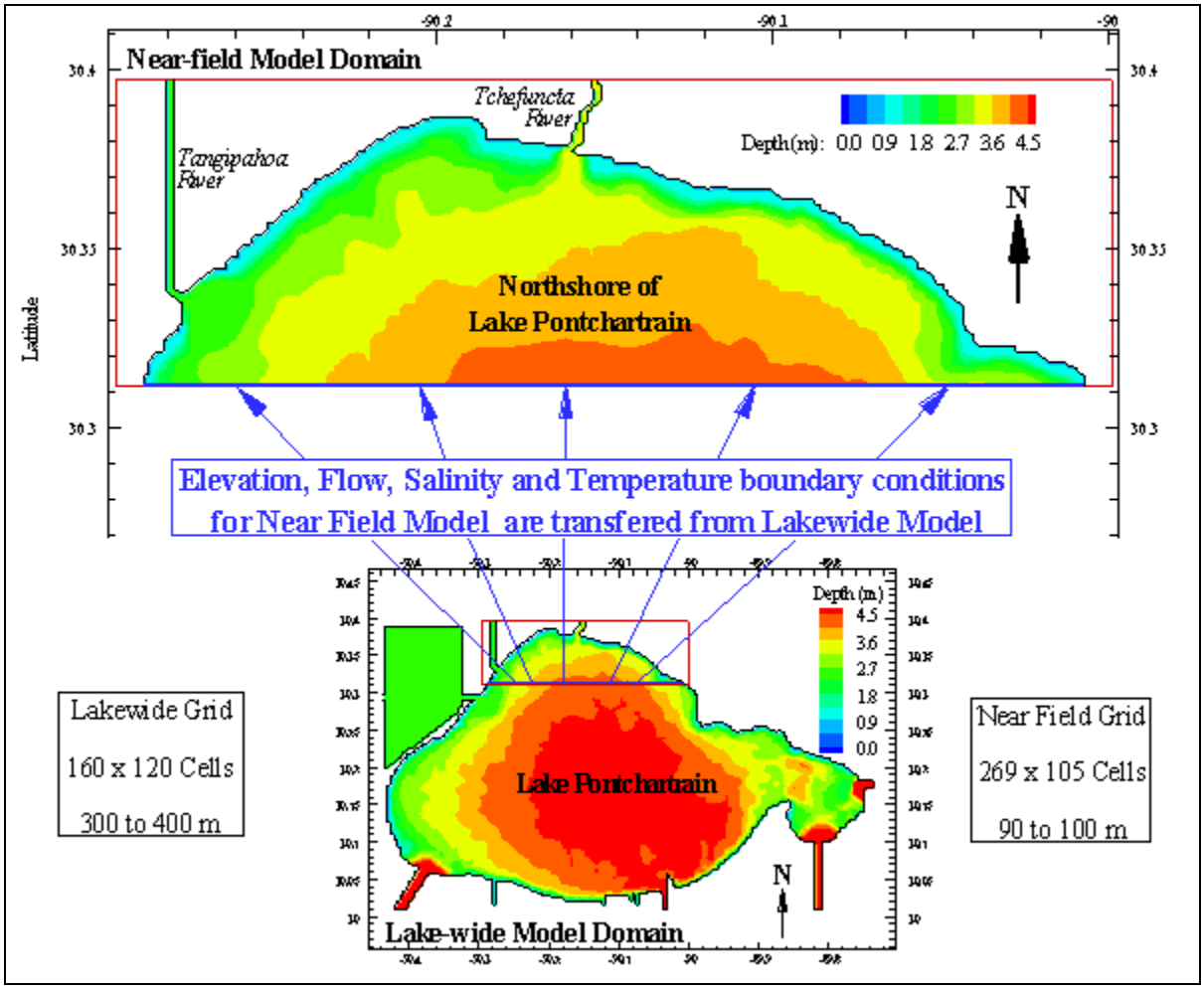

Figure 4.5 Modeling Methodology

ECOMSED was modified to accept hourly forcing of depth-averaged velocities, water surface elevations, salinity and temperatures along the southern open boundary for the north shore Near-field model. The Near-field model was driven with wind, waves, flows and time-dependent fecal coliform levels for the rivers in the north shore. In addition, hourly water surface elevations, depth-averaged velocities, salinity and temperatures extracted from the Lake-wide model and interpolated onto the southern open boundary of the north shore domain, were forced. Figure 4.5 shows the described modeling methodology.

4.3.3 Model Inputs

4.3.3.1 Initial Conditions

The Lake-wide model was initiated with background salinity and temperature values. The salinity values were interpolated over the model domain between the values observed at the LUMCON gage and the Rigolets gage. Water temperatures obtained from the Midlake gage were forced throughout the lake. The locations of these gages are shown in the Figure 3.1. The water surface elevation and currents were set to zero. The entire model forcing functions were ramped from zero to their full values in one day. The Near-field model was started with the initial conditions interpolated from the Lake-wide model onto the Near-field grid.

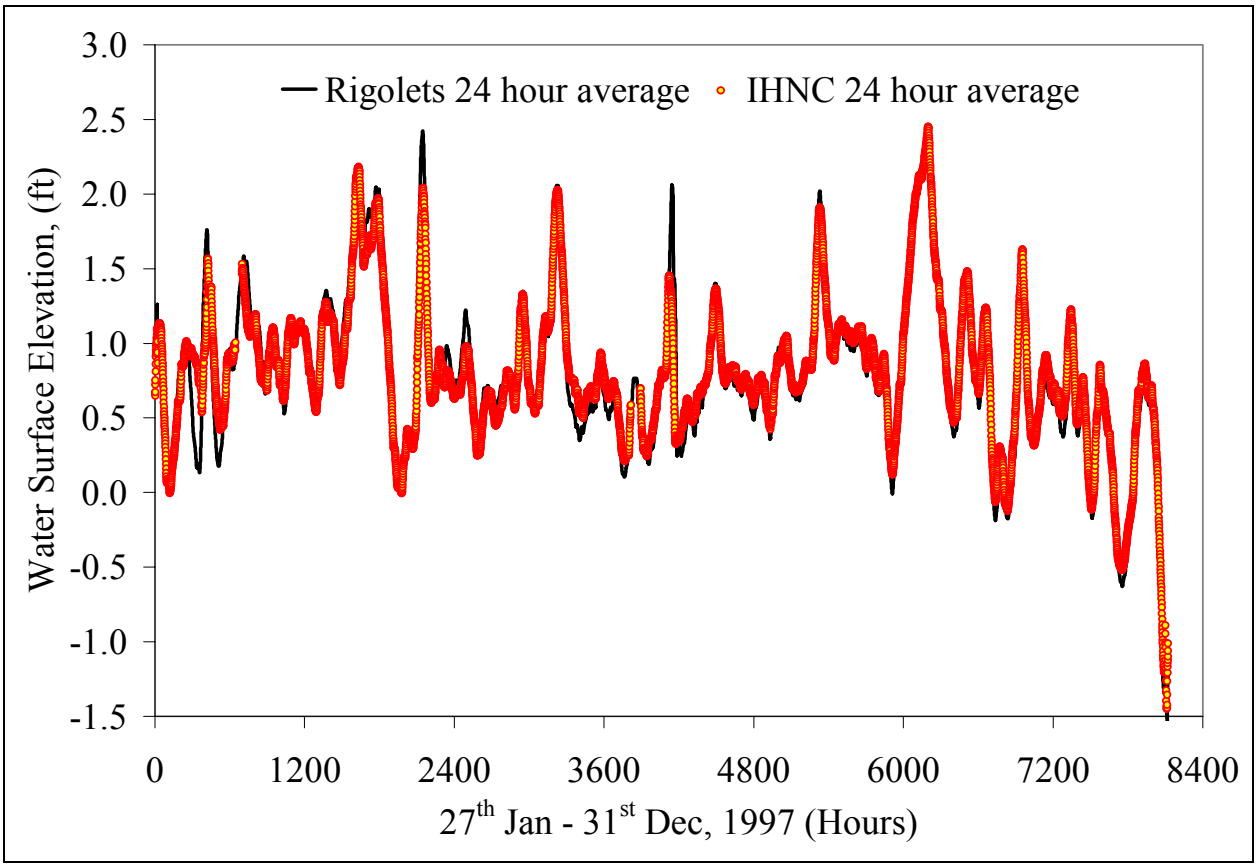

Figure 4.6 Comparison of water surface elevations observed at the Rigolets gage and the Seabrook gage for January 27th to December 31st, 1997 period

4.3.3.2 Boundary Conditions

The surface boundary conditions for the Lake-wide model were prescribed using the hourly wind speed, wind direction, heat flux, precipitation, and evaporation data obtained from the LUMCON gage or the National Weather Service (NWS) Midlake gage. Water surface elevations, salinity and temperatures obtained from the USGS Rigolets gage were used to force the tide at Rigolets, Chef Menteur Pass, and IHNC tidal open boundaries. A comparison of the 24-hour average of the tide observed at the Rigolets gage and the Seabrook gage for the year 1997 is shown in the Figure 4.6. A statistical analysis performed on the water surface elevation data from the USGS gage at the Rigolets and the gage at Seabrook Bridge on the IHNC for the

year 1997 showed that the tide was similar at both the locations. However, due to the lack of measured elevation data at the Chef Menteur Pass, the Rigolets data were used. The inflow open boundaries data were prescribed using the discharge, salinity and temperature data obtained from the USGS gages near Covington, Robert, and Denham Springs for Tchefuncte, Tangipahoa, and Amite rivers respectively. The locations of these gages are shown in the Figure 3.1.The Tchefuncte flow obtained from the Covington was transformed into the flow at the mouth of the Tchefuncte River based on a correlation developed by performing water shed analysis as described in Leal (2004). Figure 4.7 shows the time series of the river flows and water surface elevations used in the Lake-wide model for the calibration simulation.

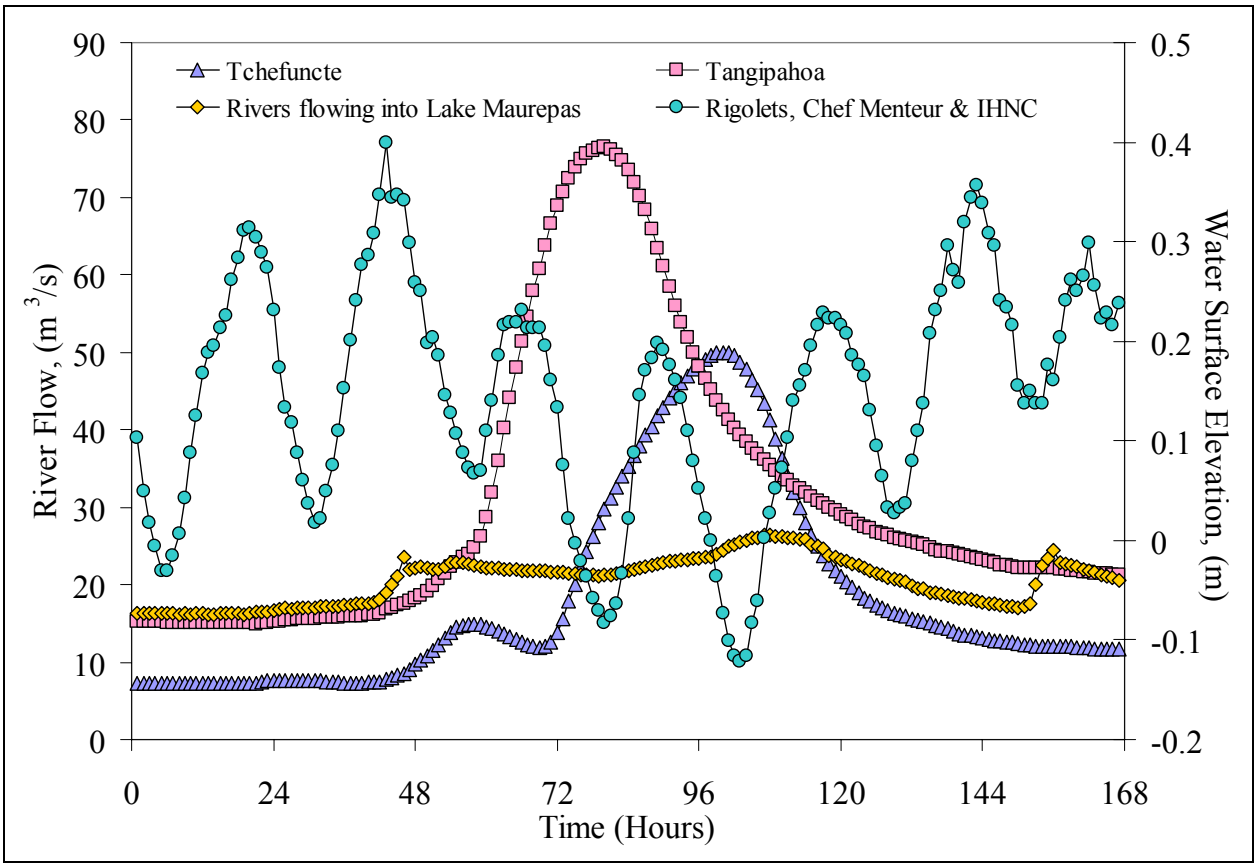

Figure 4.7 Flow and tidal boundary conditions for the Lake-wide model for the calibration simulation (April 24th – 30th, 2004) (Data source: USGS)

The meteorological data and the rivers inflow data used in the Lake-wide model were applied as the surface and inflow boundary conditions for the Near-field model as well (Figure 4.8). The interpolated hourly water surface elevations, depth-averaged velocities, salinity and temperature from the Lake-wide model were forced along the southern open boundary in the Near-field model. In addition, the surface wind waves' data interpolated from the Lake-wide model was forced hourly into the Near-field model to use it in the sediment transport computations. The sediment characteristics of Lake Pontchartrain, including resuspension and deposition have been documented by Haralampides (2000) and USGS (2001). Data from these authors were used to initialize and describe the settling and depositional properties of the Lake sediments. The coefficients required for the sediment model were derived from the shaker tests performed on the Lake sediments by these authors and are shown in Table 4.1.

Table 4.1 Values used in the sediment transport model for various model parameters

Critical bed shear stress (dynes/cm^2)	Coefficient a_0 in Equation 20	Coefficient n in Equation 20	Exponent m in Equation 20
1.0	2.05	0.4228	0.5

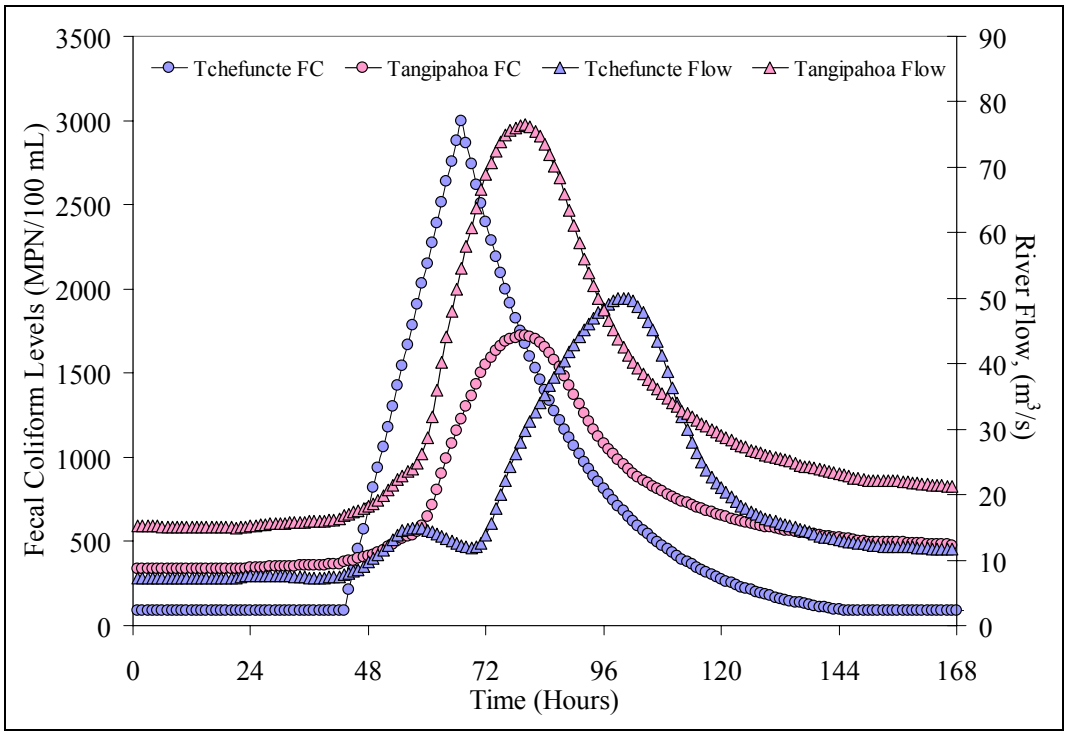

Figure 4.8 Flow and fecal coliform loadings used in the north shore Near-field model for the calibration simulation (April 24th – 30th, 2004)

5. MODEL CALIBRATION, TESTING and SENSITIVITY ANALYSIS

5.1 Lake-wide Model Calibration

5.1.1 Hydrodynamics

5.1.1.1 Inter-model Comparison

The hydrodynamics simulated by the Lake-wide model (Figure 5.1) were compared to the results obtained from models by other researchers such as Georgiou (2002) (Figure 5.2), Haralampides (2000) (Figure 5.3), and Signell and List (1997) (Figure 5.4). The circulation patterns, water surface elevations and currents predicted by ECOMSED were in good agreement with these models under the same external forcing.

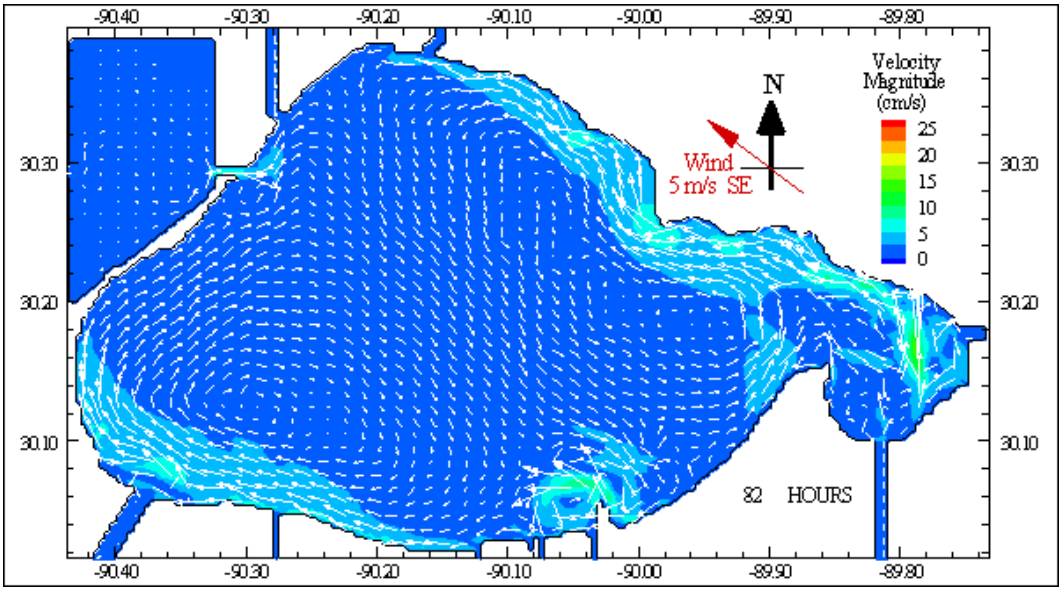

Figure 5.1 Depth-averaged circulation for a southeasterly wind at 5 m s^{-1} predicted by the Lake-wide model

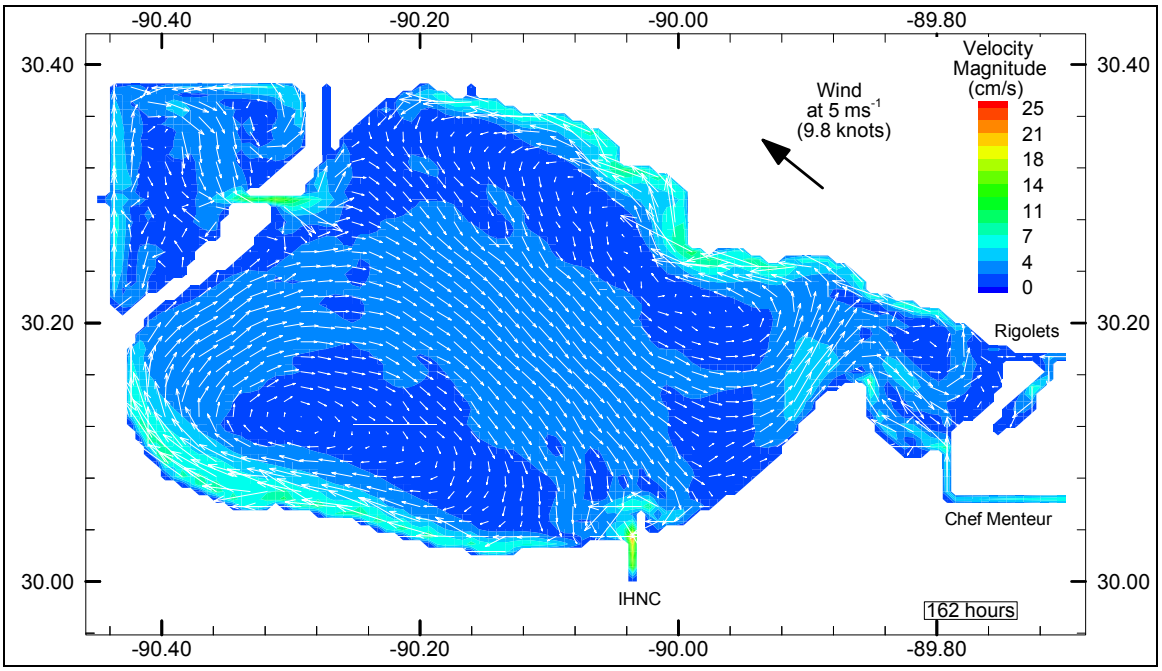

Figure 5.2 Depth-averaged circulation in Lake Pontchartrain due to southeasterly wind at 5 m s^{-1} using POM (Georgiou, 2002)

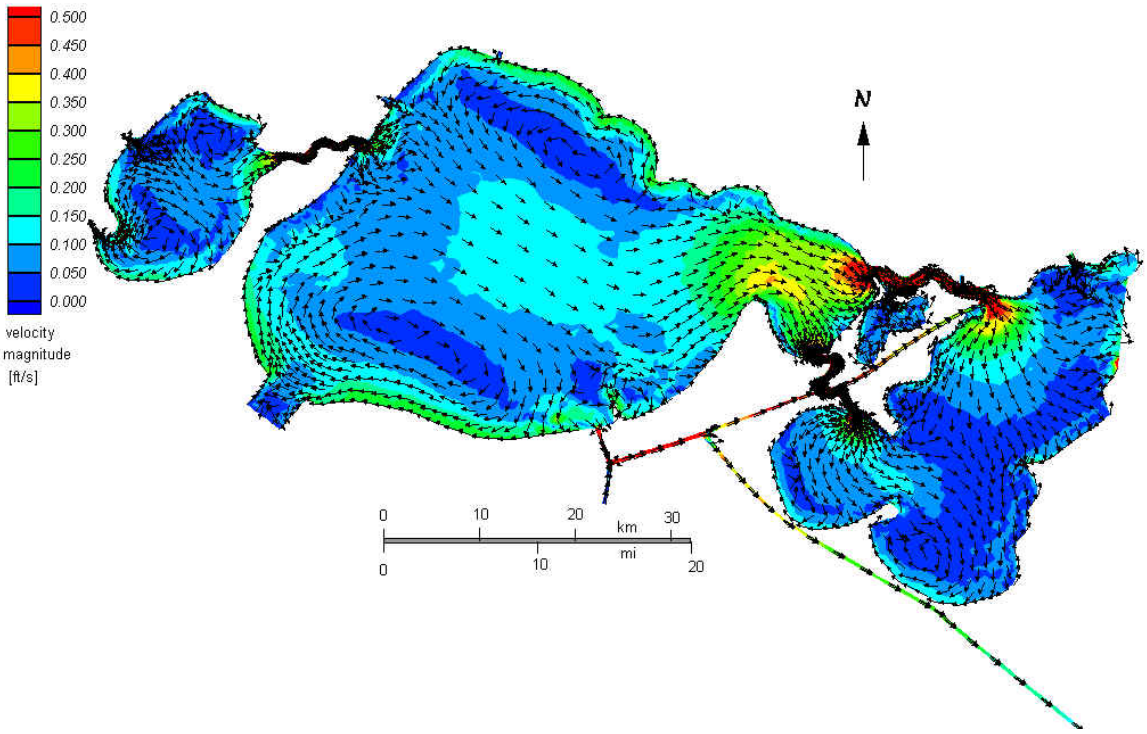

Figure 5.3 Depth-averaged circulation in Lake Pontchartrain due to southeasterly wind at 6 m s^{-1} using RMA2 (Haralampides, 2000)

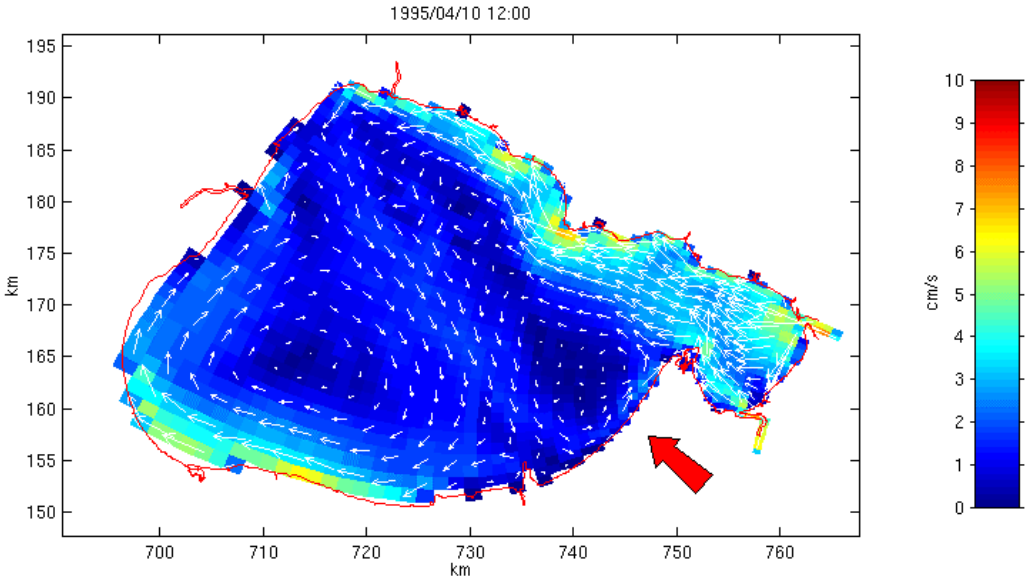

Figure 5.4 Simulated depth-averaged circulation in Lake Pontchartrain due to a southeasterly wind of 5 m s^{-1} using ECOM-si (Signell and List, 1996)

5.1.1.2 Water Surface Elevation Calibration

The free surface water level component of the model was calibrated with observed data from the five USGS monitoring stations (East Lake, Mandeville, Mid-Lake, Westend and West Lake) located as shown in Figure 3.1. Figure 5.5 shows a comparison of the predicted and measured lake water levels at the Westend station for a period that included wind and barometric effects from the Gulf of Mexico as well as normal tidal conditions. The performance of the model in comparison with the stage data at the Mandeville gage is shown in the Figure 5.6.

The simulated water levels match very well with the measured stages in both the cases. The same is shown in the scatter plots between observed and modeled elevation data in Figures 5.7 and 5.8. Table 5.1 gives the root mean square (RMS) values of the modeled and measured water surface elevations and their corresponding root mean square errors (RMSE) at various

locations in the model domain. The RMS values for simulated and measured water levels were very close; the difference was less than 0.02 ft.

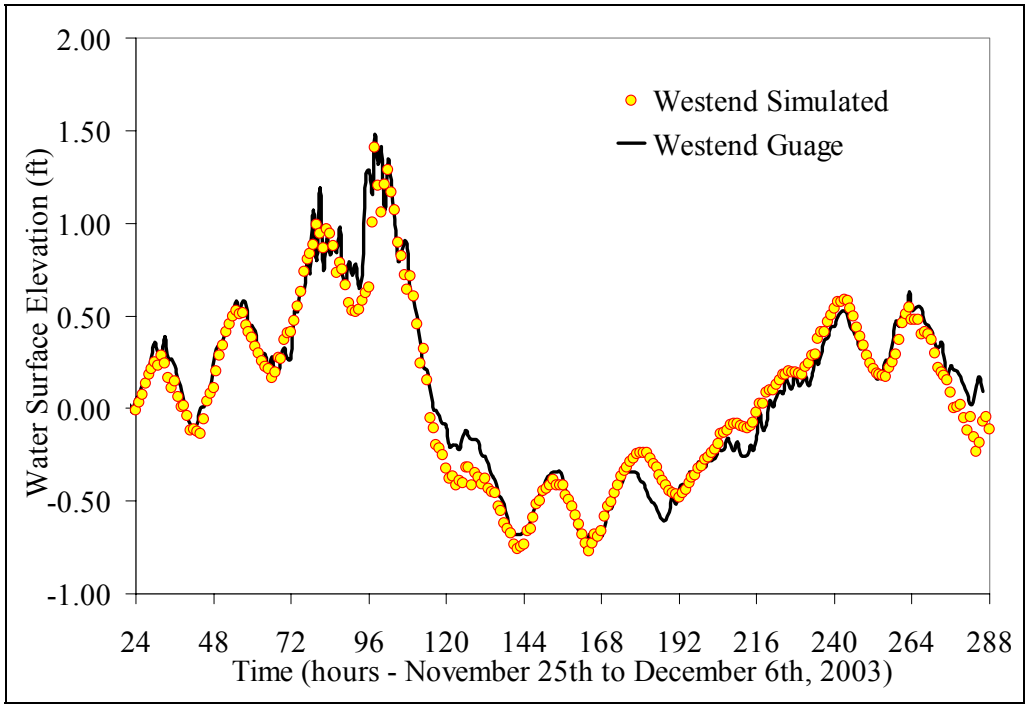

Figure 5.5 Water surface elevation calibration at the Westend gage

Table 5.1 RMS and RMSE values of simulated and measured water surface elevations

Site	RMS Water Level, ft		RMS Error in Measured Vs Modeled Water Levels, ft
	Measured	Modeled	
Mandeville	0.46	0.44	0.17
Westend	0.50	0.49	0.13
LUMCON	0.46	0.44	0.14
Midlake	0.45	0.44	0.12
Pass Manchac	0.44	0.44	0.13

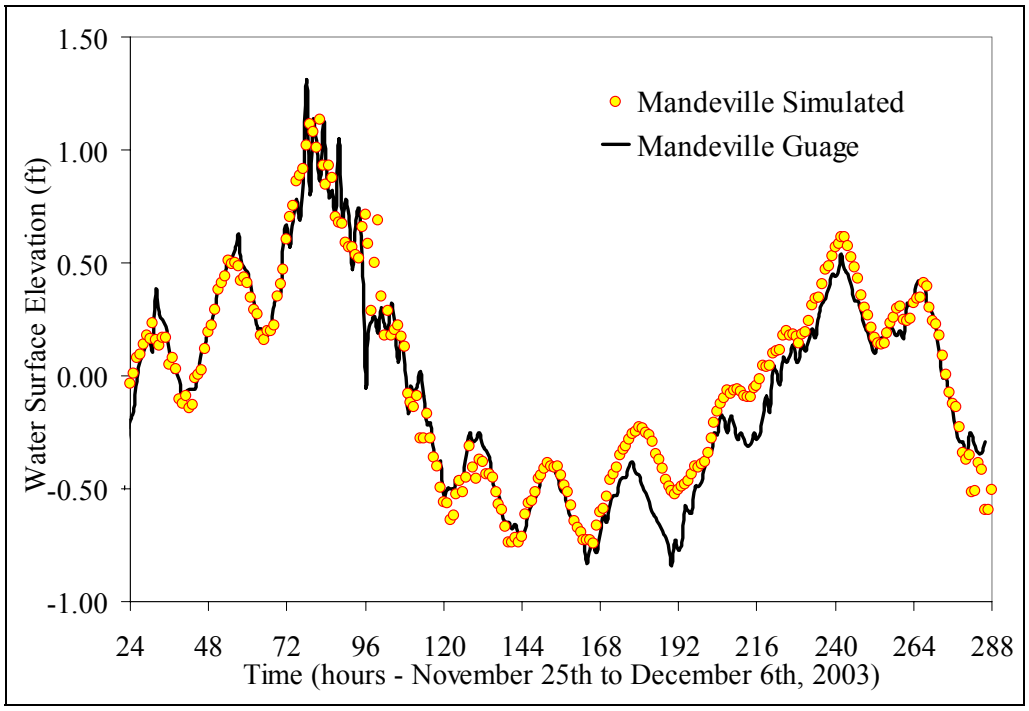

Figure 5.6 Water surface elevation calibration at the Mandeville gage

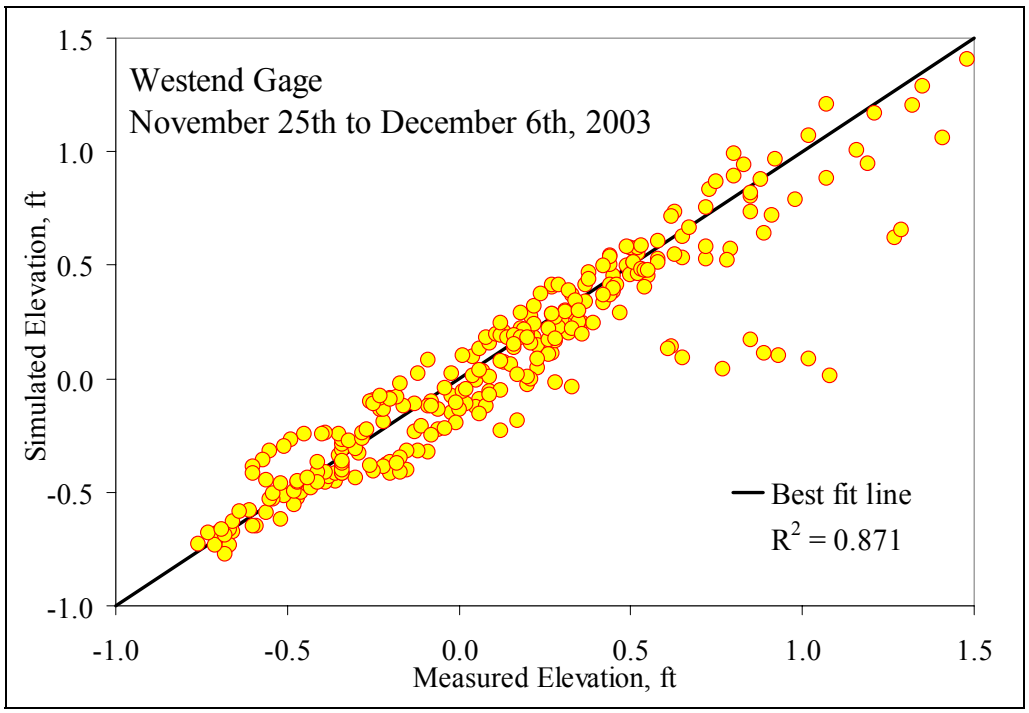

Figure 5.7 Comparison of measured and modeled water surface elevations at the Westend gage

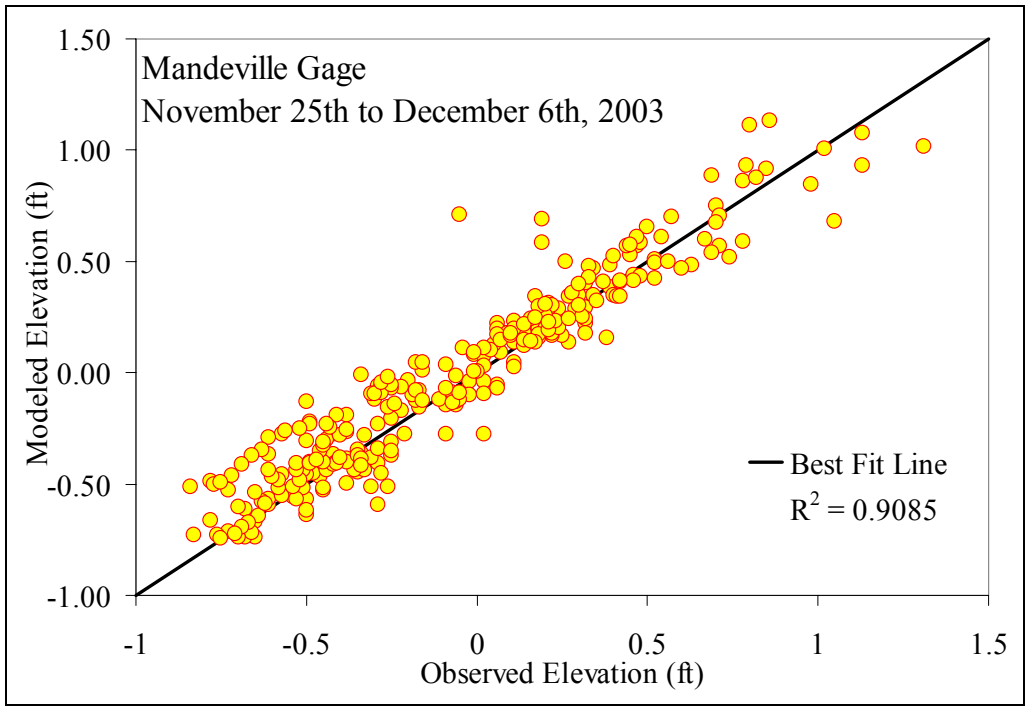

Figure 5.8 Comparison of measured and modeled water surface elevations at the Mandeville gage

5.1.1.3 Depth-averaged Currents Calibration

Model computed depth-averaged currents were compared with the velocity values measured by USGS in Lake Pontchartrain 1998 (USGS, 2001) at Mid Lake and South Lake sites. Figures 5.9 and 5.10 show the comparison of measured and simulated depth-averaged 'U' and 'V' velocity components for the south shore location respectively. The model captured the overall trend of variations in the currents fairly well. Table 5.2 gives the RMS values of the modeled and measured depth-averaged velocities at both locations and corresponding RMSE values at the South Lake and the Mid Lake sites (Locations A and D in the Figure 5.29). Again, it can be observed that the difference between RMS values of the measured and modeled velocities were less than ~7 mm/s. The root mean square error accentuates the phase difference between two signals, if there is any. Small phase differences between the modeled and measured

velocities were inherent as the wind field imposed in the model was assumed to be spatially constant and was interpolated temporally. Figures 5.11 and 5.12 show the scatter in the observed and the modeled data for the two velocity components.

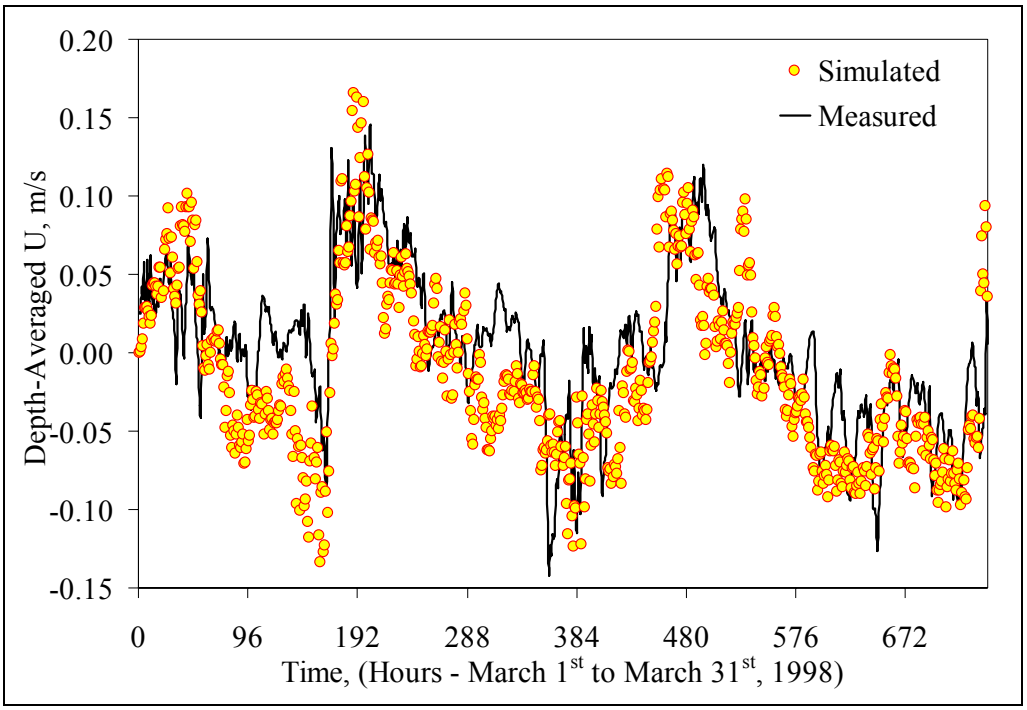

Figure 5.9 Calibration of U-component of the depth-averaged velocity at the south lake site for the period of March 1st to March 31st, 1998 (Source: USGS, 2001)

Table 5.2 RMS and RMSE values of simulated and measured depth-average velocities

Site	RMS depth-averaged velocity, m/s				RMS Error, m/s	
	U		V		U	V
	Measured	Modeled	Measured	Modeled		
South lake	0.05	0.058	0.025	0.019	0.045	0.0195
Mid lake	0.025	0.028	0.028	0.024	0.037	0.027

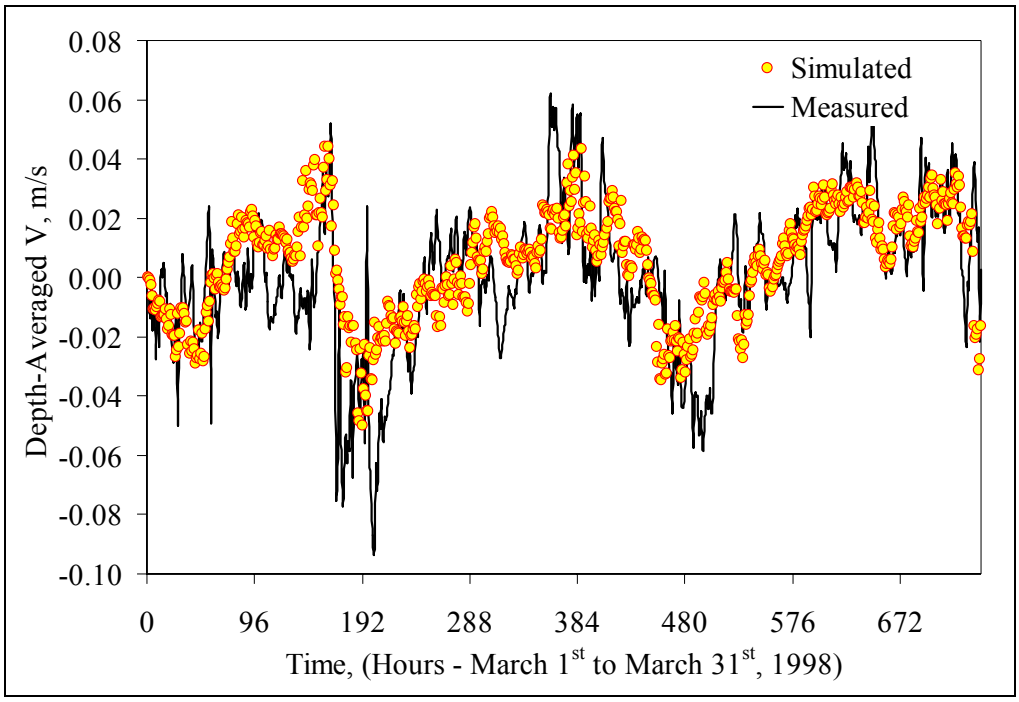

Figure 5.10 Calibration of V-component of the depth-averaged velocity at the south lake site for the period of March 1st to March 31st, 1998 (Source: USGS, 2001)

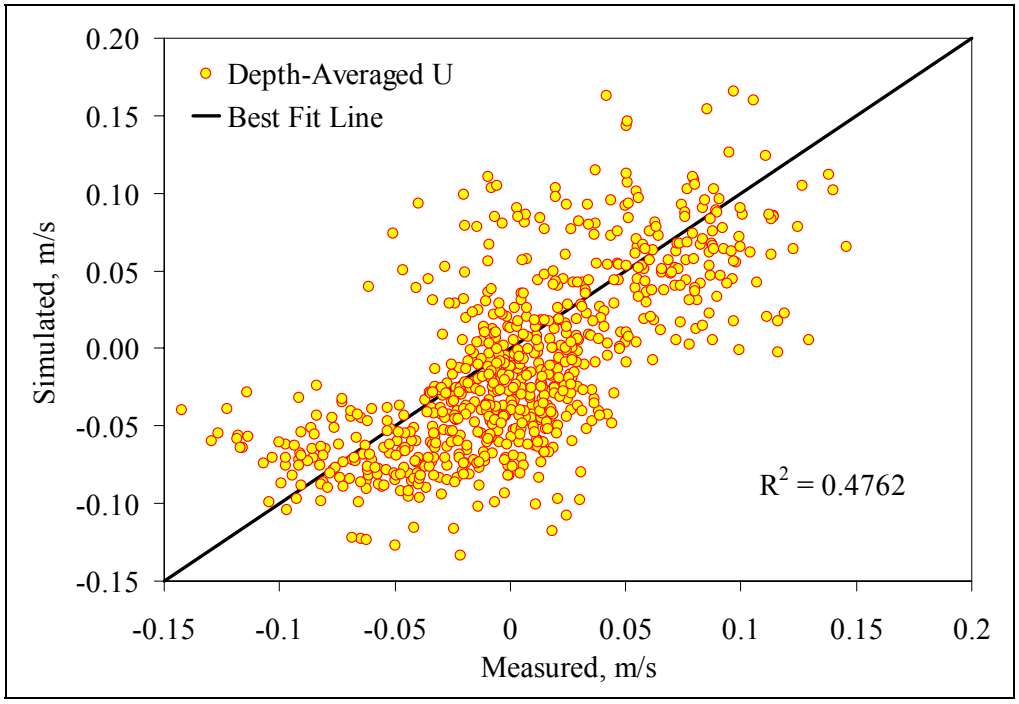

Figure 5.11 Comparison of measured and modeled U-component of the depth-averaged velocity at South Lake site (Source: USGS, 2001)

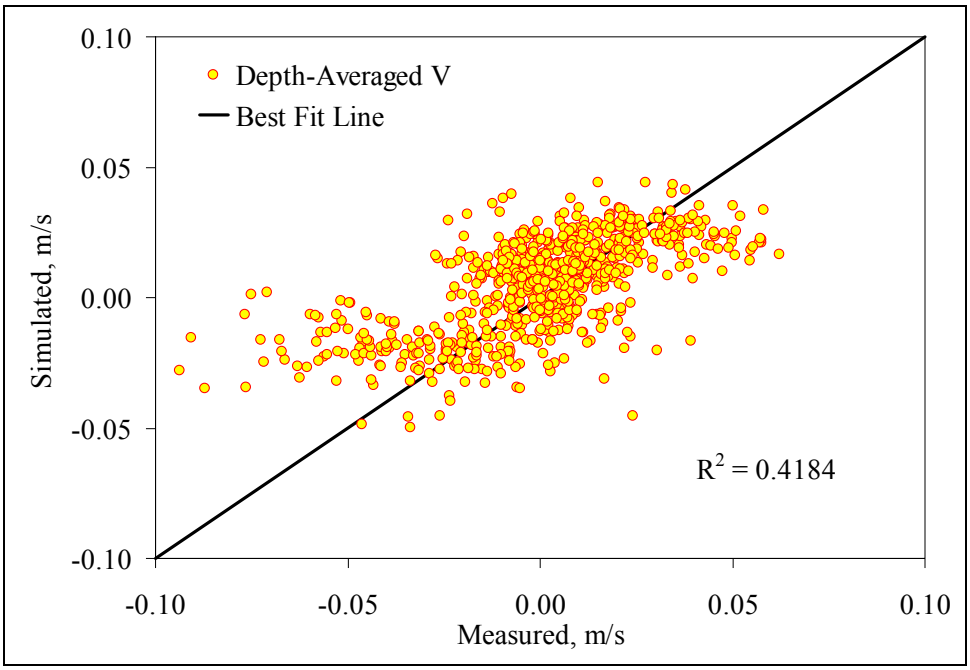

Figure 5.12 Comparison of measured and modeled V-component of the depth-averaged velocity at South Lake site (Source: USGS, 2001)

5.1.2 Transport Calibration

The transport component of the model was calibrated using the 1997 Bonnet Carré Spillway Opening dataset. The 1997 spillway opening was simulated by transporting a tracer representing the turbidity. Actual flow, tide, and wind forcing data corresponding to the simulation period were used. The turbidity plume simulated by the model was compared to the satellite reflectance images obtained from NOAA Advanced Very High Resolution Radiometer (AVHRR) data (Stumpf, 2001) and water surface temperature images obtained from the Southern Regional Climate Center at LSU. Figures 5.13 to 5.26 present the comparison of the satellite reflectance images of the Mississippi River plume and the model predicted turbidity plume over a period of 20 days beginning on March 21st to April 9th, 1997.

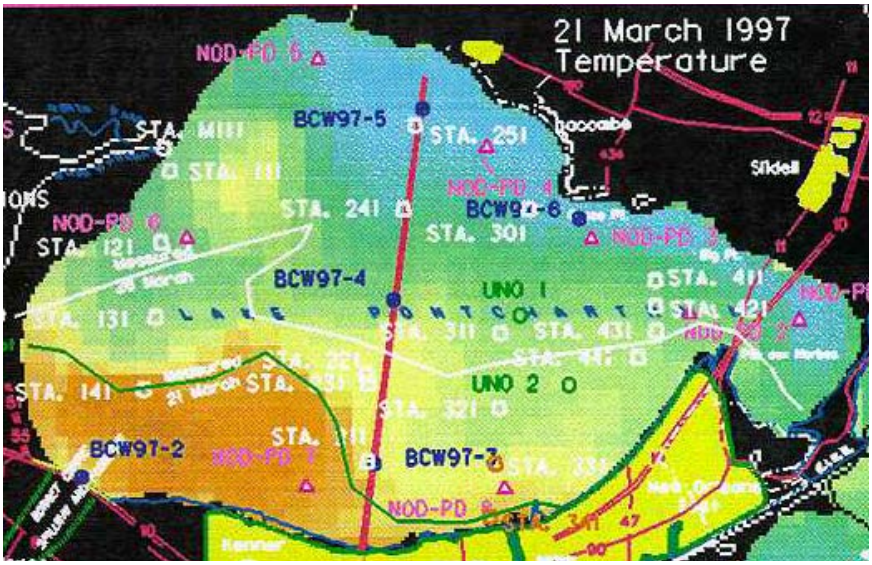

Figure 5.13 Surface water temperature image of Mississippi River plume during the 1997 Bonnet Carré Spillway opening on March 21st, 1997.

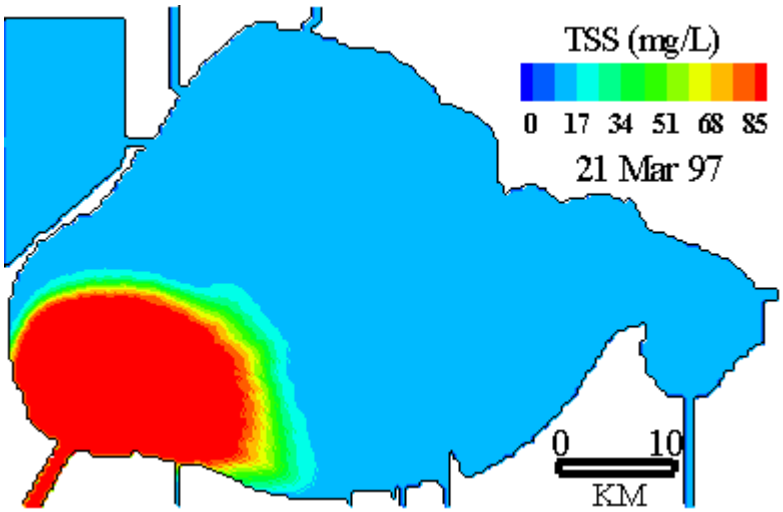

Figure 5.14 Model predicted Mississippi River turbidity plume for the period shown in the Figure 5.13

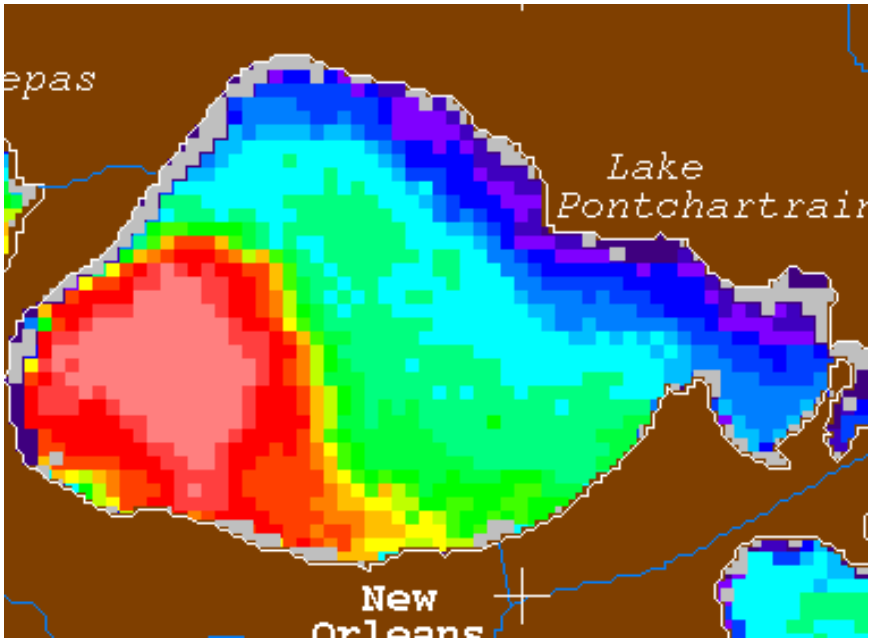

Figure 5.15 Satellite reflectance image of Mississippi River plume during the 1997 Bonnet Carré spillway opening on March 23rd, 1997.

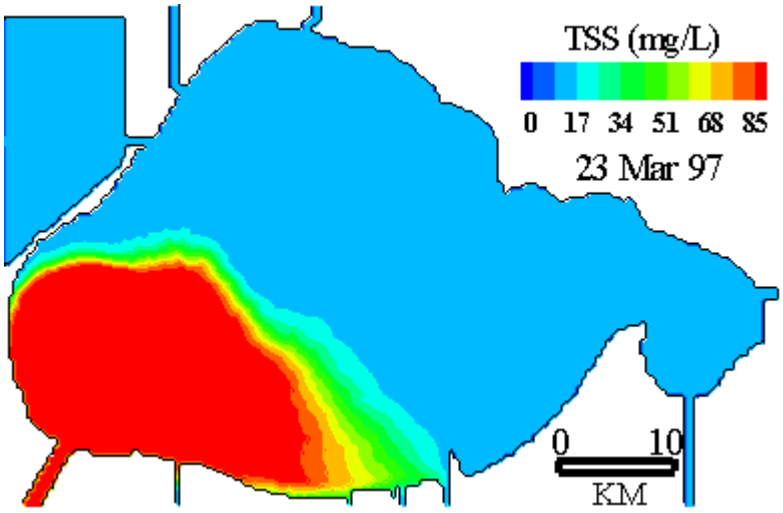

Figure 5.16 Model predicted Mississippi River turbidity plume for the period shown in the Figure 5.15

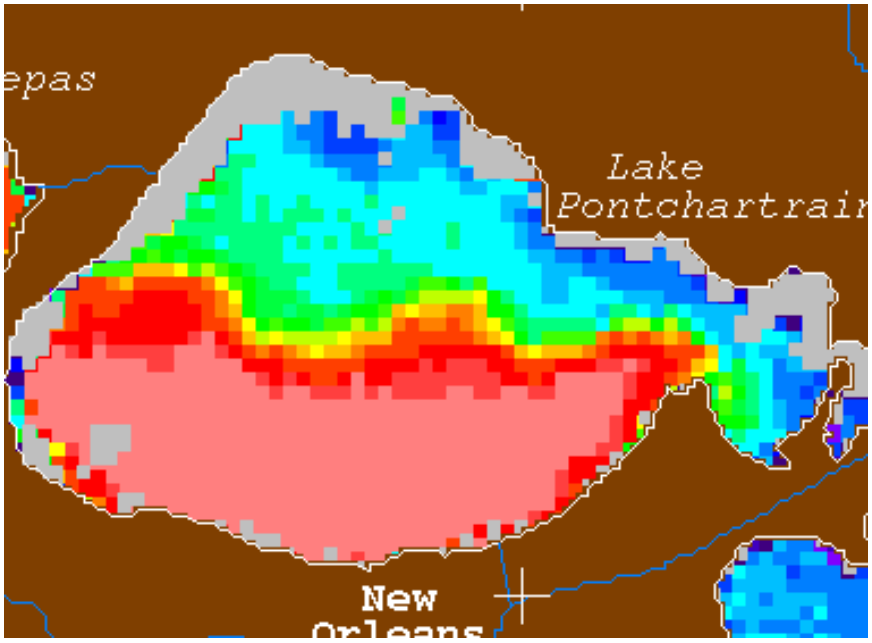

Figure 5.17 Satellite reflectance image of Mississippi River plume during the 1997 Bonnet Carré spillway opening on March 26th, 1997.

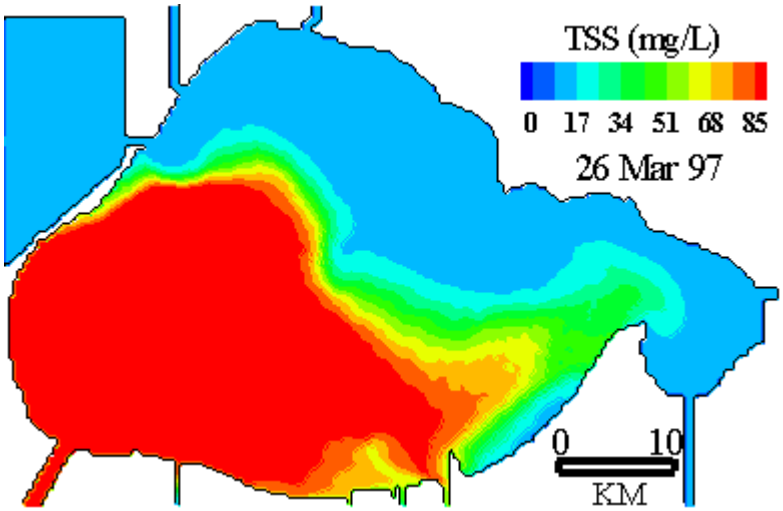

Figure 5.18 Model predicted Mississippi River turbidity plume for the period shown in the Figure 5.17

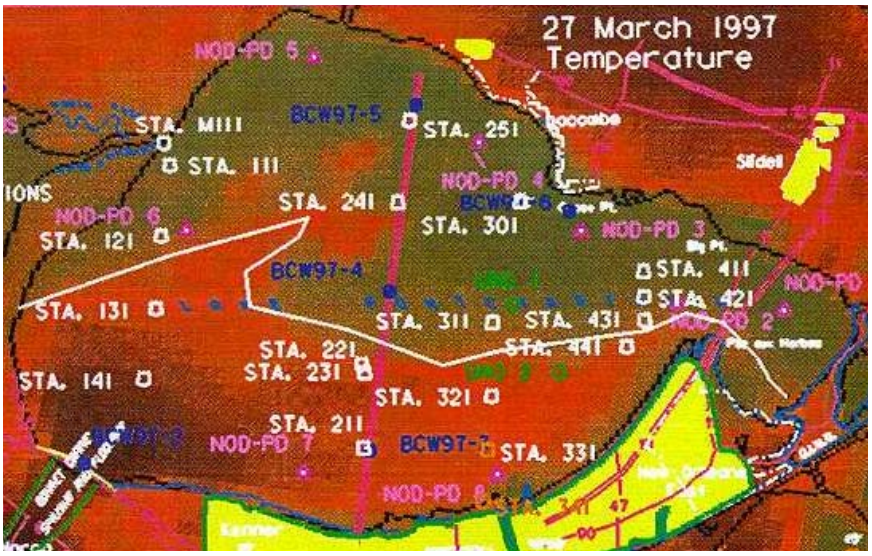

Figure 5.19 Surface water temperature image of Mississippi River plume during the 1997 Bonnet Carré spillway opening on March 27th, 1997.

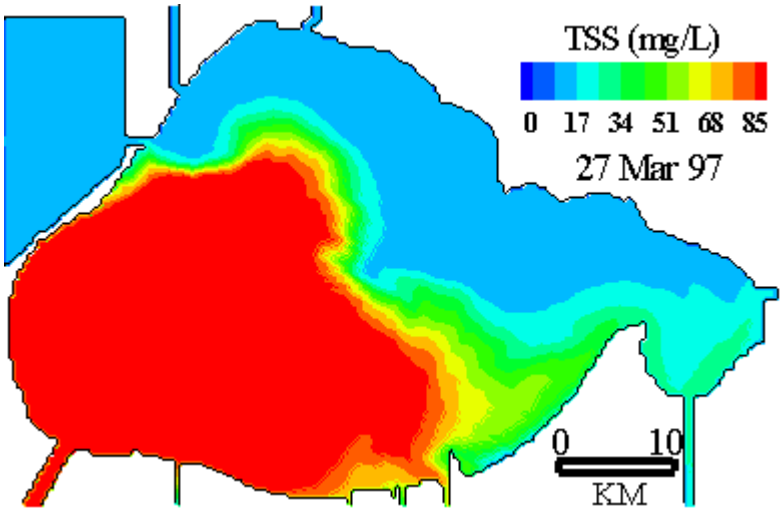

Figure 5.20 Model predicted Mississippi River turbidity plume for the period shown in the Figure 5.19

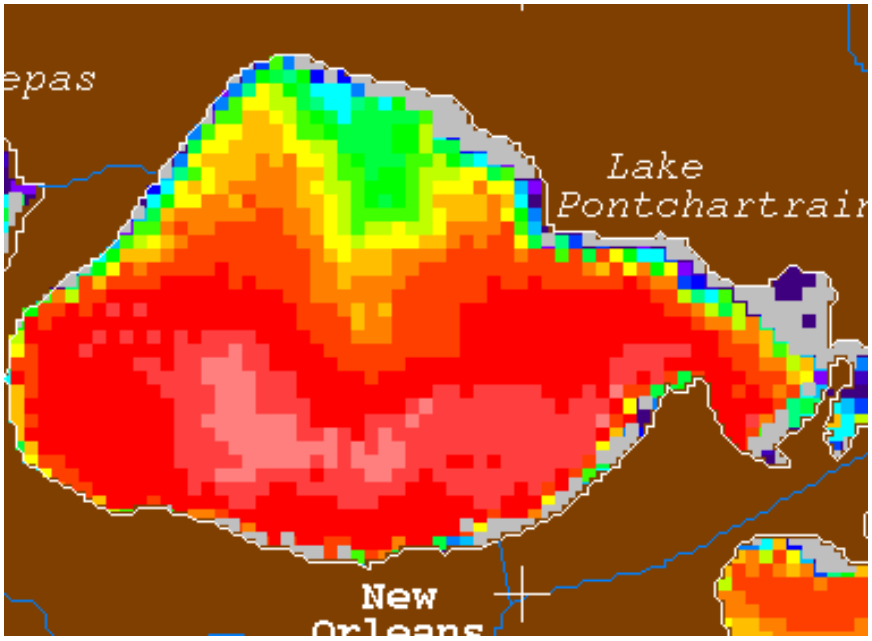

Figure 5.21 Satellite reflectance image of Mississippi River plume during the 1997 Bonnet Carré spillway opening on April 6th, 1997.

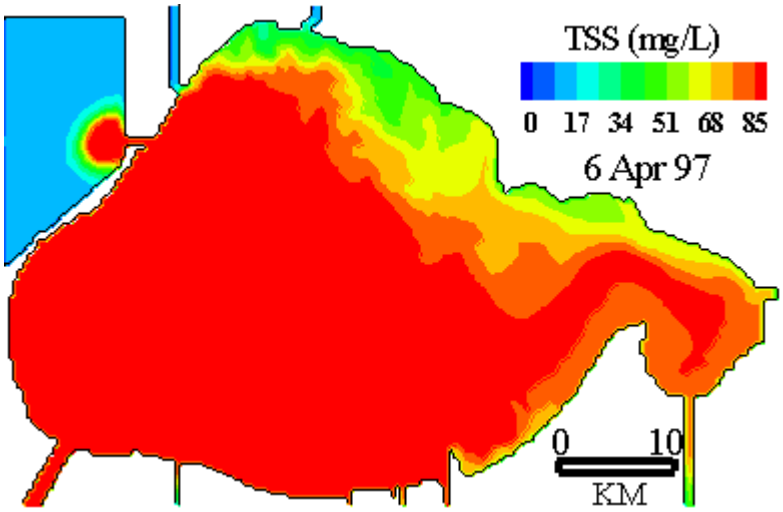

Figure 5.22 Model predicted Mississippi River turbidity plume for the period shown in the Figure 5.21

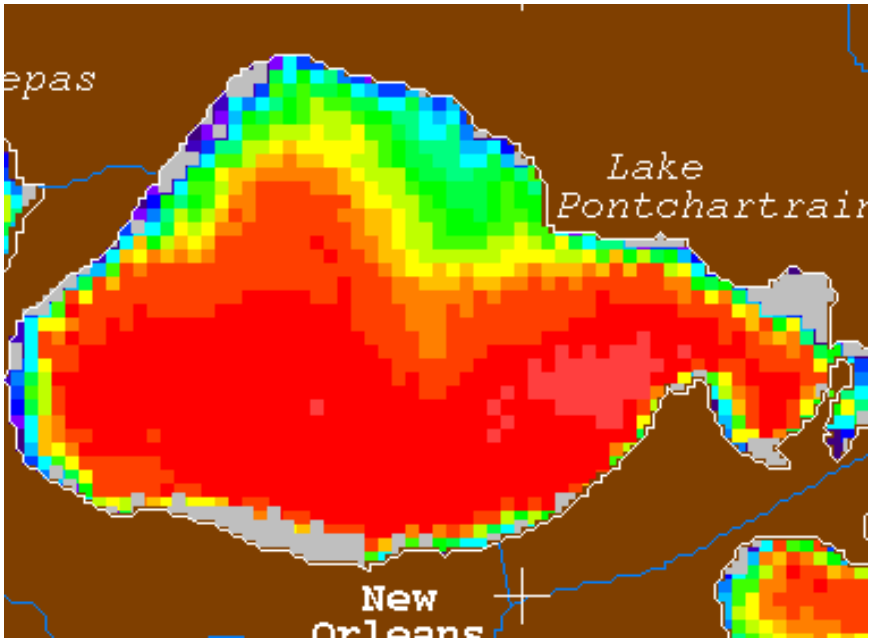

Figure 5.23 Satellite reflectance image of Mississippi River plume during the 1997 Bonnet Carré spillway opening on April 7th, 1997.

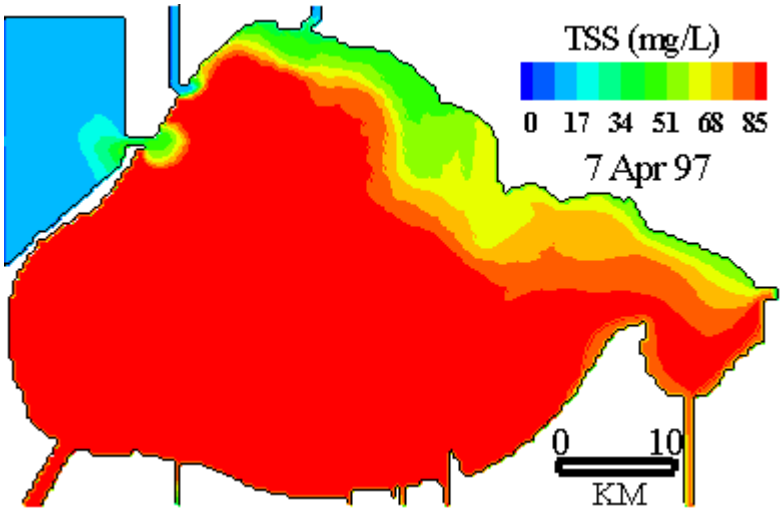

Figure 5.24 Model predicted Mississippi River turbidity plume for the same period shown in the Figure 5.23

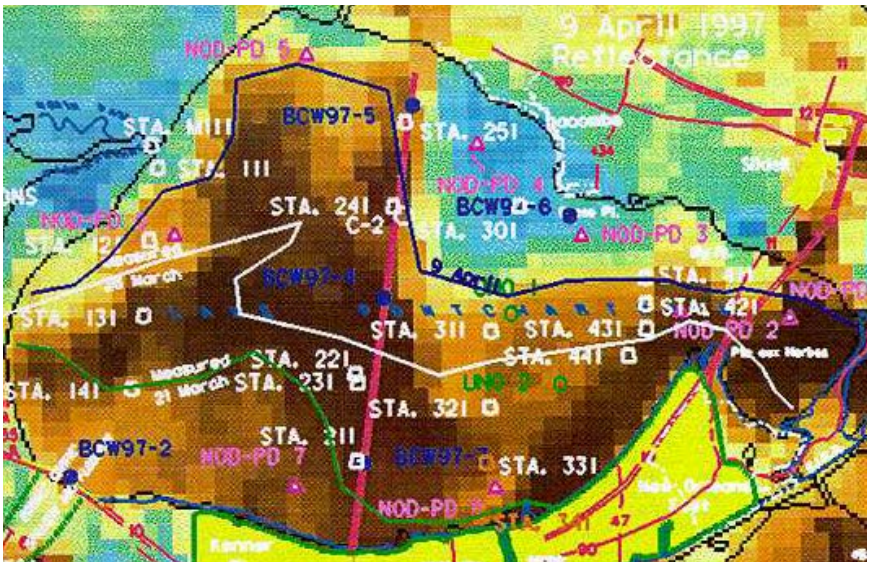

Figure 5.25 Surface water temperature image of Mississippi River plume during the 1997 Bonnet Carré spillway opening on April 9th, 1997.

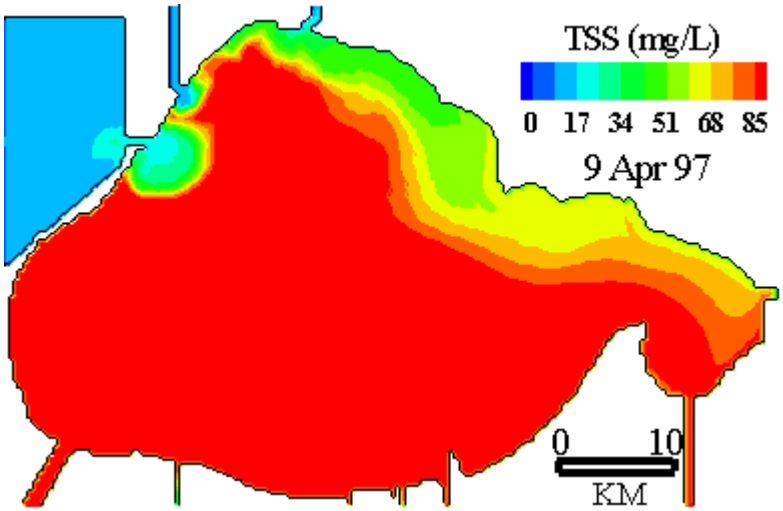

Figure 5.26 Model predicted Mississippi River turbidity plume for the period shown in the Figure 5.25

The extent of the turbidity plume predicted by the model was in very good agreement with the plume observed in the satellite images for the entire period. The model under-predicted

the extent of the freshwater plume, initially. This may be attributed to the fact that there was significant amount of leakage flow from the spillway before it was officially opened.

Although forcing a spatially constant wind field captured the trend of the Mississippi River plume, it was necessary to apply a spatially variable wind field to reproduce some of the circulation features observed in satellite images. The observed wind data at 6 stations were interpolated using the inverse distance weight approach to determine the spatially variable wind field. A micro-circulation was observed in the mid-lake region. This circulation helped the plume to migrate northward. A detailed description about the effect of spatially variable wind is provided in Chapter 7.

5.1.3 Calibration of the Wave Model

The wave model was initially calibrated by visually comparing the results generated by the Lake-wide model with the results predicted by a wave model developed and calibrated for Lake Pontchartrain by List and Signell (1997). The contour plots of the wave heights generated by the two models for a southwesterly wind of 5 m s^{-1} were compared as shown in the Figures 5.27 and 5.28. There was a reasonable agreement between the results of the two models. However, the Lake-wide model slightly under-predicted the wave heights compared to the List and Signell Model.

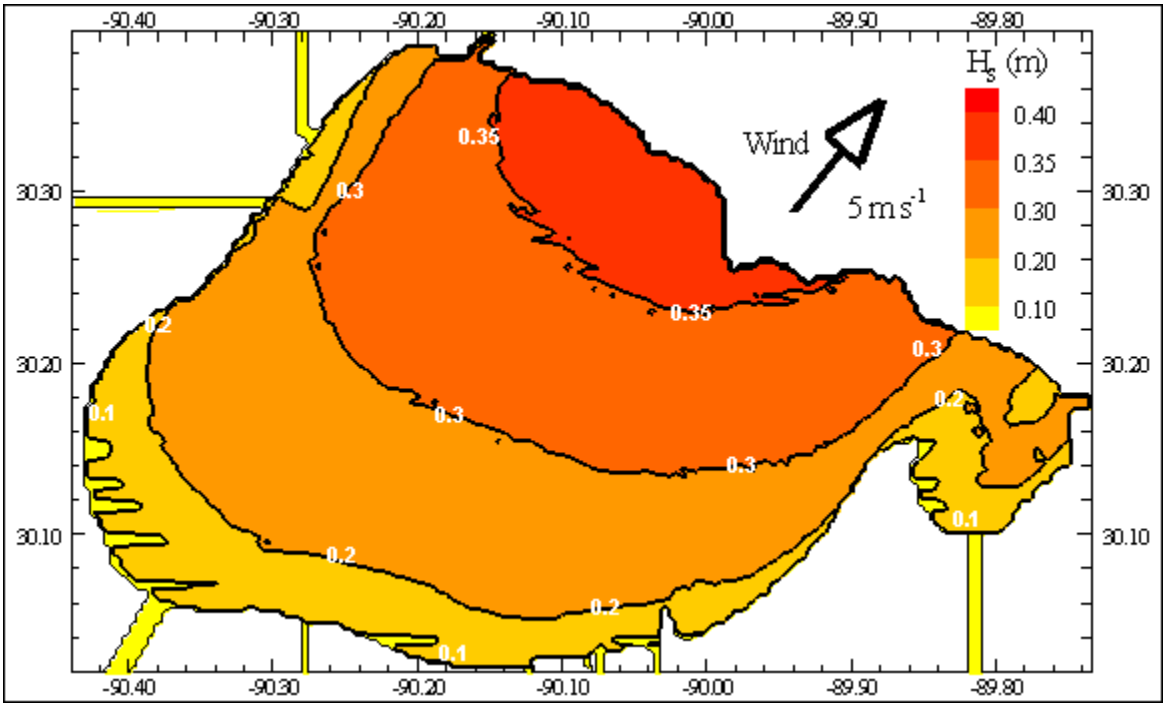

Figure 5.27 Significant wave heights simulated by the Lake-wide model for a constant southeasterly wind of 5 m s^{-1}

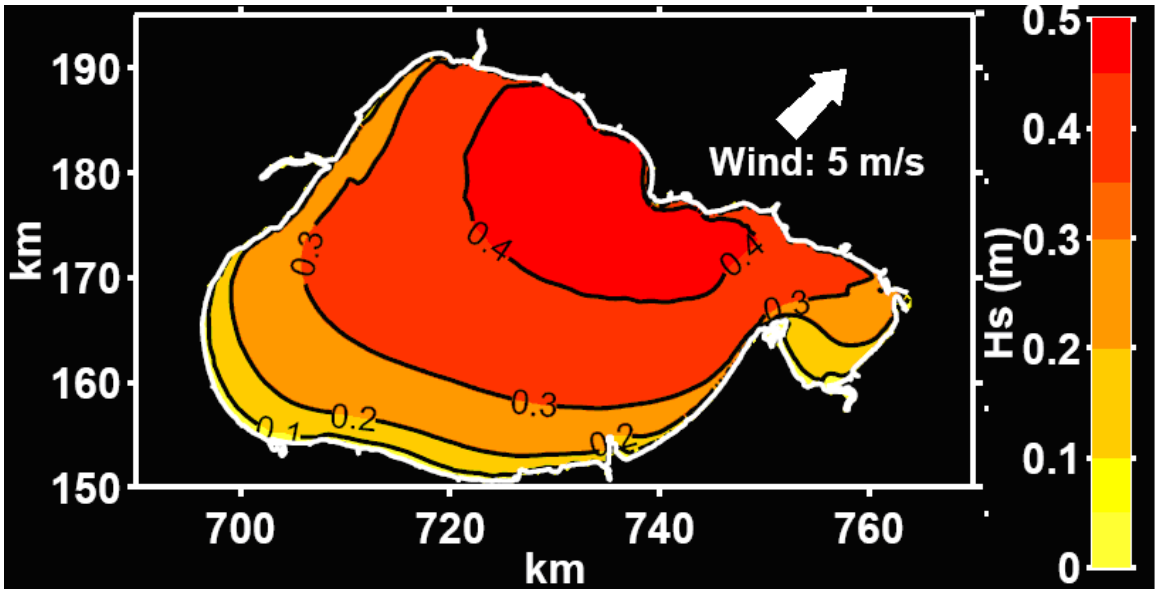

Figure 5.28 Significant wave heights simulated by the HISWA model for a constant southerly wind of 5 m s^{-1} (List and Signell, 1997)

Further, the wave model was calibrated based on the wave data collected by Signell and List for USGS (USGS, 2001) in Lake Pontchartrain during the period January to May, 1995. The location of the stations is shown in the Figure 5.29. The data used for calibration was collected from the location marked as 'A' in the Figure 5.29. The Lake-wide model was simulated using the existing wind and tide conditions from May 1st to May 31st, 1995.

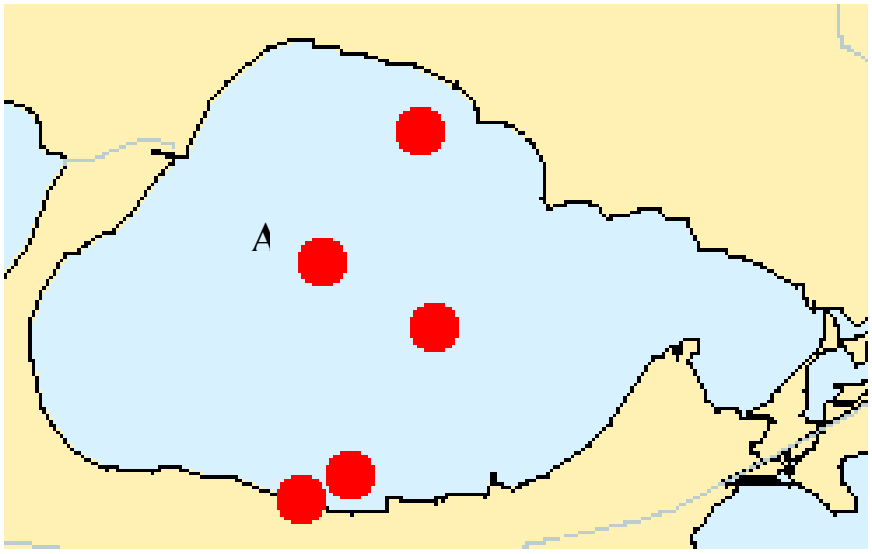

Figure 5.29 Location of the moorings setup to collect the wave data in Lake Pontchartrain by Signell and List for USGS (USGS, 2001)

The time series of the modeled significant wave heights were then compared to the observed values at the station 'A' as shown in the Figure 5.30. There was a reasonable agreement between the two data sets. However, the model seemed to slightly under-predict what was observed. This may be attributed to the fact that SMB wave model used in ECOMSED does not account for the wave transformation and other non-linear processes. The RMS value of the observed wave heights was found to be 34.25 cm and that of the predicted to be 33.91 cm, thus indicating a reasonably good performance by the model.

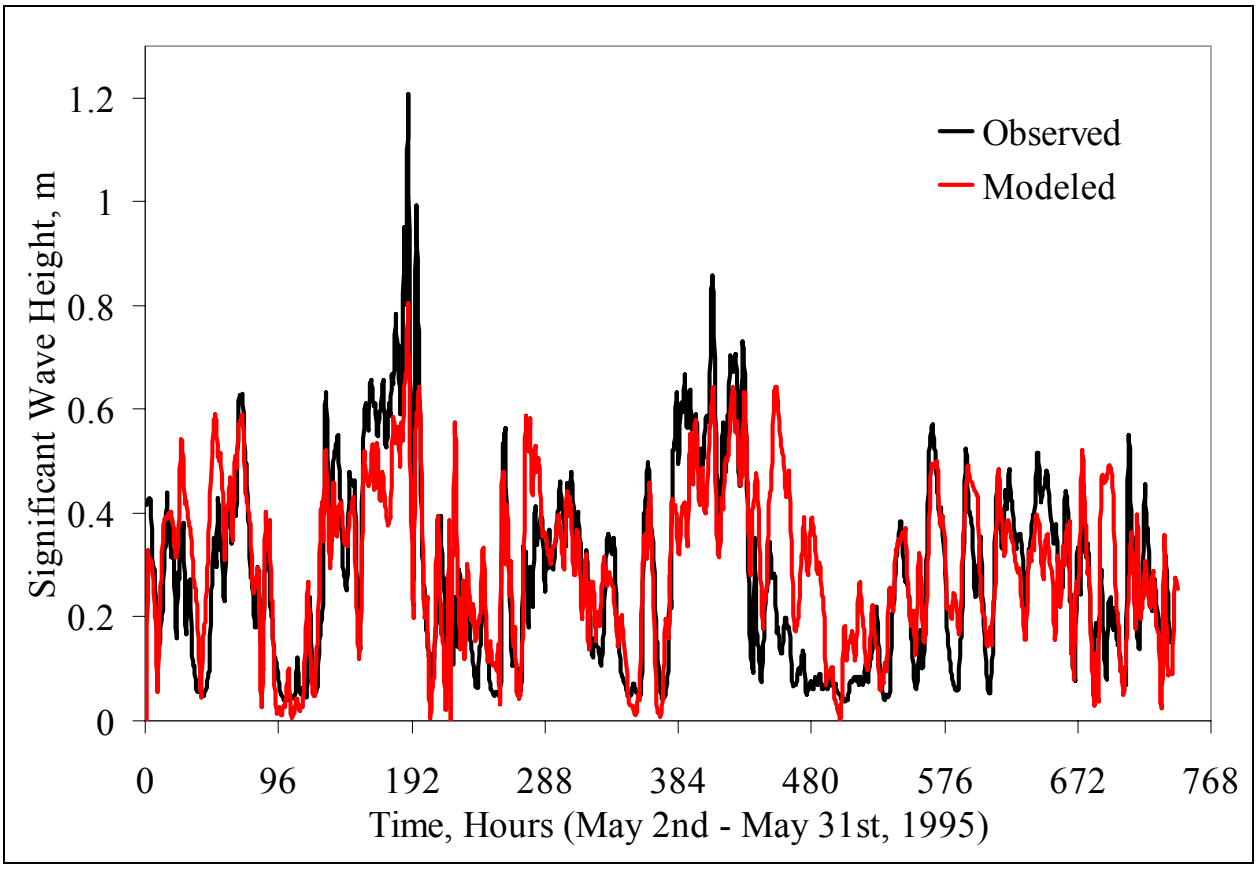

Figure 5.30 Comparison of measured and simulated significant wave heights in the lake at the location A in the Figure 5.27 for the period indicated (Field data source: USGS, 2004)

5.1.4 Calibration of the Sediment Transport Model

Data obtained from Haralampides (2000) and USGS (2001) were used for an initial calibration. The final calibration of the sediment model was achieved by comparing sediment concentrations predicted by the model with the TSS data obtained from NASA MODIS Terra satellite images based on a correlation developed by Miller and McKee (2004) for the period of May 15-23, 2002. The MODIS image for May 15, 2002 was used to define the initial conditions for the model. The remaining images were used for calibration and validation. Limited temporal field data are sufficient for initial calibration and parameter initialization; however, spatial as well as temporal TSS data, such as those obtained from MODIS, are essential for the dynamic

calibration of the model. The coefficients and exponents that affect the depositional and erosional properties of sediments in the model were adjusted. Model refinement was conducted until the observed pattern was sufficiently reproduced by the model. Figure 5.31 shows the TSS data obtained from a satellite reflectance image and corresponding model generated surface sediment concentration on May 22nd and 23rd, 2002. The concentrations in both cases are comparable.

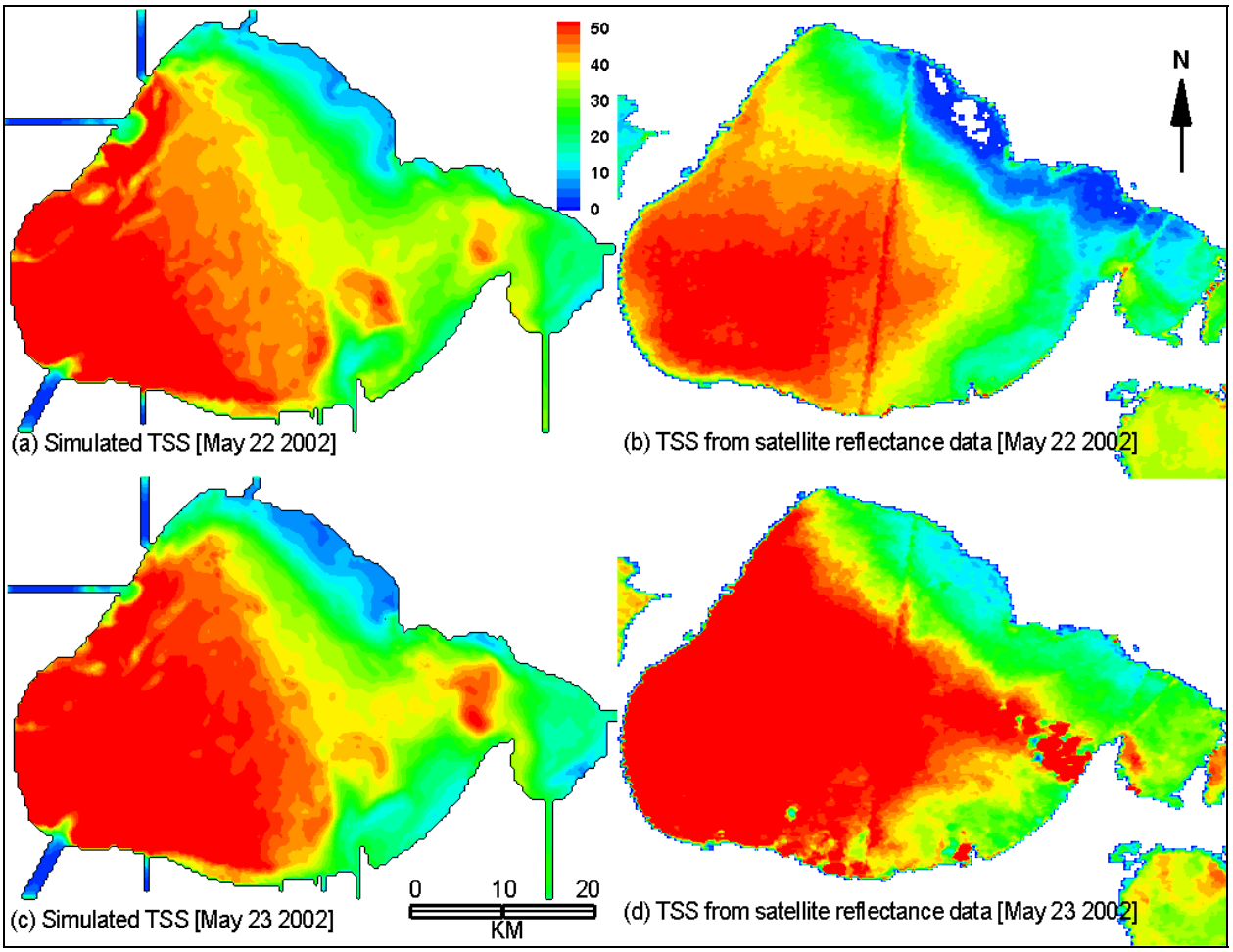

Figure 5.31 Comparison of simulated and observed TSS for May 22nd and 23rd, 2002

5.2 Near-field Model Calibration

5.2.1 Hydrodynamics

The hydrodynamics in the Near-field model were validated by comparison with the Lake-wide model. Figure 5.32 show the depth-average circulation patterns in the north shore predicted by the Near-field model and the Lake-wide model when driven with the same boundary conditions. The Near-field model captures the large scale circulation features as observed in the Lake-wide model results both in terms of magnitude and direction (Length of the vectors indicate magnitude).

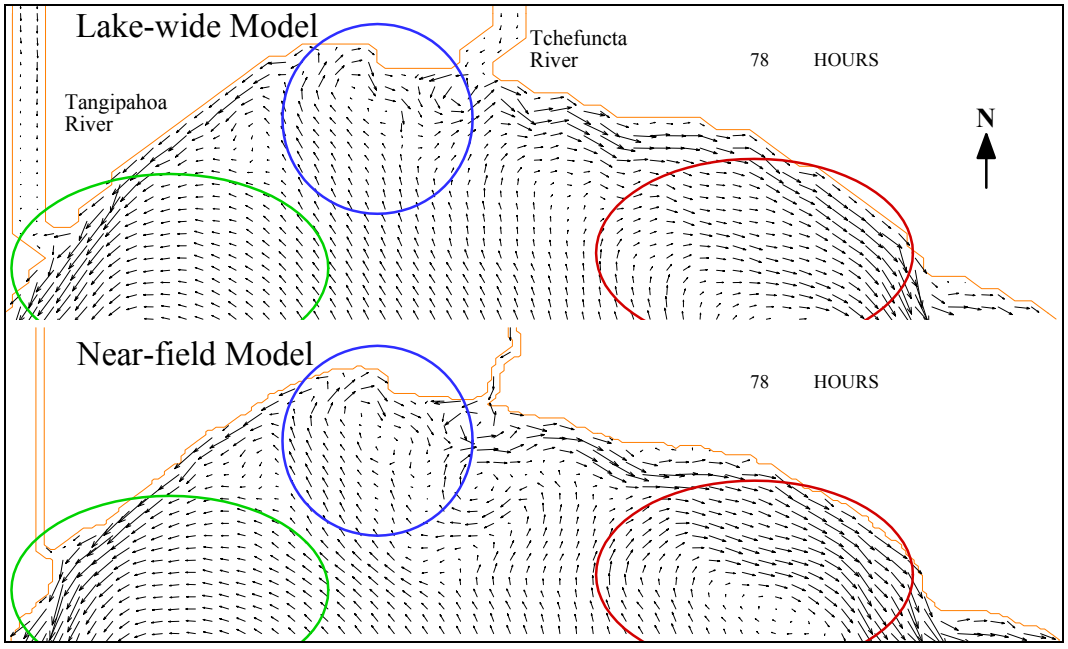

Figure 5.32 Comparison of depth-averaged circulation patterns predicted by the Lake-wide and Near-field models

It was necessary to prescribe the depth-averaged velocities and water surface elevations at the southern open boundary of the Near-field domain, in addition to the surface wind forcing,

to obtain the necessary equivalency in the hydrodynamics between the two models. Moreover, the coefficient α in the Smagorinsky formulation (Equation 14) which controls the horizontal diffusion was increased to 0.75, from a value of 0.1 (used for the Lake-wide model) so as to achieve a stable solution.

5.2.2 Transport Calibration

Transport of conservative tracer was simulated in the Near-field model for the April 24th to 30th, 2004 period. The dissolved inorganic nitrogen (DIN) levels measured in the field were compared with the tracer concentrations predicted by the model at each sampling grid location (Figure 5.33). It was assumed that DIN is nearly conservative over a period of 24 hours.

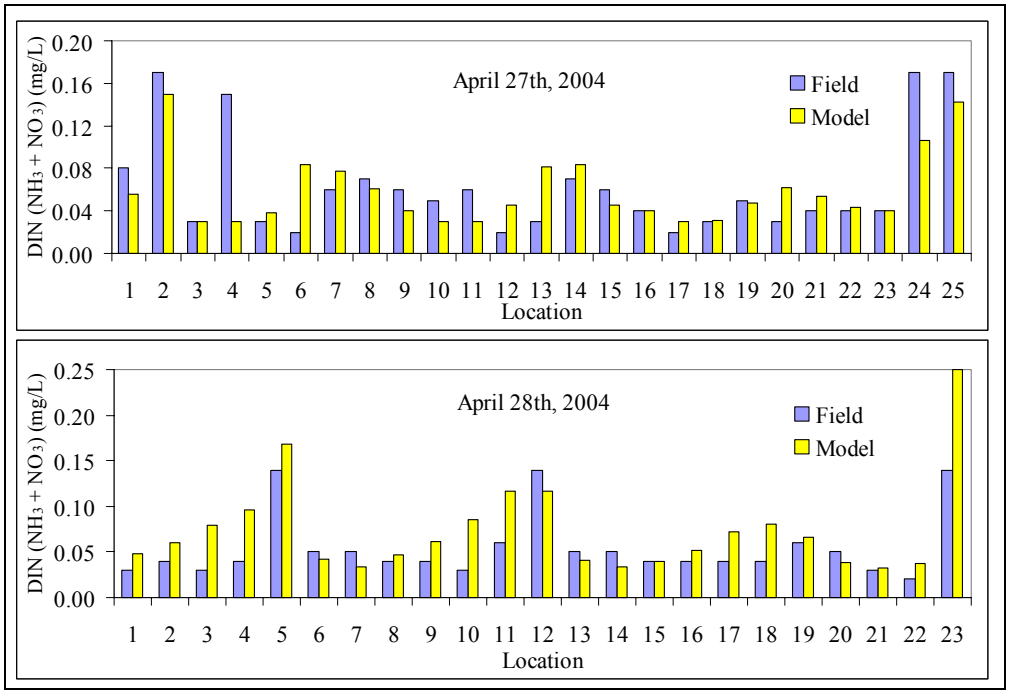

Figure 5.33 Comparison of the simulated and the observed DIN at various sampling locations for April 2004 rain event

To verify if the model was generating similar DIN concentrations as those observed in the field, independent of spatial location, the DIN concentrations from the field and the model were sorted separately and were plotted against each other (Figure 5.34). This was a check on the mass conservation of the nutrient loading. Moreover, if there was any difference in the orientation of the predicted plume and the plume observed in the field, this check would verify whether the model can actually predict the concentrations observed in the field.

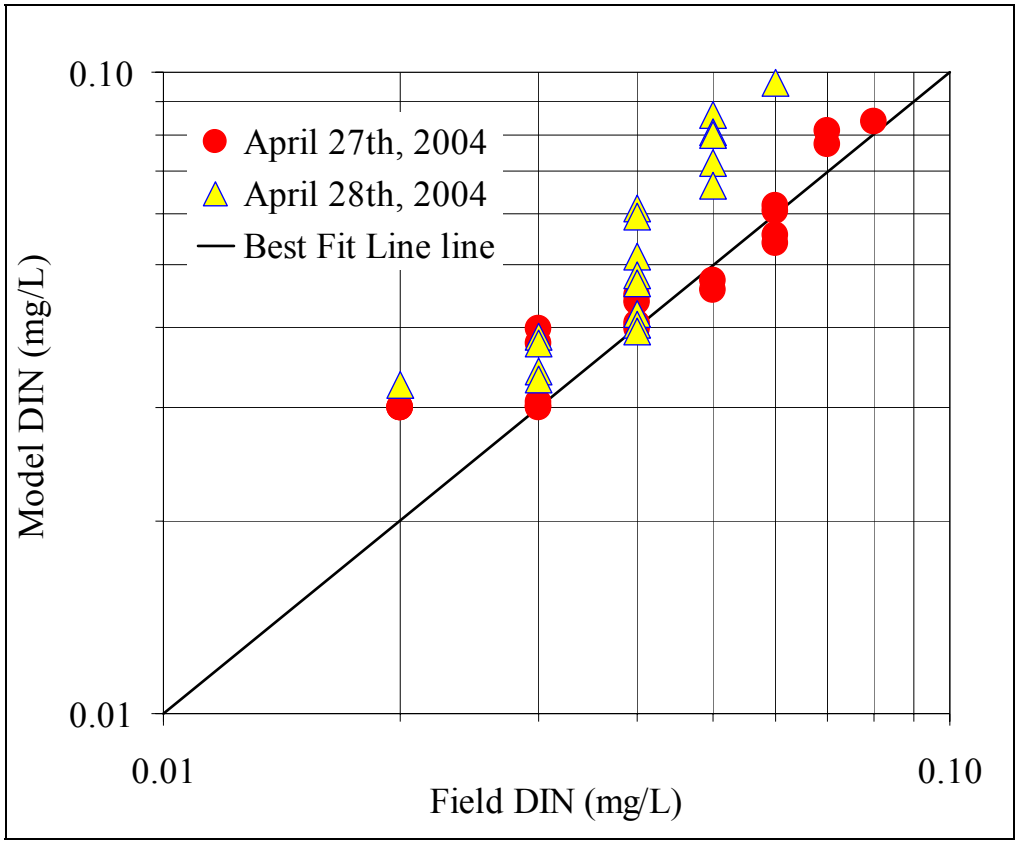

Figure 5.34 Comparison of the simulated and the observed DIN for April 2004 rain event independent of location

On the 27th there was a good agreement between the model and the field DIN concentrations; however, the model over-predicted DIN on the April 28th. This could be attributed to the fact that the time series data at the source was very limited. The source DIN was

interpolated temporally to fill the gaps in the available time series data. The forcing used in the model may have failed to capture the fluctuations in the DIN loading thus causing a disagreement.

5.2.3 Fate and Transport Calibration of Fecal Coliform

The April 2004 rain event data set was used to calibrate the pathogen indicator model. The Near-field model was simulated for a period of seven days from April 24th to 30th, 2004. The model was initialized with the mean background levels and was ramped up for one day. Due to the limited amount of data available at the source, the fecal coliform loading pollutograph for the simulation period was synthesized. The value obtained for the "high loading" was used as the peak concentration of the pollutograph as the measured rainfall for this event was 1.1 inches. The falling limb of the pollutograph was modeled exponentially as shown in the Figure 4.8. The curve of the pollutograph was fitted to pass through the few available data points. A check was made to ensure that the mass of the load was at least equal to the mass observed in the receiving water.

The fecal coliform levels from the field and the model were plotted for each sampling location. The levels matched fairly well as shown in the Figure 5.35. Moreover, as described in the transport calibration section, a plot to verify that the mass loading was conserved in the model was developed as shown in the Figure 5.36. The simulated and observed data were in good agreement for both days; however, a small error in the pollutograph at the source could have caused the model to slightly under-predict the fecal coliform levels on April 27th.

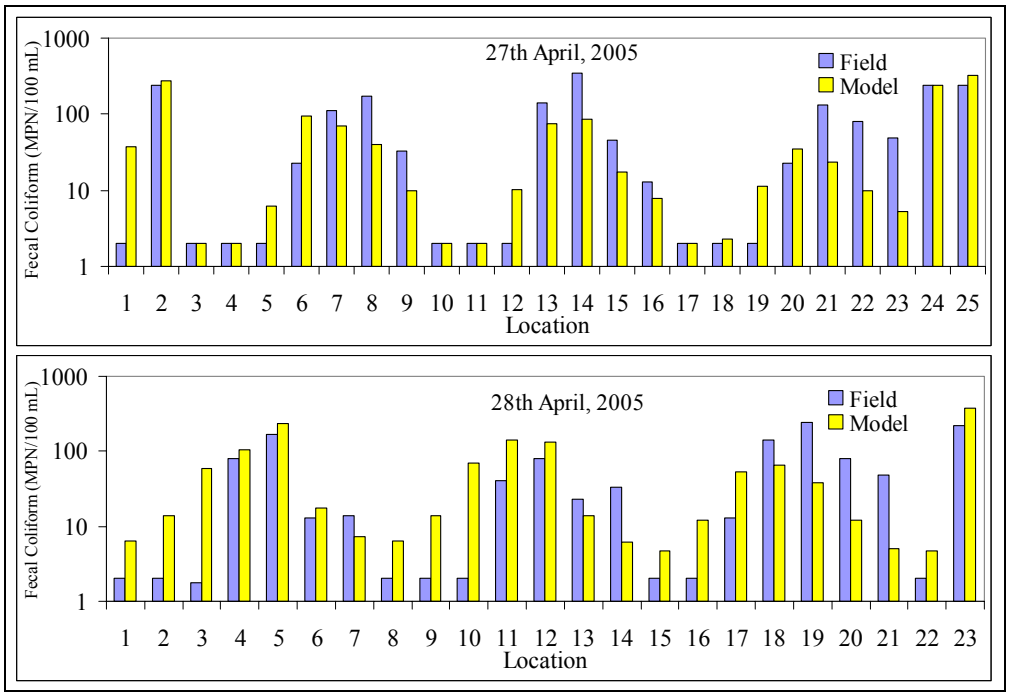

Figure 5.35 Comparison of the simulated and the observed fecal coliform levels for April 2004 rain event independent of location

A student t-test was employed to make sure the means of the predicted and observed values were not significantly different. It was found that 95 % of the times, the difference between the predicted and the observed means was insignificant for both April 27th and 28th. Moreover, it was observed that the extent of the plume predicted by the model was similar to that observed in the field as shown in the Figure 5.37.

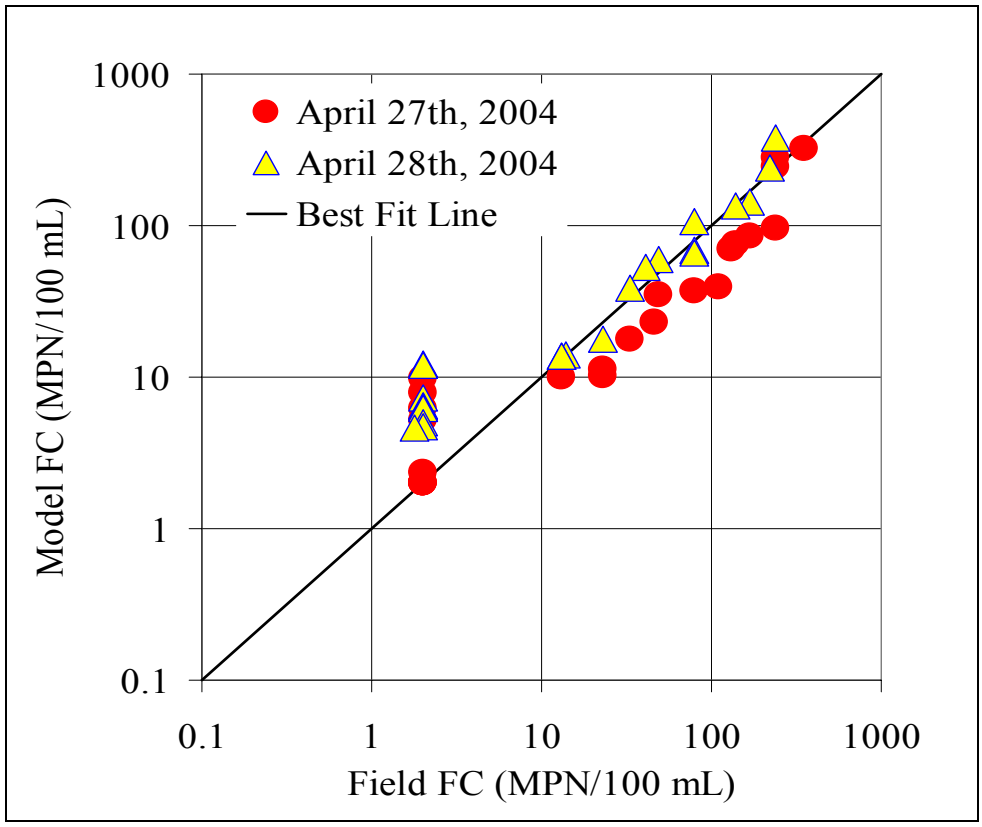

Figure 5.36 Comparison of the simulated and the observed fecal coliform levels for April 2004 rain event independent of location

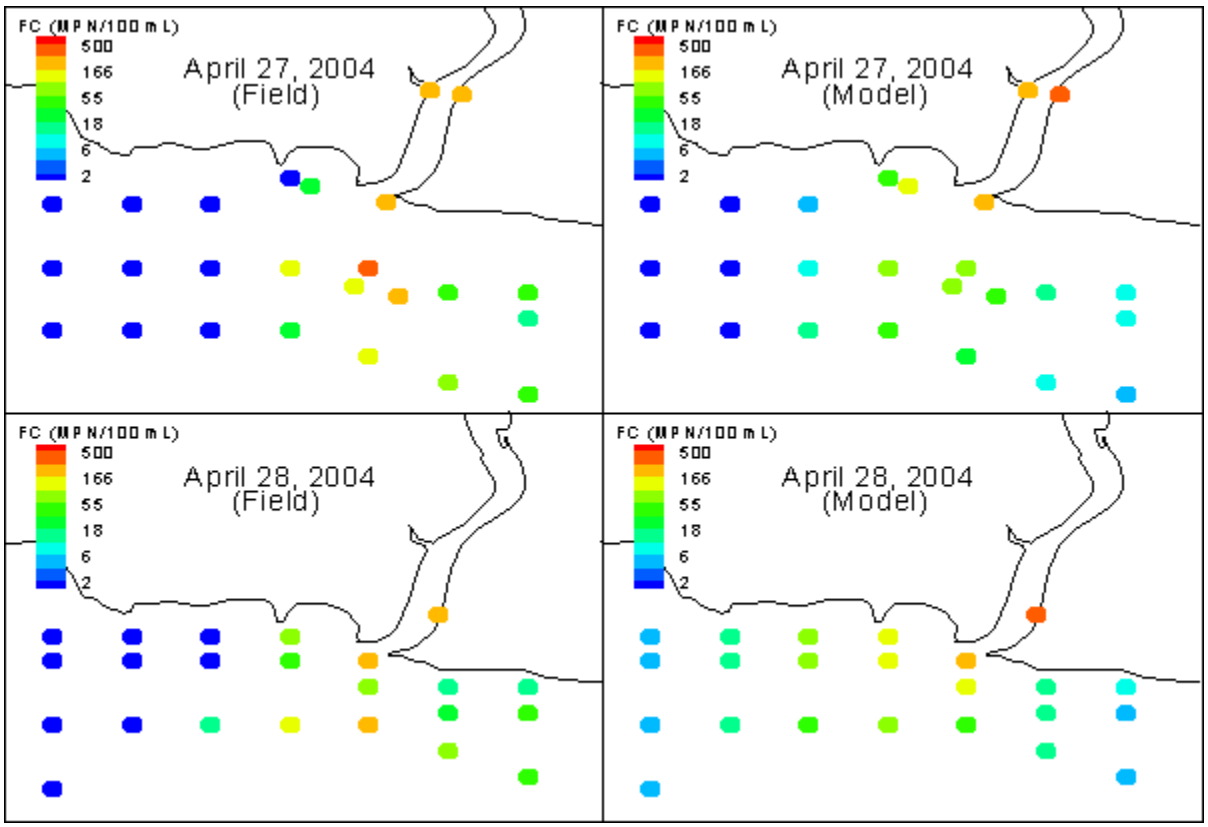

Figure 5.37 Comparison of the observed and simulated extents of the fecal coliform plumes for April 2004 rain event

5.3 Model Testing and Sensitivity

5.3.1 Effect of Various Horizontal Resolutions

The ability of the Lake-wide model to simulate the observed water surface elevation for various horizontal grid sizes (1200 m, 800 m, 400 m, and 300 m) was tested. The water levels predicted using the four grids were compared to the observed data at the Mandeville gage. The simulated data matched with the observed water levels very well and with equal precision in the four cases indicating that the model was independent of the grid size.

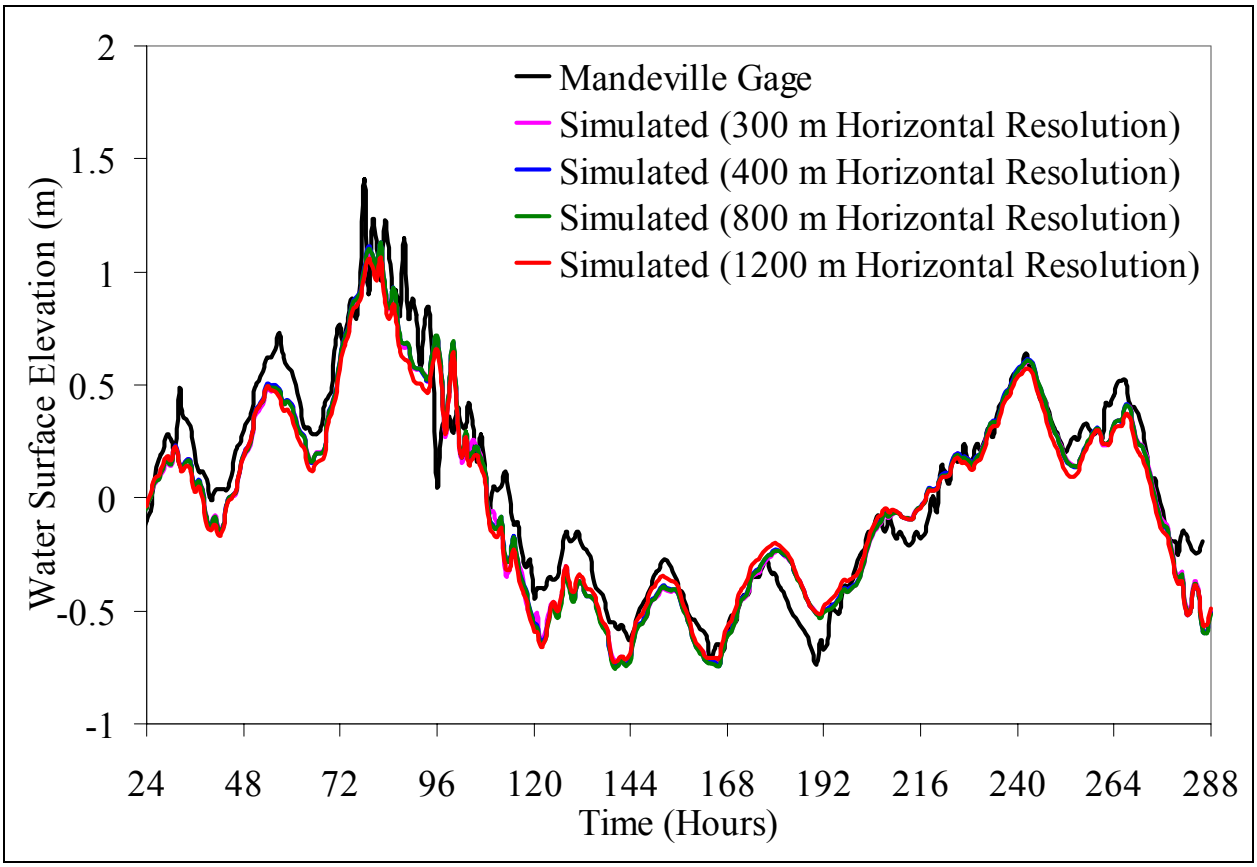

Figure 5.38 Comparison of the water levels at the Mandeville gage for various grid sizes for November 25th to December 6th, 2003 period

Further, the depth averaged currents simulated by the Lake-wide model using various grids were compared (Figure 5.39). Again, the results show that the currents simulated by the 300 m, 400 m, and 800 m grids were very similar. However, the 1200 m grid slightly under-predicts the currents when compared to other grids. The difference in the water levels and currents simulated using 400 m and 300 m grids was insignificant proving that the model was grid independent. The 400 m resolution was used as the final grid for the Lake-wide model. The root mean square difference (RMSD) values were computed for the currents simulated in the 300 m, 800 m and 1200 m cases with respect to the results in the 400 m case (Table 5.3). It was

observed that the 300 m case has the least difference whereas the 1200 m resolution resulted in a higher value.

Table 5.3 Root mean square difference in depth-averaged currents for 300 m, 800 m and 1200 m resolution grids compared to the 400 m resolution grid case

Grid Size, m	300	800	1200
RMSD, cm/s	0.28	0.72	2.68

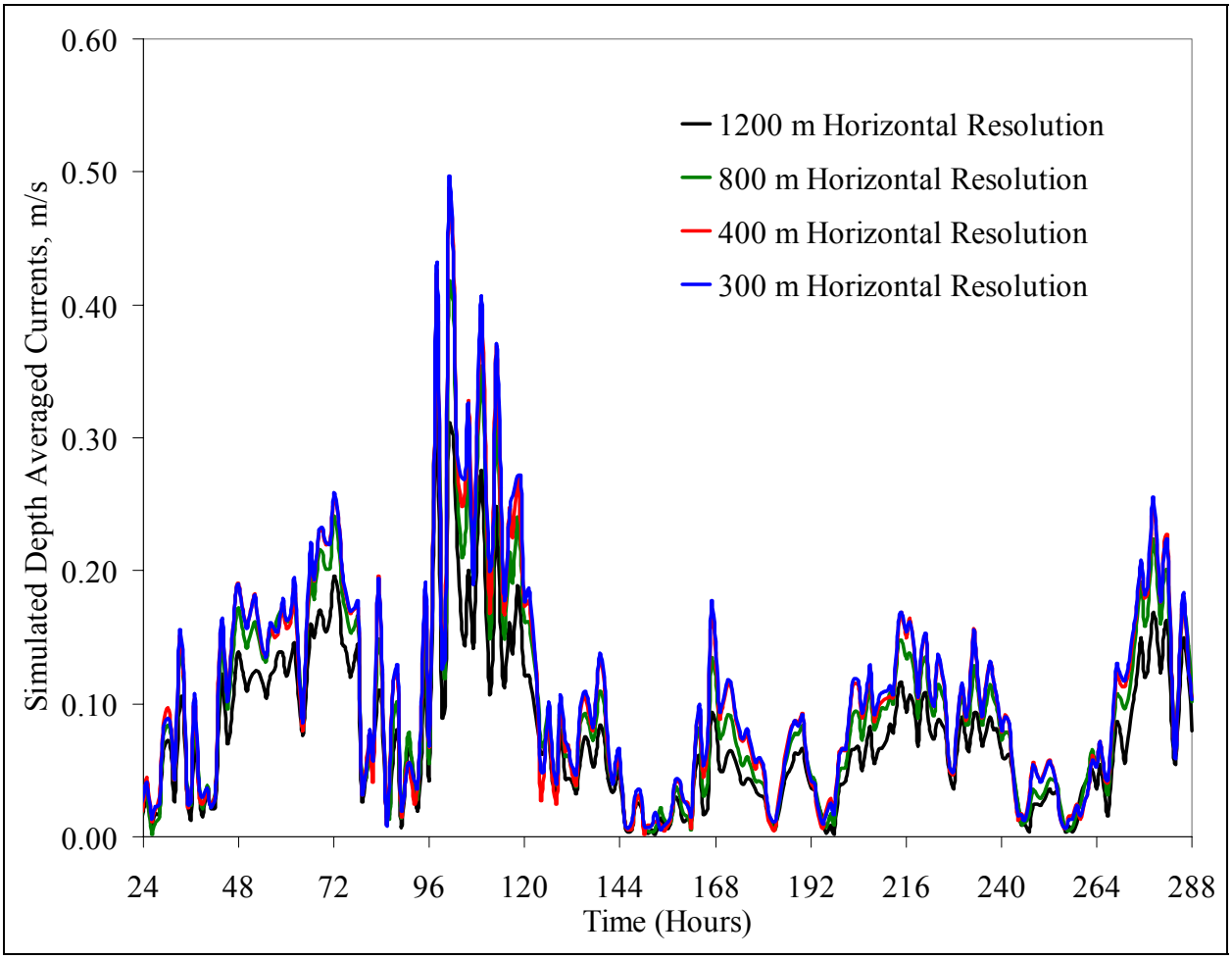

Figure 5.39 Comparison of the depth averaged currents at the Mandeville gage for various grid sizes

5.3.2 Effect of Various Time Steps used in the Model

The water levels predicted by the model at the Westend gage were simulated for various time steps of 3 s, 2 s, 1 s and 0.5 s and were compared with the actual record as shown in Figure 5.40. The results in all the four cases were in very good agreement with the observed values. Moreover, comparing the simulated depth averaged velocities (Figure 5.41) also indicated that the difference among the solutions generated using these four time steps was trivial. Thus it was concluded that the model was independent of the time step used. Although 3 s produced equally good results as in the case of 2 s, the model generated small oscillations near the regions of higher currents when a time step of 3 s was used. Consequently, an external mode time step of 2 s was used for all purposes in the Lake-wide model. Table 5.4 shows the RMSD values for the modeled currents in 0.5 s, 1 s and 3 s cases with respect to 2 s results.

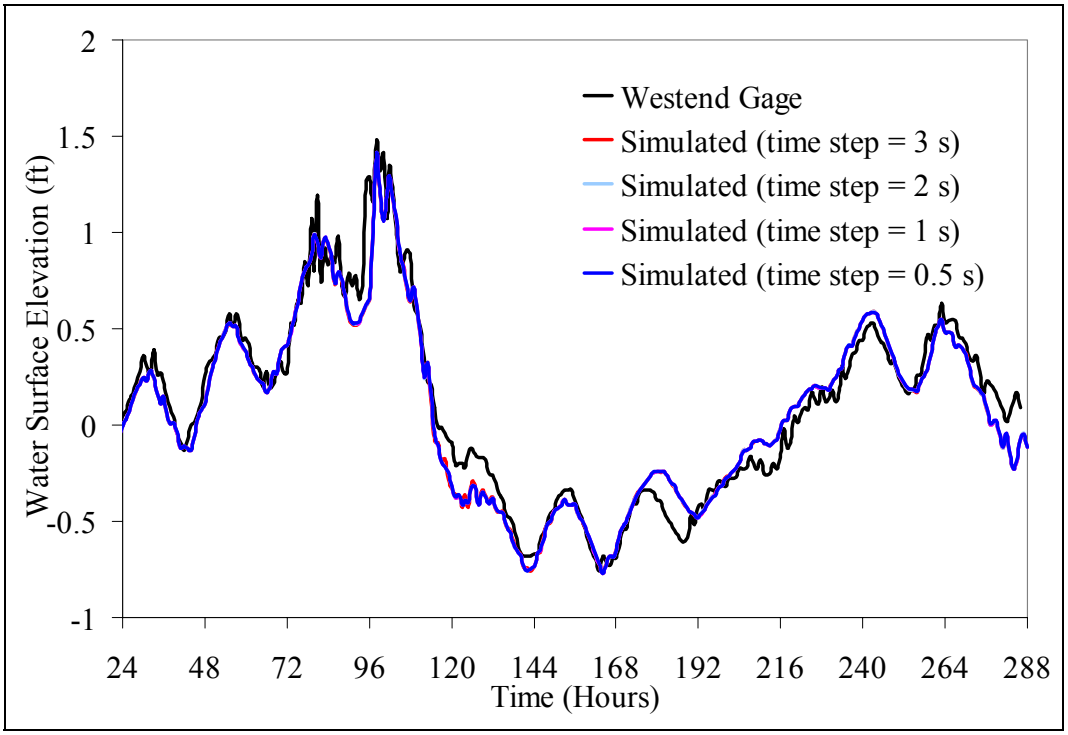

Figure 5.40 Comparison of the water levels at the Westend gage for various time steps

Table 5.4 Root Mean Square difference in depth-averaged currents for 3 s, 1 s and 0.5 s time steps compared to the 2 s time step case

Time Step	3 s	1 s	0.5 s
RMSD, cm/s	0.36	0.24	0.28

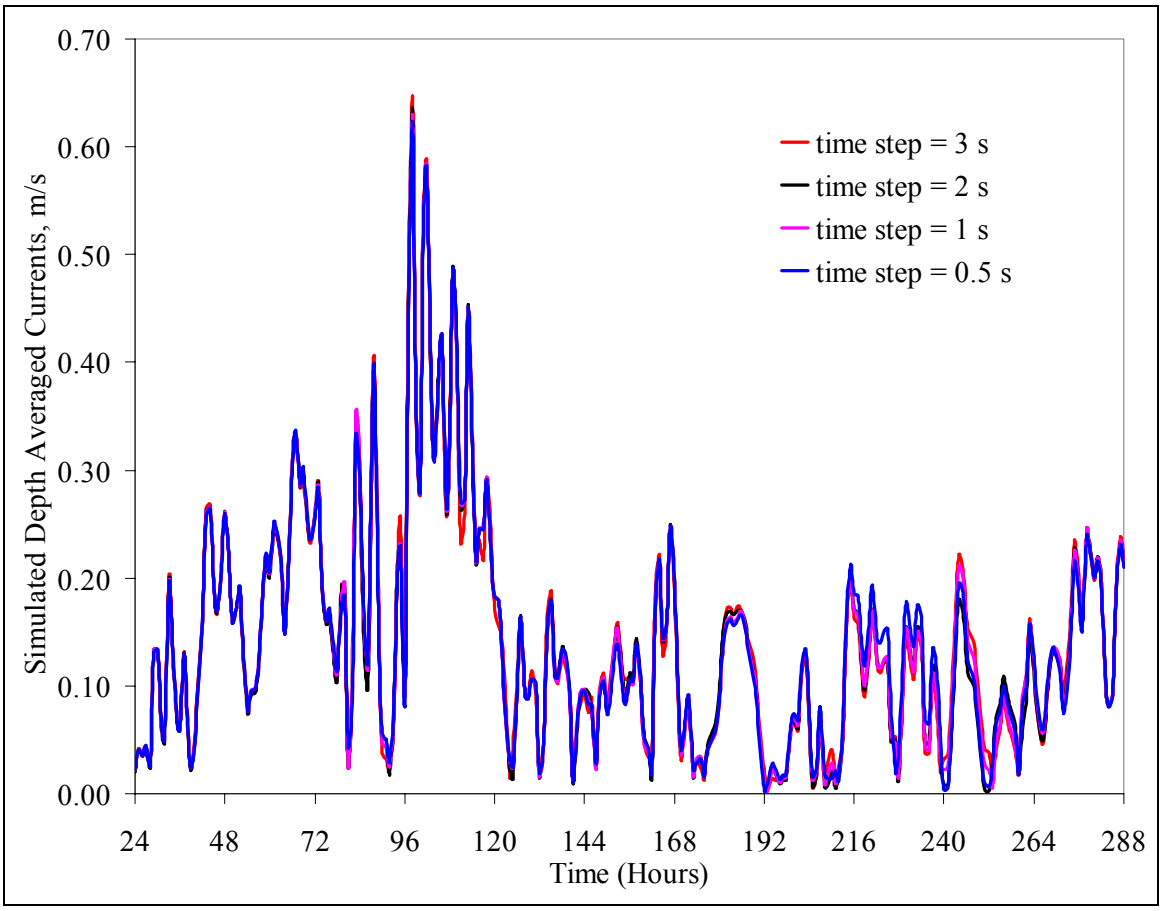

Figure 5.41 Comparison of the depth averaged currents at the Westend gage for various time steps

5.3.3 Effect of Various Vertical Resolutions

The sensitivity of the model to the number vertical layers used was tested for 10, 7 and 3 layers. The variation in the water levels simulated in the three cases was negligible. All the results were in good agreement with the observed values as shown in the Figure 5.42. This was unlike what was observed when the simulated depth averaged currents were compared in the

three cases. In the three layers case the model under-predicted the currents as can be seen in the Figure 5.43. This was especially true when the currents were higher during which additional vertical resolution was required. As the results generated in 7 and 10 layers cases were very similar, 7 layers were used for modeling purposes. Table 5.5 shows the RMSD values for the modeled currents in 10 and 3 vertical layers cases with respect to 7 layers case results.

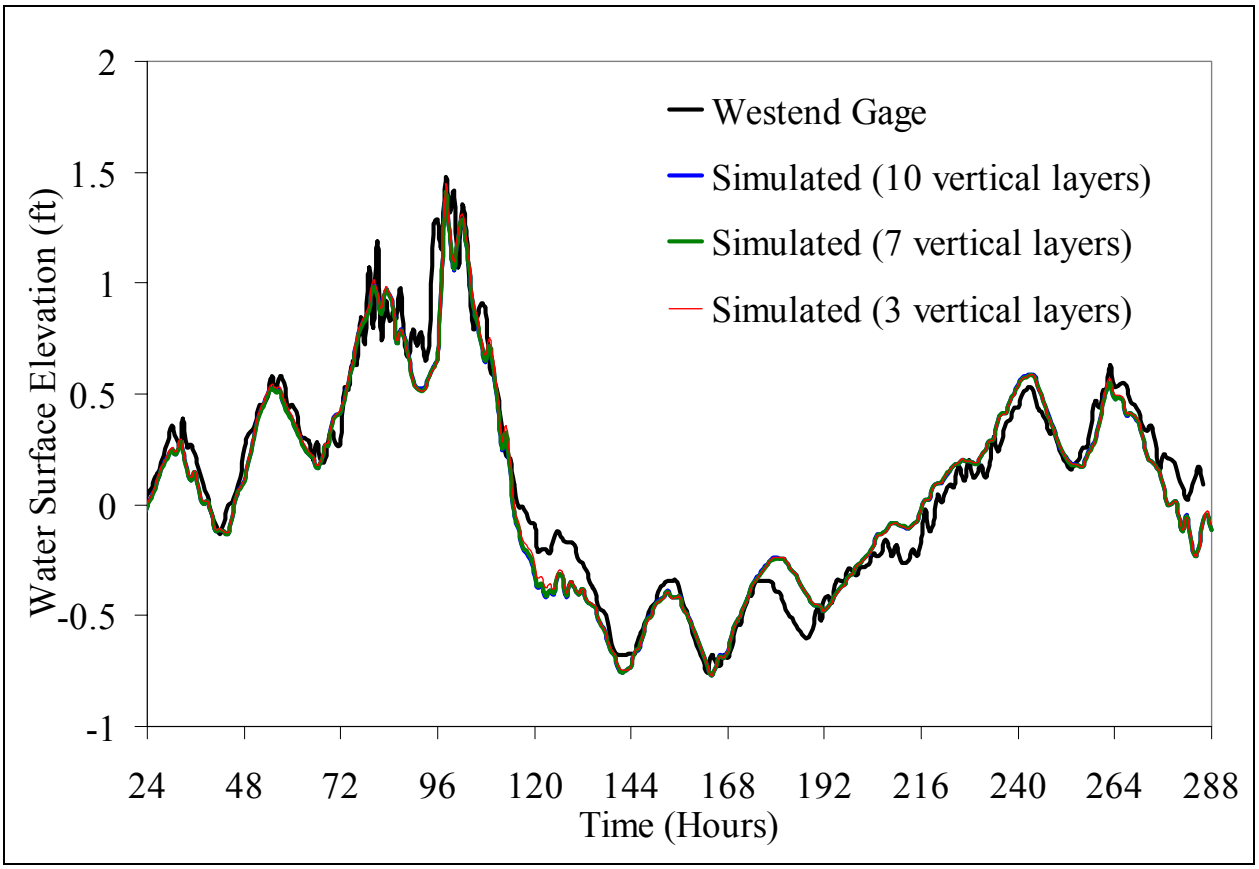

Figure 5.42 Comparison of the water levels at the Westend gage for various vertical resolutions

Table 5.5 Root Mean Square difference in depth-averaged currents for 3 and 10 vertical layer cases compared to the 7 layers case

Vertical Layers	3	10
RMSD, cm/s	5.19	2.15

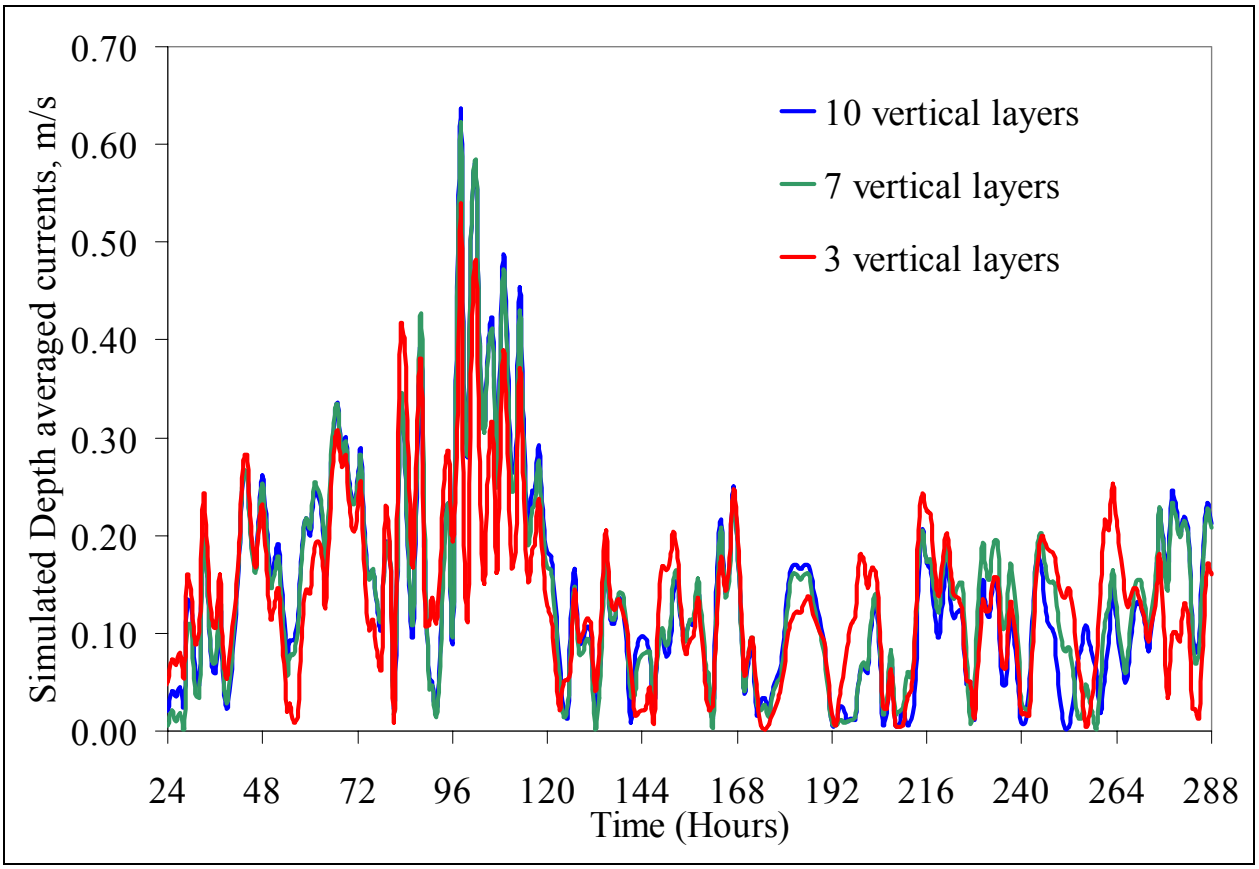

Figure 5.43 Comparison of the depth averaged currents at the Westend gage for various vertical resolutions

5.3.4 Effect of Various Bed Roughness Heights

The performance of the Lake-wide model for various bed roughness height values (0 cm, 1 cm, 2 cm, and 3 cm) was tested. ECOMSED uses bed roughness height to compute the bed friction. The model assumes a specified minimum bed friction value (0.0025) when the user specified bed roughness height is 0 cm, i.e. hydraulically smooth. The model results in each case seemed to be in general agreement with other cases and with the observed water levels (Figure 5.44). The water levels simulated in the 0 cm case were under or over the observed data. The high frequency fluctuations were smoothened in the 2 cm and 3 cm cases.

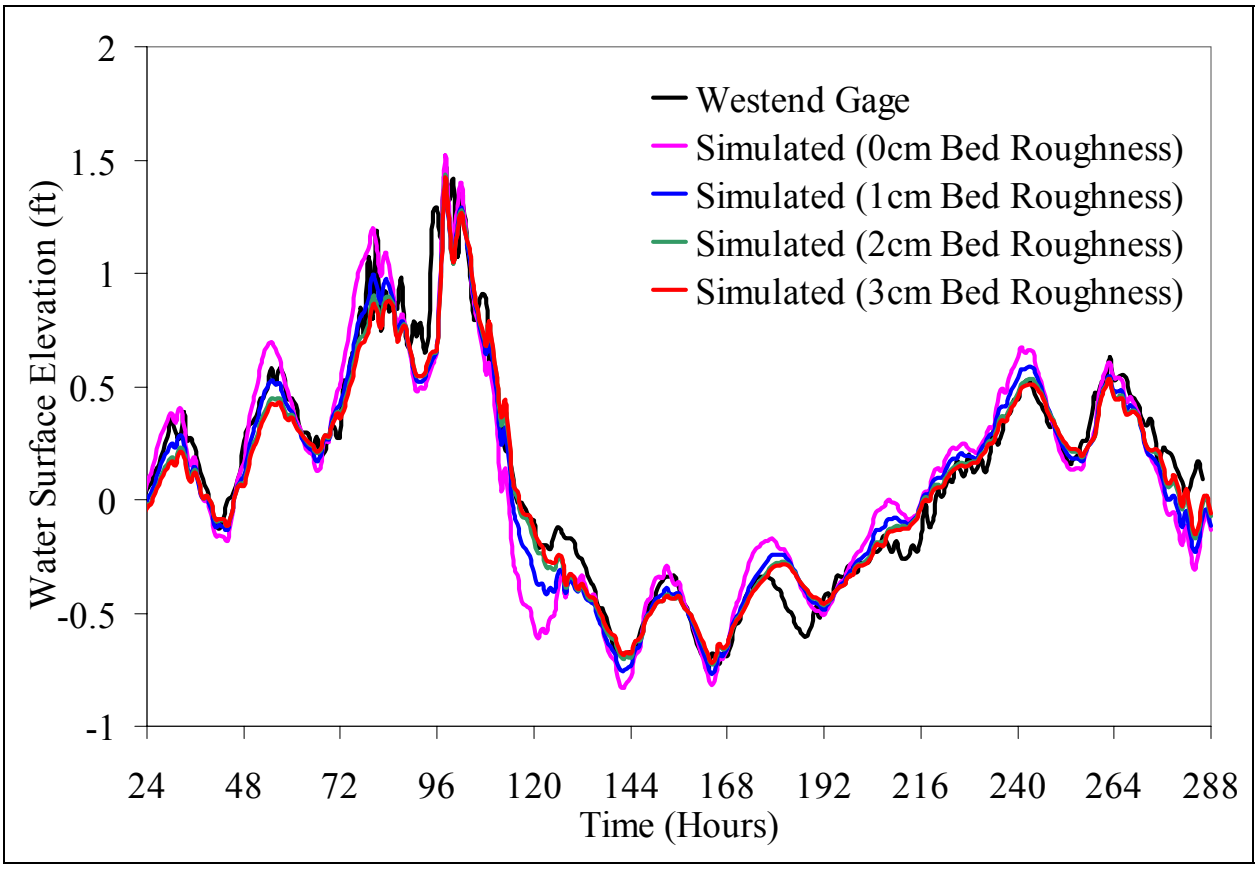

Figure 5.44 Comparison of the water levels at the Westend gage for various bed roughness heights

Further, the depth averaged currents produced in the four cases were compared as shown in the Figure 5.45. The merit of each solution was more visible in this case. As was observed previously, the currents simulated in the 0 cm case were unfeasibly higher. The currents in the 2 cm and 3 cm cases were damped when compared to those in the 1 cm case. Thus a bed roughness height of 1 cm, which allowed the model to perform well and which further provides a closer representation of the conditions in the Lake Pontchartrain due to the presence of clams was used in the Lake-wide model for this study. Table 5.6 shows the RMSD values for the modeled currents in 0 cm (smooth bed), 2 cm and 3 cm bed roughness cases with respect to 1 cm roughness case results.

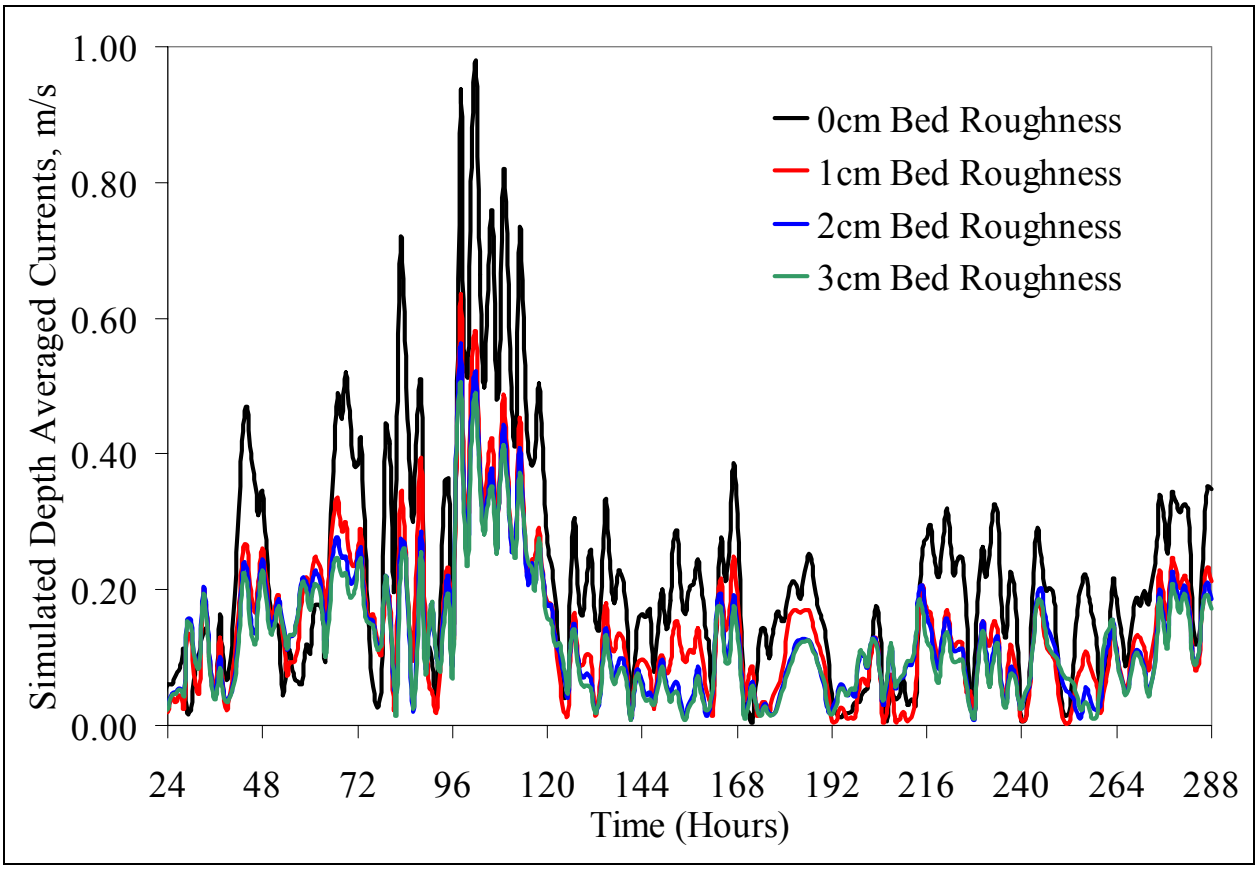

Figure 5.45 Comparison of the depth averaged currents at the Westend gage for various bed roughness heights

Table 5.6 Root Mean Square difference in depth-averaged currents for 0 cm (smooth), 2 cm and 3 cm bed roughness cases compared to the 1 cm bed roughness case

Bed Roughness	0 cm	2 cm	3 cm
RMSD, cm/s	11.70	3.53	4.45

5.3.5 Effect of Various Horizontal Diffusivities

As stated earlier ECOMSED uses Smagorinsky's formulation to compute horizontal mixing coefficients. The horizontal diffusivity in the model can be modified by varying the α parameter (HORCON) in the Equation 14. Increasing the value of HORCON would increase the diffusivity and vice versa. The model performance for various diffusivities was tested. The

model simulation failed when the HORCON value was outside the range of 0.02 to 0.4. When the value was out of this range the model failed near the IHNC. Figure 5.46 shows the comparison of the simulated water level elevations and the observed values at the Westend gage. The simulated water levels were fairly insensitive to the various HORCON values used and were in good agreement with the observed water levels.

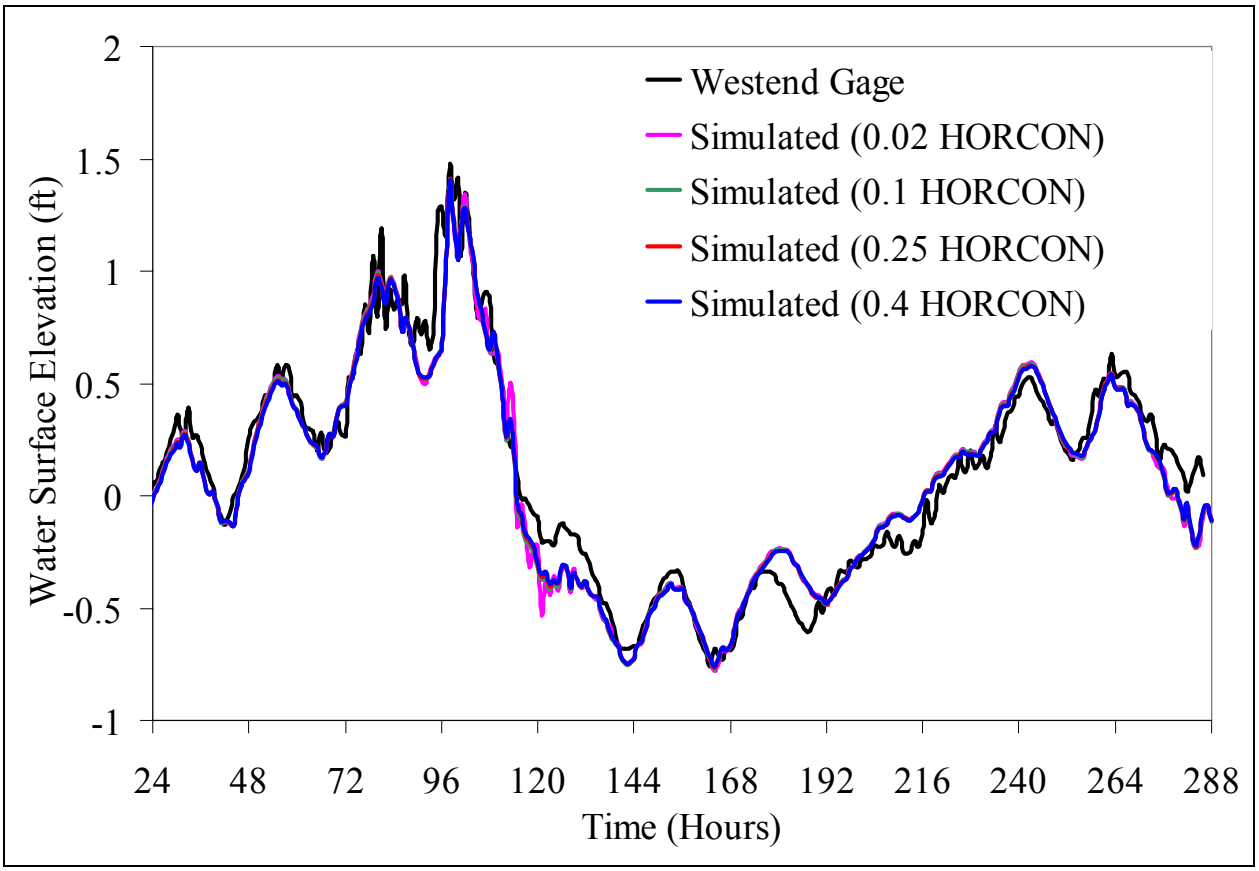

Figure 5.46 Comparison of the water levels at the Westend gage for various horizontal diffusivities

A comparison among the depth averaged currents generated by the model for various HORCON values helped to zero on the best suited value for the Lake-wide model. The currents in the 0.02 case were generally higher than those observed in the other cases. Moreover, there

was a pronounced disparity when the velocities were high. Although the currents generated in the cases of 0.1, 0.25, 0.4 HORCON were found to be agreeing with each other, in the cases of 0.25 and 0.4 as the HORCON value increased the peaks were smoothed down as shown in the Figure 5.47. For the current study a HORCON value of 0.1 was used in the Lake-wide model. Table 5.7 shows the RMSD values for the modeled currents in the 0.02, 0.25 and 0.40 HORCON cases with respect to 0.10 HORCON case results.

Table 5.7 Root Mean Square difference (RMSD) in depth-averaged currents for 0.25, 0.40 and 0.02 HORCON values compared to the 0.1 HORCON case

HORCON	0.25	0.40	0.02
RMSD, cm/s	1.81	2.54	4.12

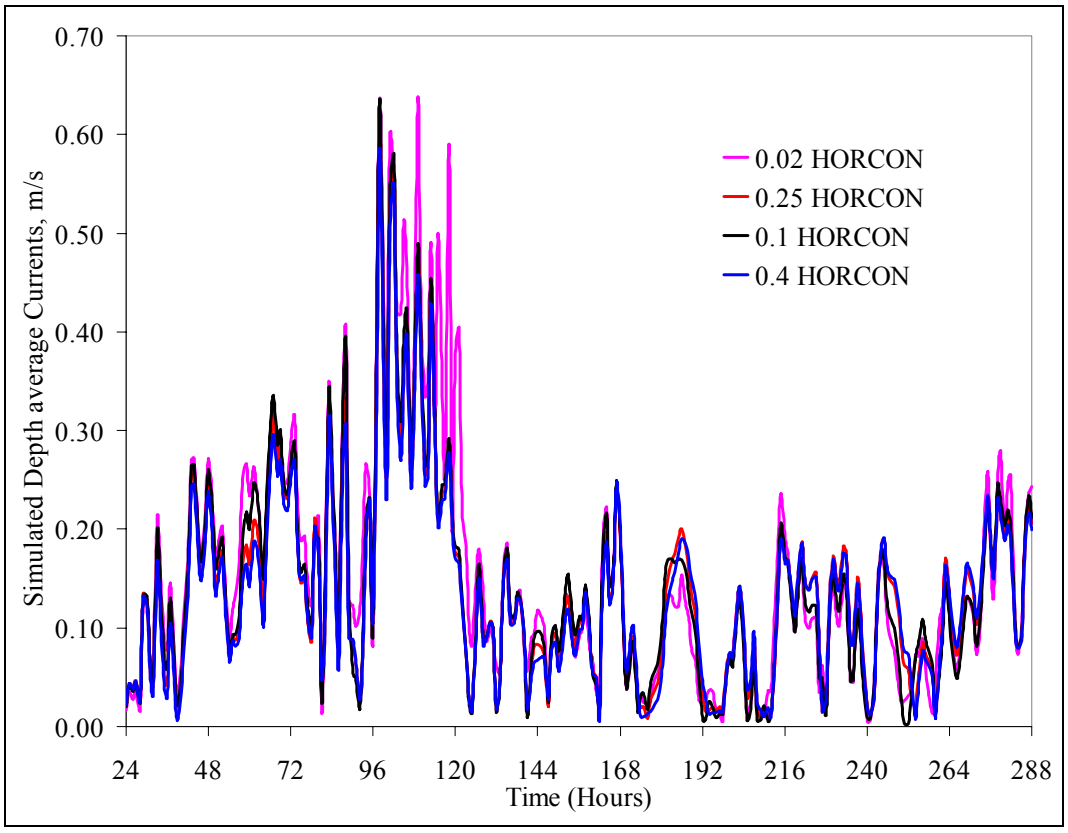

Figure 5.47 Comparison of the depth averaged currents at the Westend gage for various horizontal diffusivities

5.3.6 Sensitivity of the Near-field Model to the Horizontal Diffusivity

Although sensitivity testing was performed using various HORCON values in the Lake-wide model, considerable effort was put in to identify the specific HORCON value suitable for a stable Near-field model. To remind the reader, Smaogorinsky formulation shown in the Equation 14 is used to estimate the horizontal mixing/diffusion coefficient which would define the mixing characteristics of the sub-grid scale processes. Hence, as the grid size reduces one would expect the α value to decrease in the Equation 14 since the high resolution grid can capture the processes that were at a sub-gird scale in a lower resolution grid. To the contrary, it was found that the Near-field model which has four times higher resolution than the Lake-wide model, would not produce stable results for a smaller HORCON than the value used for the Lake-wide model. Even 0.4, which was the maximum HORCON value suitable for the Lake-wide model, was also insufficient. Instead, it required a HORCON value of 0.75 for the model to produce stable results. Although the reason was not quite clear, Berntsen (2002) suggested the use of HORCON values of the order of 1 in the Smagorinsky formulation for high resolution grids.

To demonstrate the above discussion, a comparison of the salinity fields, currents and circulation patterns is shown in the Figure 5.48. Figure 5.48 (a) shows the salinity field, currents and the circulation patterns as predicted by the calibrated Lake-wide model in the north shore of Lake Pontchartrain at 75 hours. Figure 5.48 (b) shows the results predicted by the Near-field model with a HORCON value of 0.10 at 75 hours. Comparing visually with the Figure 5.48 (a), the patterns in the Figures 5.48 (b), (c) consists of clustering type instabilities and do not agree. Whereas, Figure 5.48 (d) and (e) agree well with 5.48 (a).

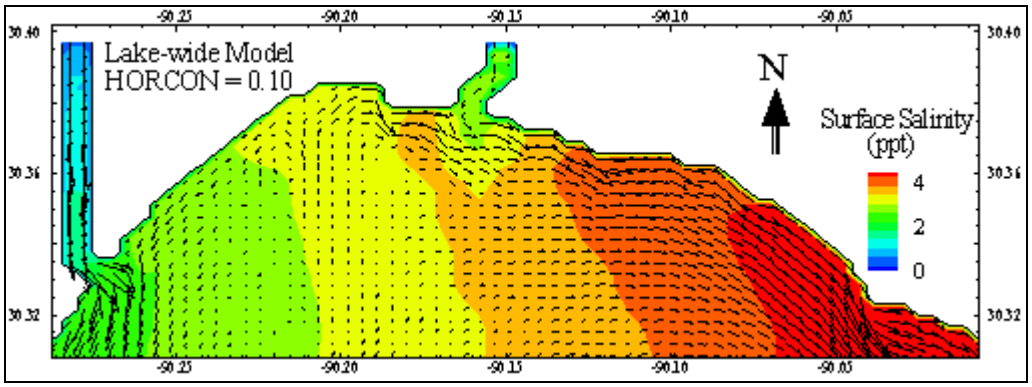

Figure 5.48 (a) Snapshot of Lake-wide model currents and the salinity levels at 75 hours

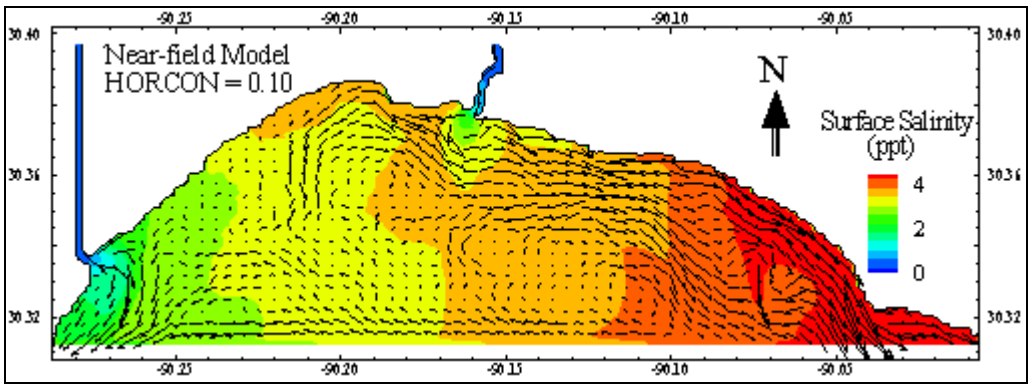

Figure 5.48 (b) Snapshot of Near-field model currents and the salinity levels at 75 hours with a HORCON value of 0.10

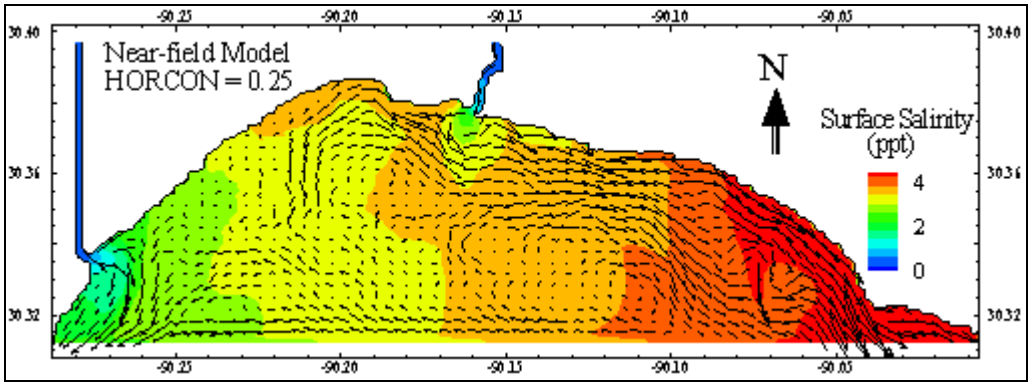

Figure 5.48 (c) Snapshot of Near-field model currents and the salinity levels at 75 hours with a HORCON value of 0.25

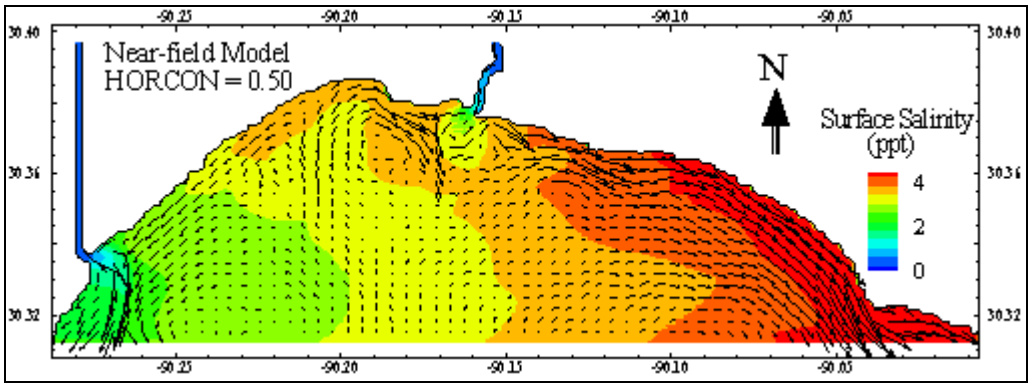

Figure 5.48 (d) Snapshot of Near-field model currents and the salinity levels at 75 hours with a HORCON value of 0.50

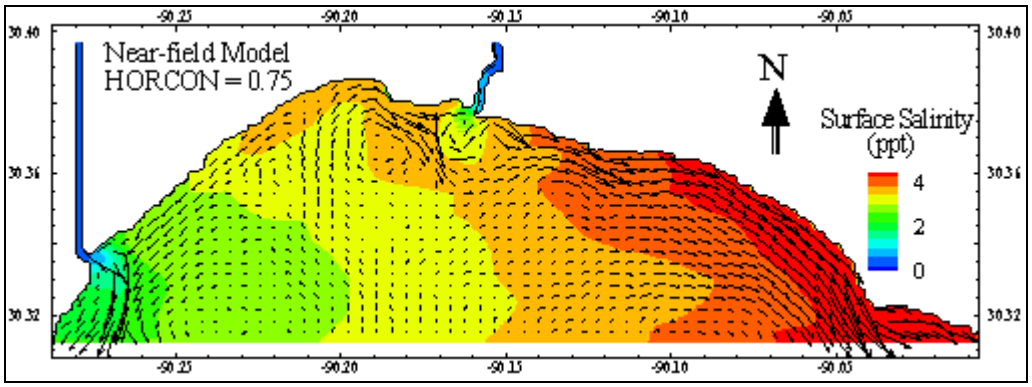

Figure 5.48 (e) Snapshot of Near-field model currents and the salinity levels at 75 hours with a HORCON value of 0.75

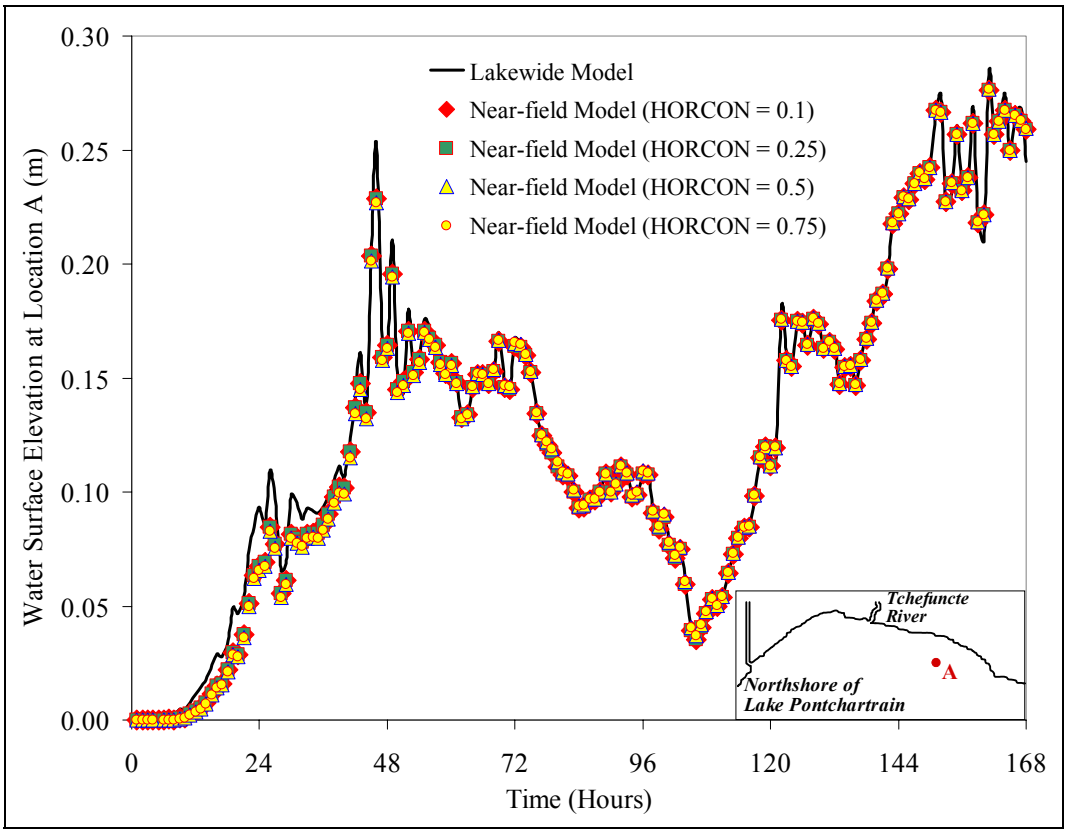

Figure 5.49 Comparison of water surface elevations predicted by the Near-field model for various HORCON values

Further, water surface elevations simulated by the Near-field model with various HORCON values were compared with that predicted by Lake-wide model at the location A as shown in the Figure 5.49. The plot suggested that the value of HORCON used in the Near-field model has no effect on the water surface elevation computations. This was confirmed by the scatter plot shown in the Figure 5.50.

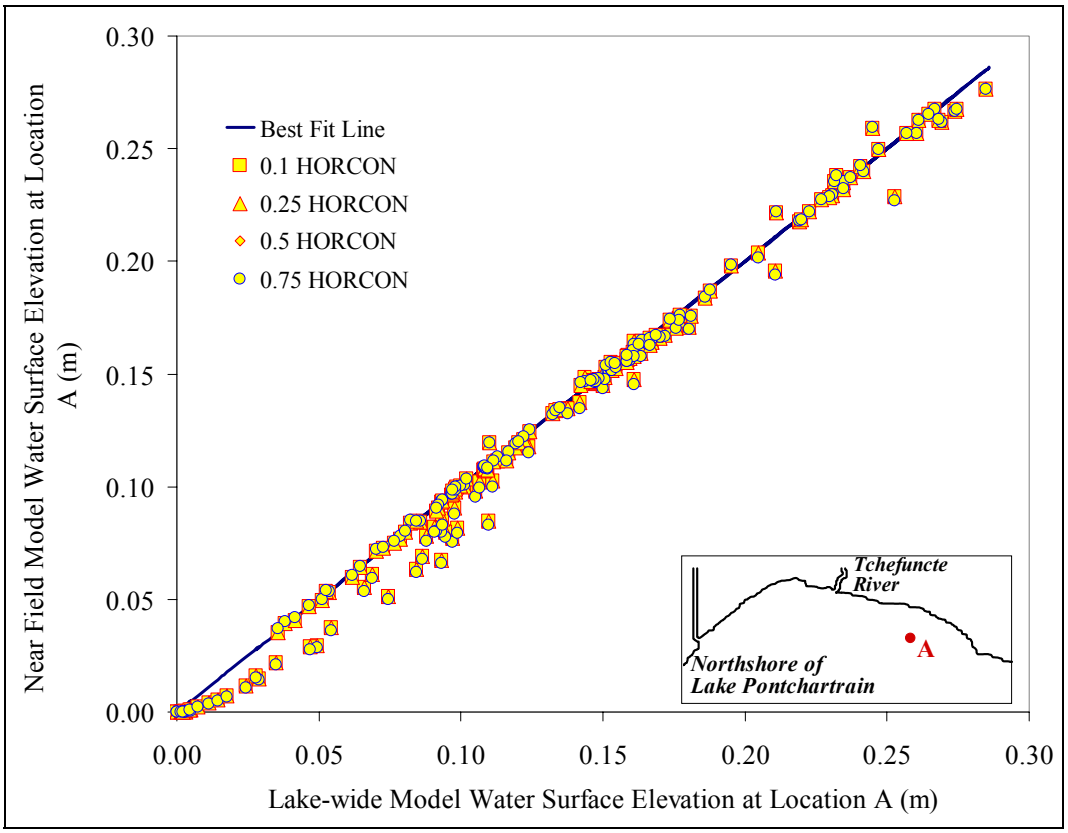

Figure 5.50 A scatter plot of the water surface elevations predicted by the Near-field model for various HORCON values and the Lake-wide model

However, this was not the case when the depth-averaged currents from the Near-field model were compared with those observed in the Lake-wide model. It was found that the Near-field model results do not agree with the Lake-wide model when HORCON values of 0.1 and 0.25 were used as shown in the Figure 5.51. There was very good agreement between the Lake-wide data and the Near-field data as shown in the Figure 5.52, when the HORCON values of 0.5 and 0.75 were used. In addition, it was found that the model was more stable when the HORCON value of 0.75 was used.

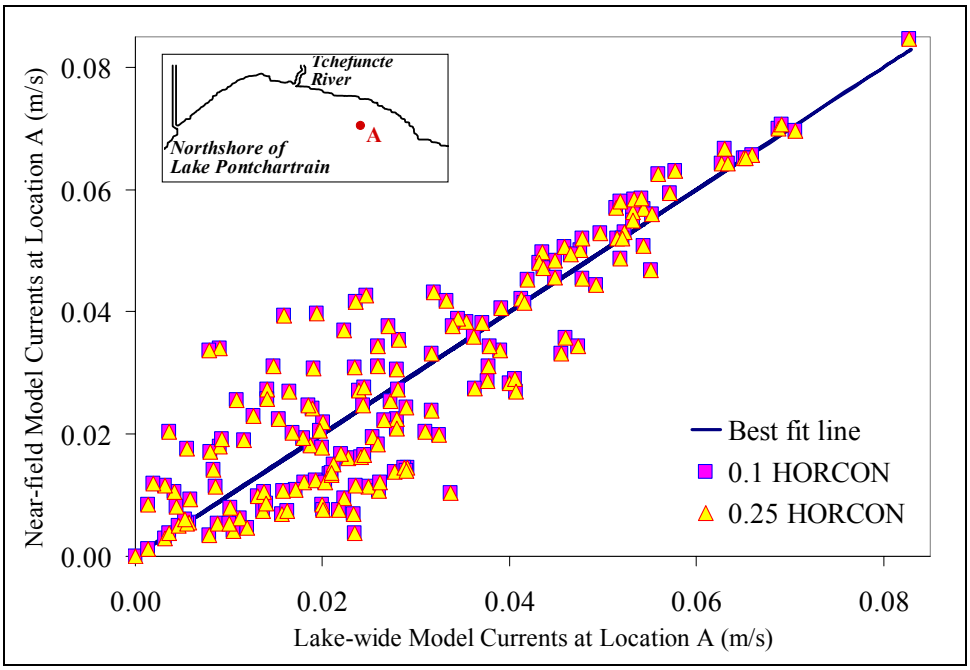

Figure 5.51 A scatter plot of the depth averaged currents predicted by the Near-field model for HORCON values of 0.1 and 0.25 and the Lake-wide model

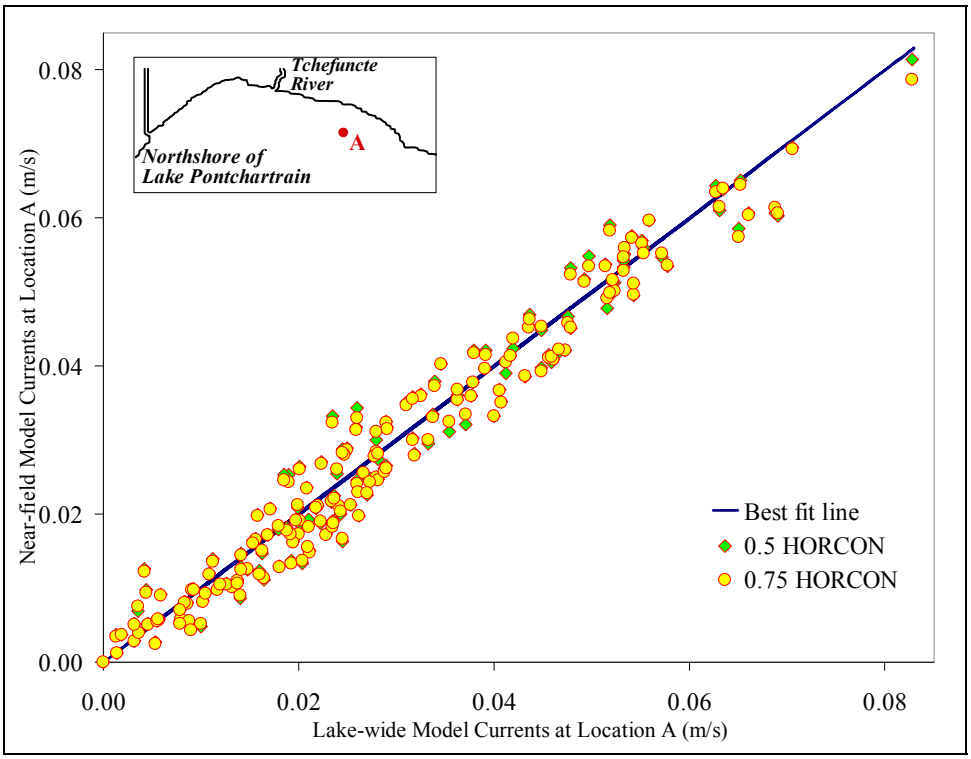

Figure 5.52 A scatter plot of the depth averaged currents predicted by the Near-field model for HORCON values of 0.5 and 0.75 and the Lake-wide model

5.3.7 Sensitivity of the Near-Field Model to Various Advection Schemes

The performance of the Near-field model with various advection schemes available in ECOMSED was tested. As noted earlier, ECOMSED allows the user to choose from CENTRAL, UPWIND, SMOLAR2 and SMOLAR_R advection schemes. The CENTRAL option represents the central difference scheme which is second-order accurate. Moreover, it does not generate any numerical diffusion. However, it can sometimes cause the over- and under-shooting of the scalar variables transported. The UPWIND option represents the upwind differences which are positive definite. However, it is only first-order accurate and can introduce significant numerical diffusion. SMOLAR2 and SMOLAR_R represent two versions of the advection schemes developed by Smolarkiewicz (1984). Both the schemes use upwind differences and a recursive correction is applied to remove the numerical diffusion induced by the upwind. In SMOLAR2, the correction is applied twice and in SMOLAR_R case a single formulation of antidiffusion velocities is used. The Smolarkewicz schemes are positive definite and are second order accurate.

The Near-field model was simulated for 24th to 30th April 2004 period. Keeping other conditions the same, the response of the model to various advection schemes was investigated. Figure 5.53 shows the fecal coliform plume generated by the model at 100 hours for various advection schemes. The shape of the plume generated in each case was different from one another. The CENTRAL and SMOLAR_R schemes allow the sharp fronts in the plume to persist, whereas the UPWIND was the most diffusive of all the four as expected. The plume diffuses further offshore into the Lake in the UPWIND and SMOLAR2 cases. Although a definite improvement can be seen, the antidiffusive correction applied in the SMOLAR2 case

was insufficient to curb the numerical diffusion due to upwinding. The SMOLAR_R scheme was devoid of any numerical ripples upstream of the front interface unlike in the CENTRAL case. The fecal coliform plume at 145 hours for the four discretization schemes are shown in the Figure 5.54. There was a better agreement among all the cases indicating a convergence of the solution in the later part of the simulation. For operational purposes, the effect of advection scheme used would have a little effect on the quality of results obtained.

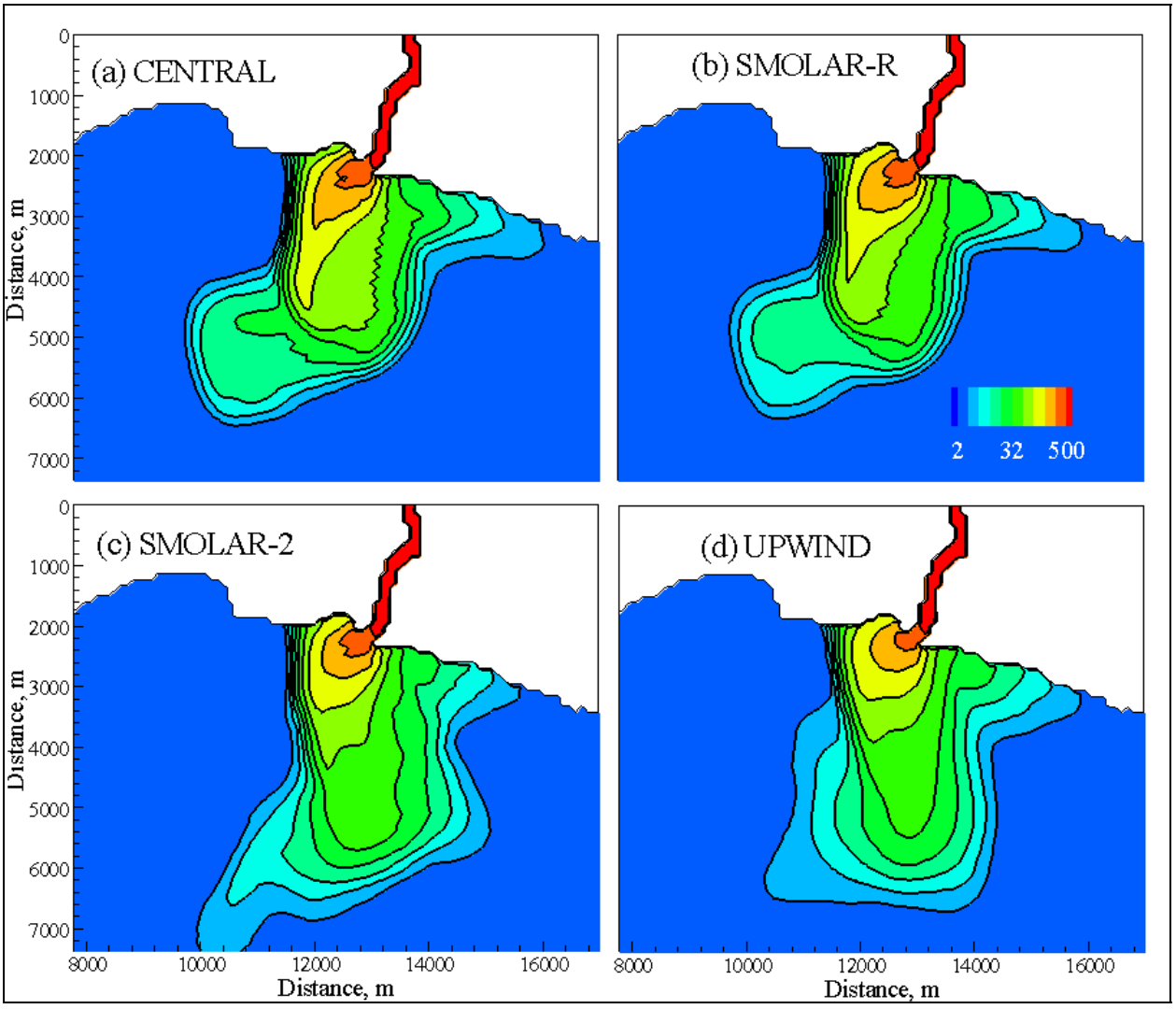

Figure 5.53 Comparison of the fecal coliform plumes generated by the Near-field model for various advection schemes at 100 hours into the simulation

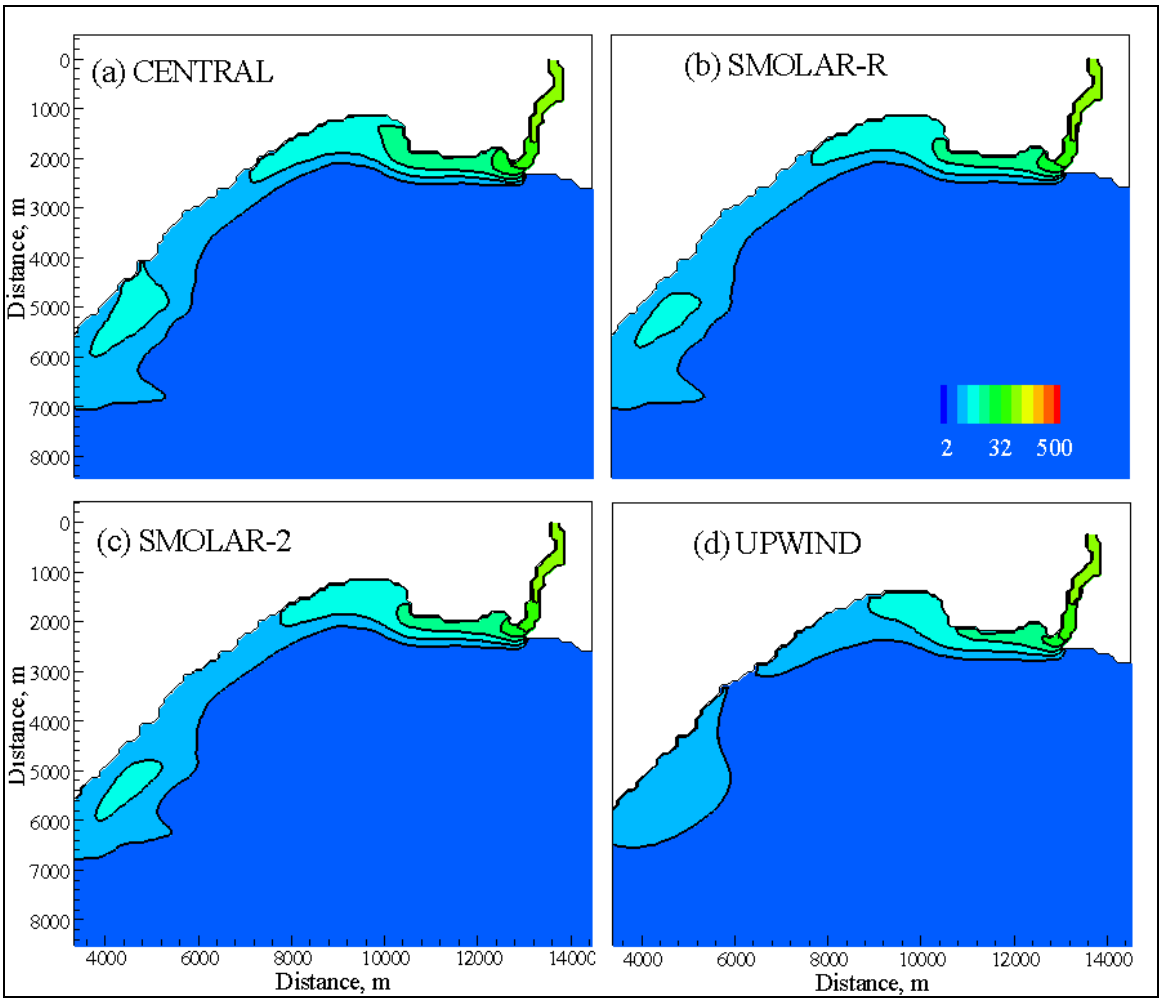

Figure 5.54 Comparison of the fecal coliform plumes generated by the Near-field model for various advection schemes at 145 hours into the simulation

Further, the fecal coliform levels predicted by each of the four schemes were compared quantitatively. Fecal coliform data was extracted along the Transect 1 shown in the Figure 5.55 at different simulation times in the above stated simulation. The predicted fecal coliform levels were plotted on the y-axis with distance from the mouth of the river on the x-axis as shown in the Figure 5.56. Figure 5.56 (a), (b), (c) and (d) show the results at 80 hours, 90 hours, 100 hours and 105 hours respectively. There was a difference of approximately 200 MPN/100 mL between the

central and upwind results at 80 hours closer to the mouth of the river where the concentrations were higher. The four cases agree well at 105 hours. The results were found to converge as the time progresses and the distance from the mouth increases.

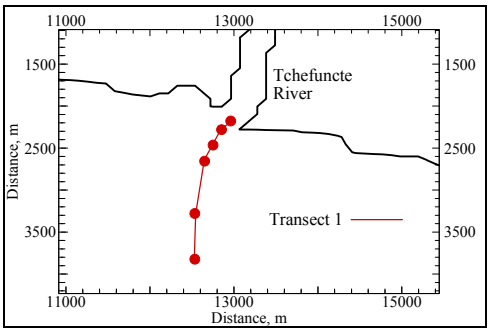

Figure 5.55 Map showing the location of the Transect 1

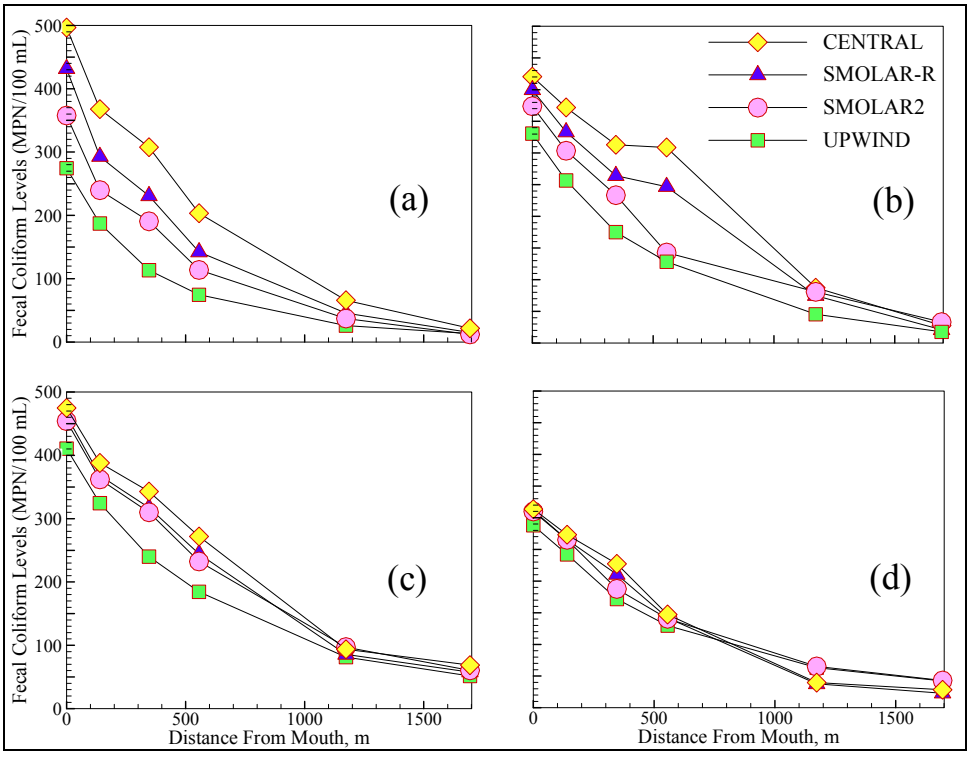

Figure 5.56 Comparison of fecal coliform levels at various simulation times for different advection schemes

6. MODEL APPLICATION

6.1 Shoreline Impact Area Assessment

Model simulations of fecal coliform loadings of various intensities can be used to develop an impact area database to assist in the risk management for the recreational zones in the Lake Pontchartrain.

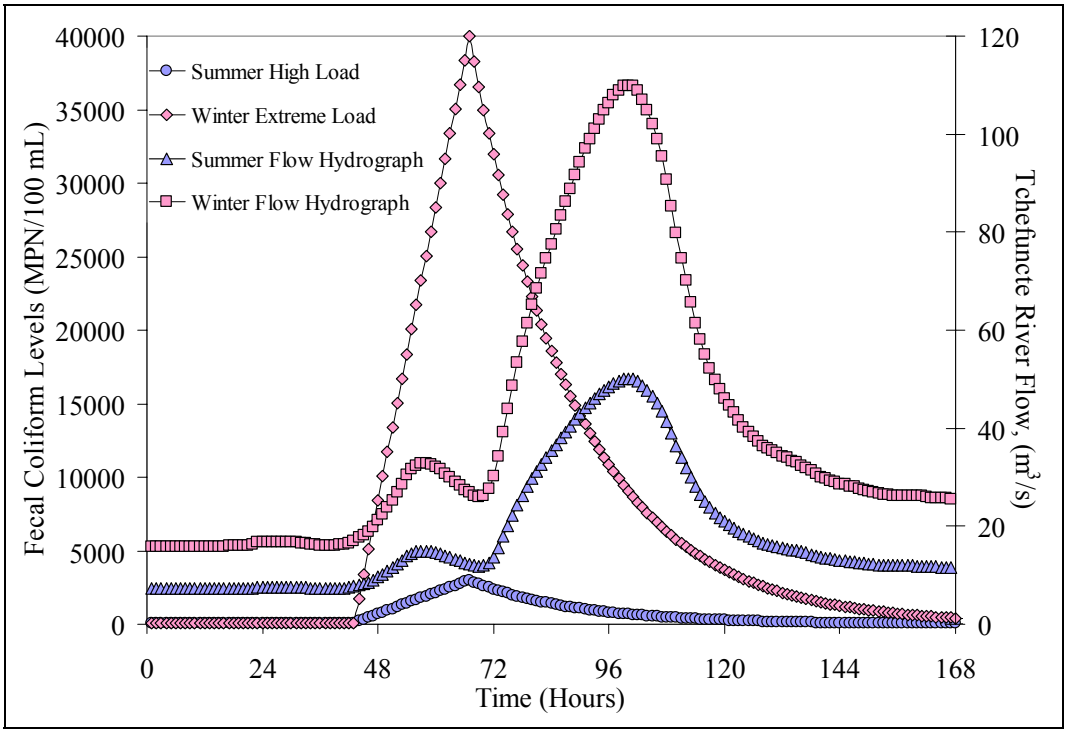

Figure 6.1 Boundary conditions for the flows and fecal coliform levels used in the summer and winter simulations of the north shore Near-field model

The Near-field model was simulated for two cases: a typical high fecal coliform loading event observed during the summer and an extreme event that could possibly occur in the winter conditions. The river discharges in each case correspond to typical summer and winter flows. The fecal coliform levels in the winter season can be an order of magnitude higher than those

observed in the summer season in the Tchefuncte River (Source: LPBF - 2003 Tchefuncte River Water Quality Survey Data). The river hydrographs and pollutographs used for the simulations are shown in the Figure 6.1. The model was run for a total of seven days with one day used for ramping the model forcing conditions to their full values.

A snap shot of the simulated "high risk fecal coliform plume" – plume containing fecal coliform concentrations of 200 MPN/100 mL or more, are shown in the Figure 6.2 for the two cases at 97 hours from the start of the simulation. The high risk plume was observed to reside in the lake for about 34 hours (~ 1.5 days) from the time it arrived at the mouth of the river in the case of the summer loading. The residence period for the high risk plume in the extreme winter loading scenario was observed to be 94 hours (~ 4days).

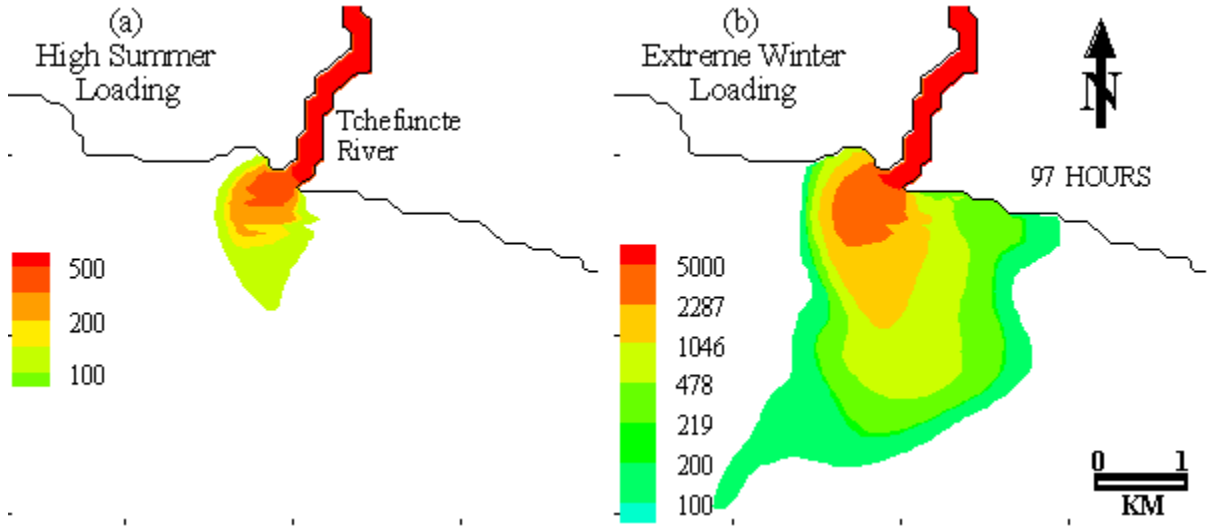

Figure 6.2 Simulated high risk fecal coliform plumes at 97 hours: (a) Summer Scenario; (b) Winter Scenario

The extent of area impacted by these high risk plumes were plotted with respect to the simulation time as shown in the Figure 6.3. During the period of simulation the maximum extent

of the impact area in the lake was found to be ~ 0.5 km^2 in the summer scenario and about 9.5 km^2 in the winter scenario. Moreover, the maximum distance along the shoreline that was impacted was found to be approximately 6.35 km in the winter scenario and 371 m in case of the summer scenario.

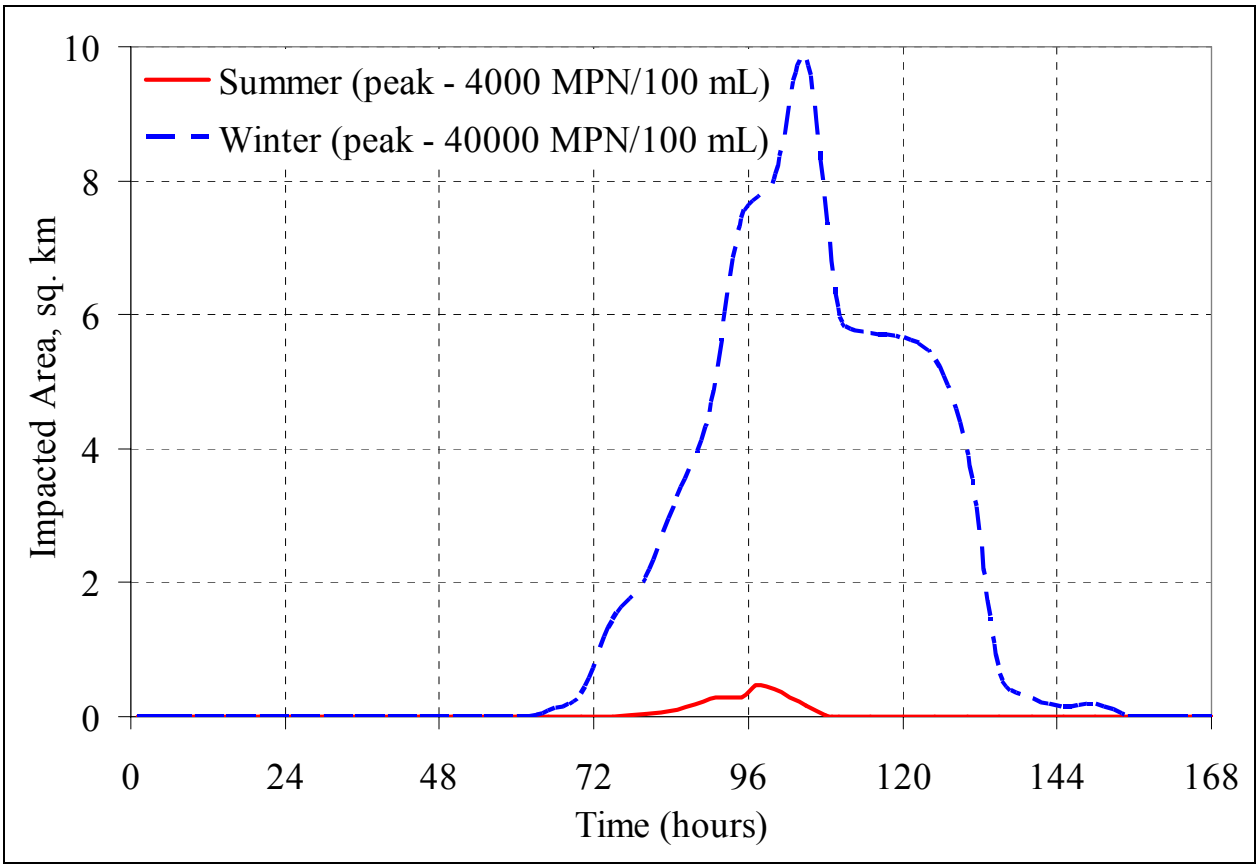

Figure 6.3 Time series of the areas of impact due to the high risk fecal coliform plume with concentrations more than 200 MPN/100 mL for the summer and winter scenarios

Figure 6.4 shows a plot of maximum fecal coliform levels observed at various radial distances from the mouth of the river over the simulation period for the winter event. A similar plot for the summer scenario is shown in the Figure 6.5.

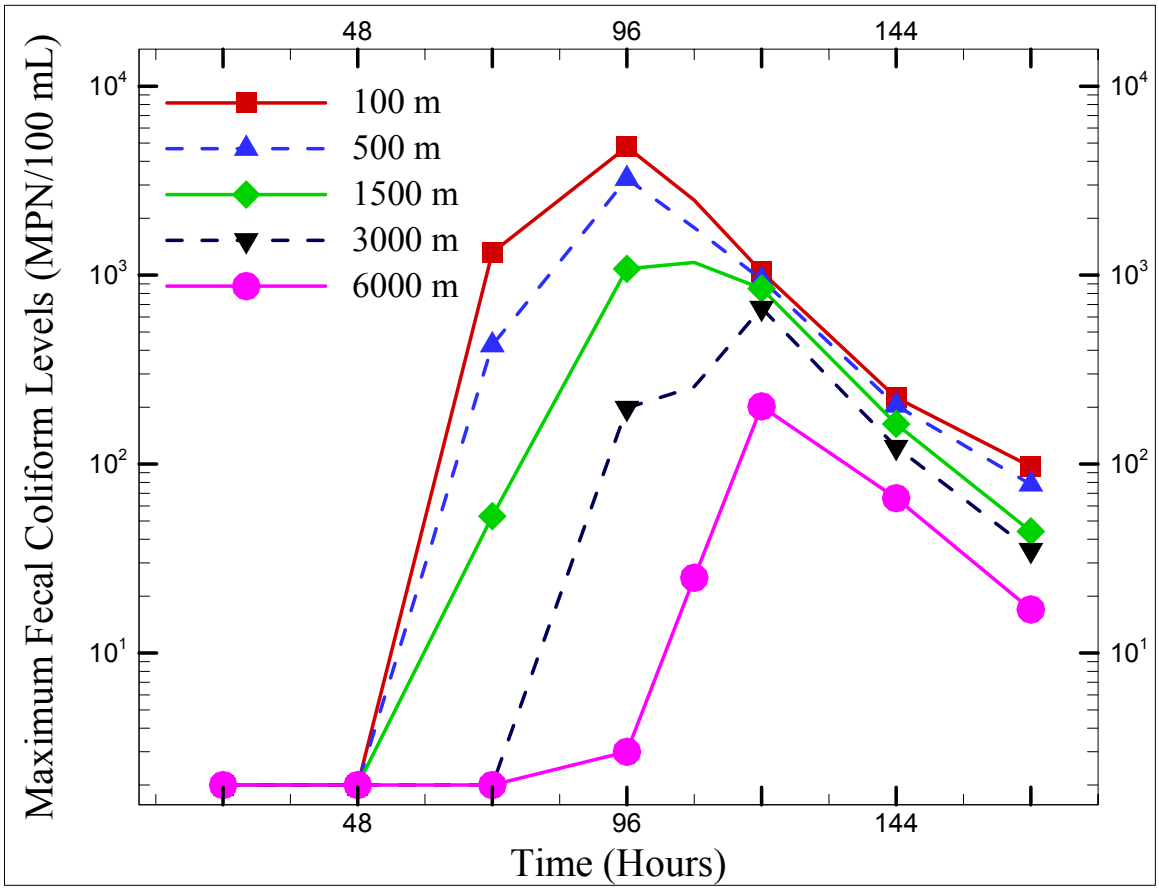

Figure 6.4 Maximum fecal coliform levels at various radial distances from the mouth of the Tchefuncte River over the simulation period for the extreme winter scenario

Plots similar to those shown here can be generated for other typical wind and tide conditions in the area. This would help to quantify the potential risk at any given location along the shoreline of Lake Pontchartrain due to the presence of a high risk fecal coliform plume with counts more than 200 MPN/100 mL, identifying the areas safe for the recreational activities at any given time.

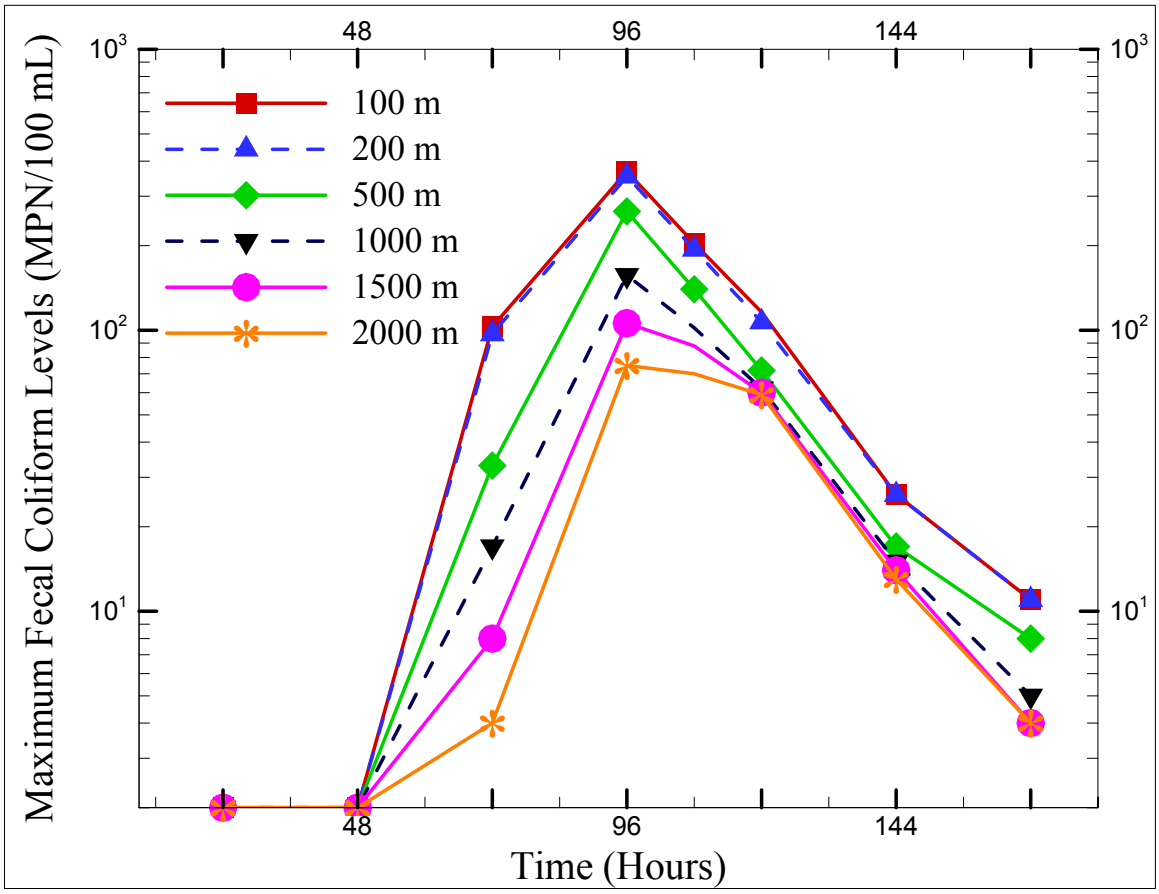

Figure 6.5 Maximum fecal coliform levels at various radial distances from the mouth of the Tchefuncte River over the simulation period for the typical summer scenario

6.2 Application of the Near-field Model to the South Shore of Lake Pontchartrain

The Near-field model developed for the north shore of Lake Pontchartrain was applied for the south shore of the lake to determine the fate and transport of the fecal coliform bacteria. The stormwater drainage outfall canals discharging the urban runoff into the lake comprise the dominant source of fecal coliforms in the south shore of the lake.

6.2.1 Grid Development

A Cartesian computational grid with a horizontal resolution of approximately 100 m and 7 equally spaced vertical layers was designed for the south shore Near-field model (Figure 6.6). The grid covers the entire south shore from the Lincoln beach in the east to the west of the Bonnet Carré Spillway. The grid includes all the major stormwater canals in the Orleans and Jefferson Parishes and the Inner Harbor Navigational Canal. Although there were quite a few inactive cells in the grid, the Cartesian grid was selected to keep the process of interpolation of the boundary conditions and the wave field data from the Lake-wide grid to the south shore grid, simple.

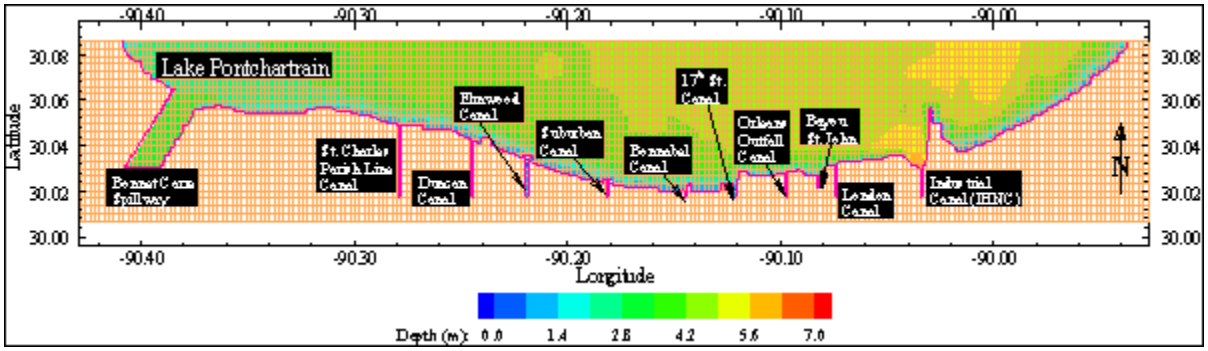

Figure 6.6 Computational grid for the south shore Near-field model (each cell represents 16 cells)

6.2.2 Initial and Boundary Conditions

The initial salinity and temperature for the south shore model were interpolated from the initial conditions of the Lake-wide model. The stormwater canals shown in the Figure 6.6 were the inflow open boundaries with intermittent discharges during the pumping events. The discharge hydrographs for these canals were collected from the pumping stations. The IHNC is the tidal open boundary in the domain. The elevation data obtained from the Rigolets gage which

were forced in the Lake-wide model were forced here too. In addition, water surface elevations, depth averaged velocities, salinity and temperatures from the Lake-wide grid were interpolated spatially and temporally along the northern open boundary of the south shore grid. This was done to ensure that the south shore model captured the Lake-wide processes due to the wind and tidal effects. Further, the wave data simulated in the Lake-wide model were interpolated spatially and temporally over the south shore grid. Due to the large extent of the area covered in the south shore model, surface wind data along with other meteorological parameters were applied.

6.2.3 Validation of the South shore Model

The hydrodynamics in the south shore model were validated by comparison of the currents and the circulation patterns with those observed in the Lake-wide model. Figure 6.7 shows the depth-average circulation patterns predicted by the south shore model and the Lake-wide model when driven with same boundary conditions. It can be noted that the south shore model captures the large scale circulation features as observed in the Lake-wide model accurately both in terms of magnitude and direction (Length of the vectors indicate magnitude). Unlike the north shore model where the HORCON value was increased to keep the model stable, the stability in the south shore model was achieved by upwinding the mass transport. This was required because of the strong currents produced by the IHNC.

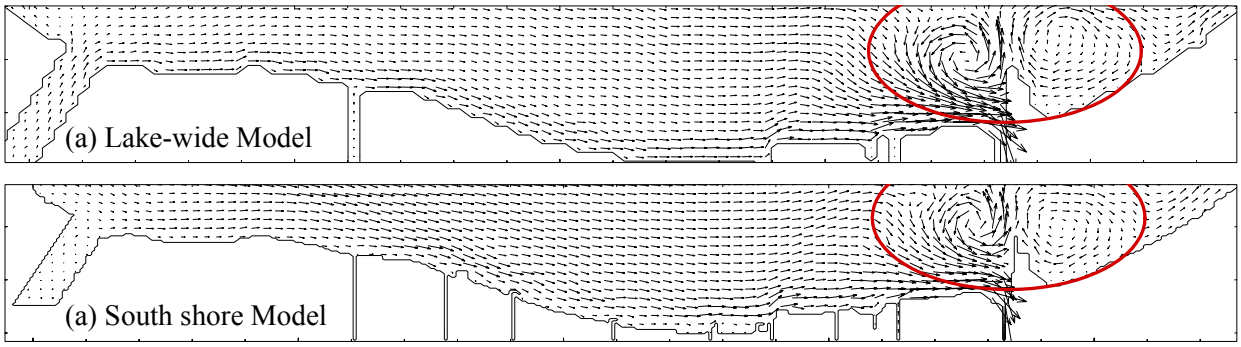

Figure 6.7 Comparison of depth averaged circulation patterns predicted by the Lake-wide model and the South shore model

For the purpose of validating the fecal coliform transport component of the south shore model, field sampling was performed in the vicinity of the Bonnabel Canal in Jefferson Parish at the locations shown in Figure 6.8. During a pumping event water samples were collected just downstream of the pumping station (Location 16 in the Figure 6.8) at frequent intervals to characterize the source concentration. Samples were collected for three consecutive days following the pumping event at predetermined locations along the shoreline of the lake between the 17th Street Canal and the Suburban Canal. These data provided information regarding the plume patterns and the kinetics of the bacteria. For a detailed description of the field study in the south shore, the reader is referred to Martinez (2005).

The data from the third wet weather sampling event from 5th to 9th April, 2005 were used to validate the fate and transport of the fecal coliform in the south shore model. A six day simulation was setup from the 4th April to the 9th April. The inflow and tidal boundary conditions used in the Lake-wide model for this simulation are shown in the Figure 6.9.

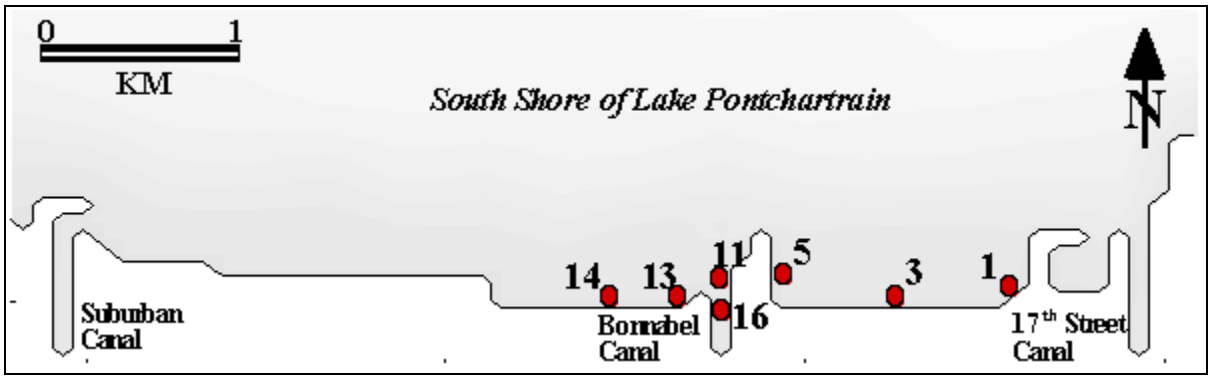

Figure 6.8 Sampling locations for the south shore field study

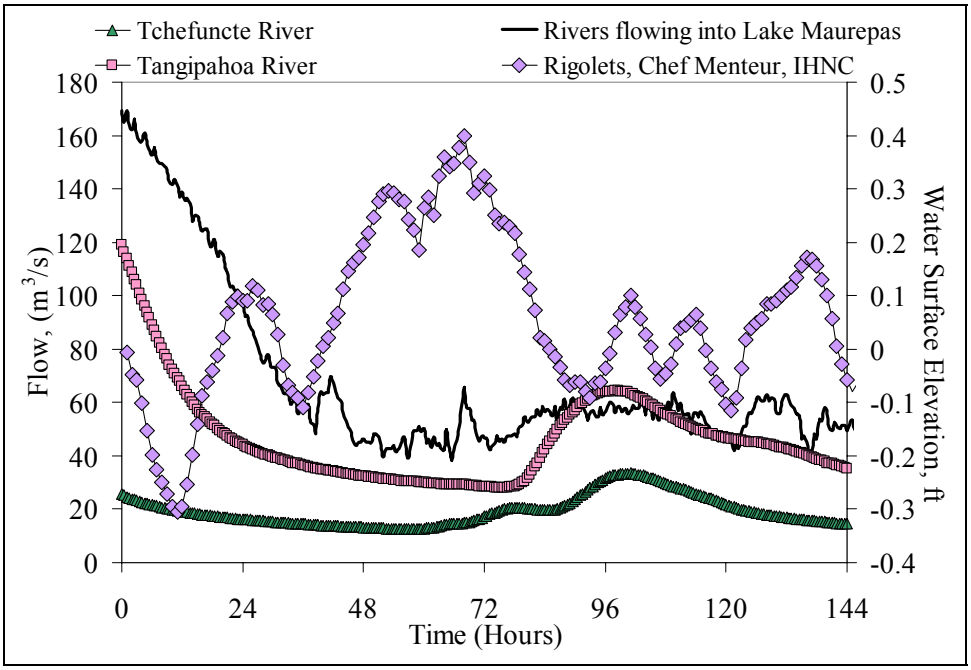

Figure 6.9 Flow and elevation data used in the Lake-wide model for the calibration simulation (April 4th – 9th, 2005) (Data source: USGS)

The flow data for the canals during simulation period were obtained from the pumping stations. The detailed pumping records for the calibration period are provided in the Table A1 of Appendix A. The elevation data for the tidal passes were obtained from the USGS gage at the Rigolets. The wind data were obtained from the LUMCON gage. Previous study by Carnelos (2003) in the south shore of Lake Pontchartrain, the storm water canals in the Orleans Parish, i.e.

London, Orleans, and the 17th Street Canals were found to discharge similar concentrations of total coliform as those observed in the Bonnabel Canal. Hence the same total coliform data were used as the source for all the canals in the south shore model. The complete information about the total coliform levels forced at each canal is provided in the Table A2 of Appendix A.

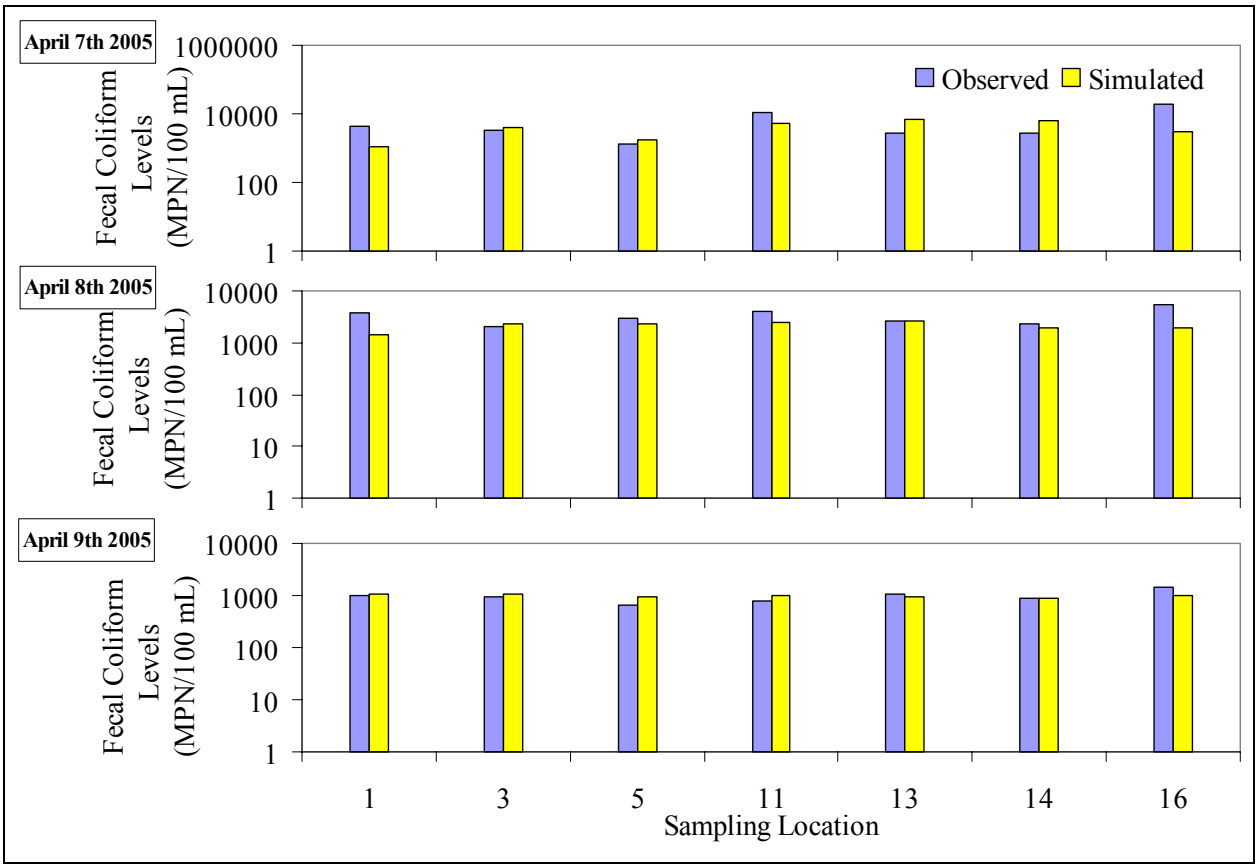

Figure 6.10 Comparison of the observed and modeled total coliform levels at various sampling locations along the south shore of Lake Pontchartrain

The modeled total coliform levels at various locations were compared to the observed field values for April 7th, 8th, and 9th as shown in the Figure 6.10. The simulated values match the measured values fairly well. A scatter plot between the observed and simulated values is shown

in the Figure 6.11. Although there was a good concurrence overall, the agreement was better on the 2nd and 3rd day of the sampling.

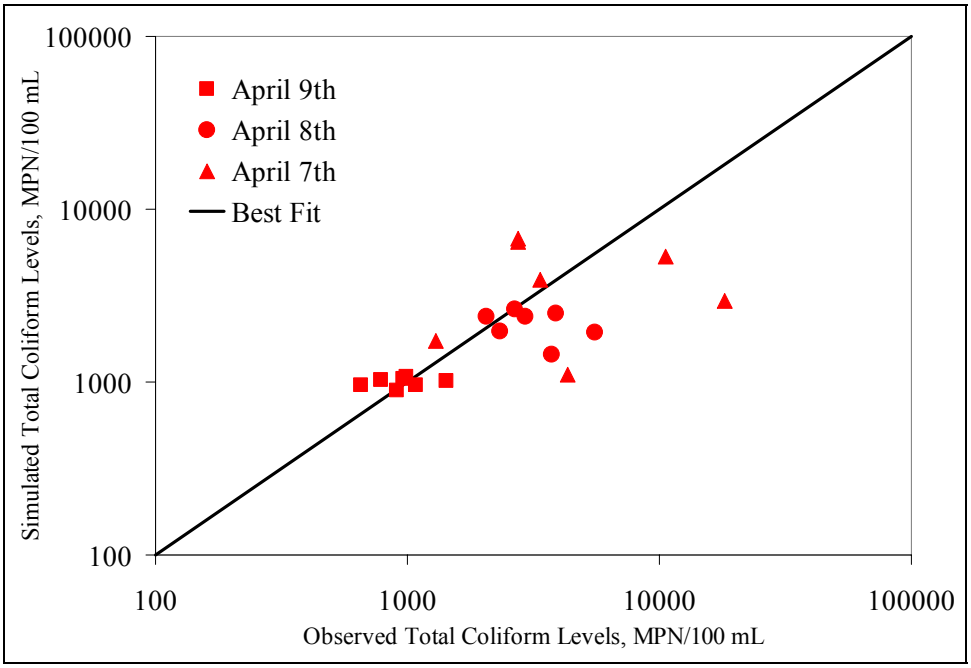

Figure 6.11 Comparison of the observed and modeled total coliform levels in the south shore of Lake Pontchartrain

A sequence of images showing the simulated total coliform plumes at various hours, for the calibration event, are shown in the Figure 6.12. It was found that the bacteria levels did not return to the background levels within the period of simulation, i.e. within 88 hours after pumping.

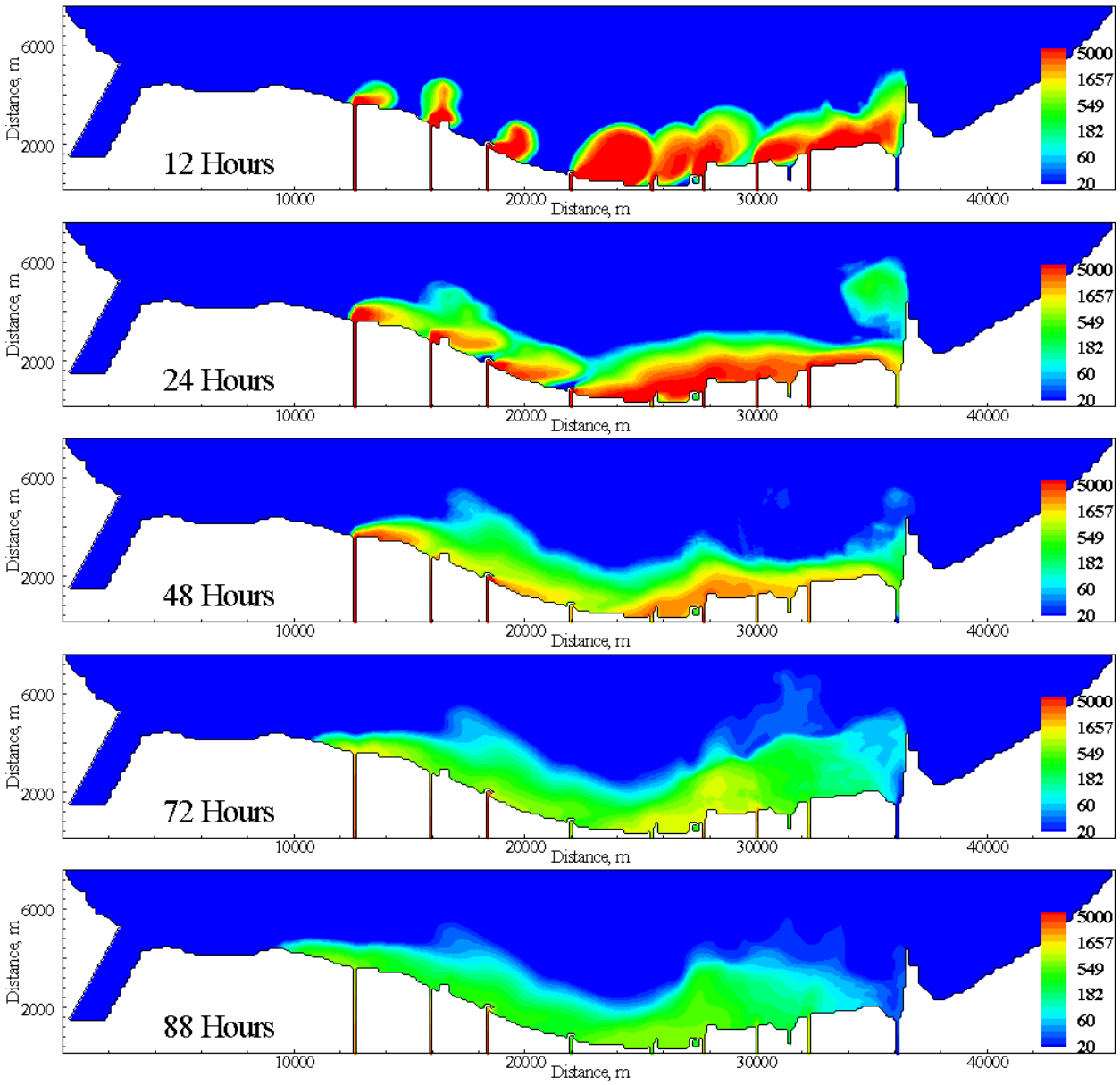

Figure 6.12 Simulated fecal coliform plumes in the south shore of Lake Pontchartrain for period April 7th to April 9th

7. DISCUSSION

7.1 Field Studies

Accurate and ample field data are necessary for adequate calibration of a numerical model. The field sampling performed in the north shore of Lake Pontchartrain provided the required water quality data to calibrate the near field model. The data indicated the presence of fecal coliform plume associated with the wet weather. However, the fecal coliform data collected in the river to quantify the source was rather too little.

The fecal coliform levels in the water column and sediments were found to be highly variable spatially and temporally. Results from a study conducted by Doyle et al. (1992) in an environment similar to that of Lake Pontchartrain indicated that both water and sediment fecal coliform populations were highly variable over the time. This is especially true in the case of rivers, where there would be continuous mixing and transport of contaminants along with the flow. Therefore collecting a single daily sample in the river would not adequately characterize the source, as was the case in the north shore study.

In a similar study in the south shore of Lake Pontchartrain, Martinez (2005) found the standard deviation of the *e coli* samples collected at the Bonnabel Canal during a pumping event to be 45%. It was concluded that, to estimate the source with reasonable accuracy, a minimum of six samples were required at a location at any given storm runoff event. Further it was found that the samples were to be collected at a high frequency in order to reduce the error due to the temporal variability in the data.

Due to the insufficient fecal coliform data available at the source in the north shore, the fecal coliform loading was corrected based on the mass of the contaminant observed in the lake. The amount of mass introduced into the lake due to the forced fecal coliform loading was equal or greater than what was observed in the lake. This process would introduce uncertainty in the results predicted by the model. To avoid or to minimize this uncertainty due to the source, high frequency sampling is necessary in the river.

7.2 Modeling Framework

As described earlier, a nested framework was developed to include the effect of wind and tide on the whole lake, in the Near-field model. So as to successfully transfer the features of the Lake-wide circulation into the Near-field model, a number of possible boundary conditions were considered. In a similar model developed by Carnelos (2003), depth-averaged currents and the water surface elevations from the Lake-wide model were forced along the western and eastern boundaries of the Near-field model respectively. The north boundary was set to radiate any gravity waves generated in the domain.

In the north shore model, in order to reproduce the hydrodynamics observed in the Lake-wide model, water surface elevations and depth-averaged currents were forced along the southern open boundary in the Near-field model. A component of the depth-averaged currents which was computed based on the existing gradient in the forced and computed elevations at the boundary nodes was also included to safely radiate any shocks generated due to this gradient. In addition to these boundary conditions, surface wind forcing was necessary due to the substantial

area in the Near-field modeling domain. This process assured the Near-field model to predict the water surface elevations accurately. However, the currents and the circulation features were not in agreement with Lake-wide model. To avoid the occurrence of the clustering type instabilities, it was found that the horizontal diffusivity had to be increased by a significant amount. In the model the amount of horizontal diffusivity available is controlled by the HORCON value (parameter α in Equation 14) specified by the user. By default, a low value of 0.1 was used for HORCON as recommended for ECOMSED. However, this value was increased to 0.75 to get the stable and consistent results compared to the Lake-wide model. This modification finally allowed the Near-field model to successfully replicate the Lake-wide hydrodynamics accurately. Berntsen (2002) noted that in similar cases with small horizontal grid spacing values and in areas with high variability, the HORCON value of the order of 1 should be used in order to avoid $2\Delta X$ oscillations.

In the case of the south shore model, a similar set of boundary conditions were forced at the northern boundary of the domain along with the wind. However, the high density gradients and currents at the IHNC in the south shore model may have induced oscillations in the solution making the model unstable. Generally, to reduce the oscillations and to make the model stable, higher diffusion is induced into the model. However, the model failed to run when the higher HORCON values similar to those in the north shore model were used. The reason for this inconsistency in the amount of horizontal diffusivity to be used between the two Near-field models was unclear. However, it may be attributed to the presence of higher velocities of the order of 1 m s^{-1} in the south shore model near the IHNC which may have generated unusually high horizontal mixing coefficients. Since the Smagorinsky formulation (Equation 14) used to

compute the horizontal mixing coefficient depends on the horizontal velocity gradients and the grid size, the high velocities at the IHNC may have lead to the failure of the south shore model, when higher HORCON values such as 0.75 were used.

The south shore model was found to generate similar clustering type instabilities as observed in the north shore model when lower HORCON values were used. Finally, a simple first order upwind scheme without any correction for the numerical diffusion was used for advection of salinity and other mass variables, in order for the south shore model to run without any instabilities and to successfully replicate the hydrodynamics in the Lake-wide model. However, the upwind scheme is only first order accurate and can cause numerical diffusion and under-predict the total coliform levels when the concentrations are high, e.g. in the vicinity of the mouth of the canals as was observed in the case of north shore model (Figure 5.56).

Thus it may be deduced that higher diffusion was required for the mass transport when the grid size was smaller as was the case in both the Near-field models. It could be induced either by using a higher HORCON value in the Equation 14 (north shore model) or by using a diffusive advection scheme for mass transport (south shore model). This may not be true for the momentum transport. The north shore Near-field model was stable although higher diffusivity was used for the momentum transport. However, lower diffusion values were necessary in the south shore model where the currents were higher.

7.3 Wind Forcing

The 1997 Bonnet Carré spillway opening event was used to calibrate the mass transport component of the Lake-wide model. As mentioned earlier, when a spatially variable wind forcing was used, the model was found to generate few circulation features which were absent when a spatially constant wind was used. These circulation patterns were in better agreement with the satellite reflectance images which were used in the calibration process. To demonstrate this, the turbidity plumes generated by the models with and without spatially variable wind forcing were compared to the satellite reflectance images. Figure 7.1 shows the satellite reflectance image of the turbidity in Lake Pontchartrain on 26th March, 1997. The model results for this day when spatially constant wind and variable wind were forced are shown in the Figures 7.2 and 7.3 respectively.

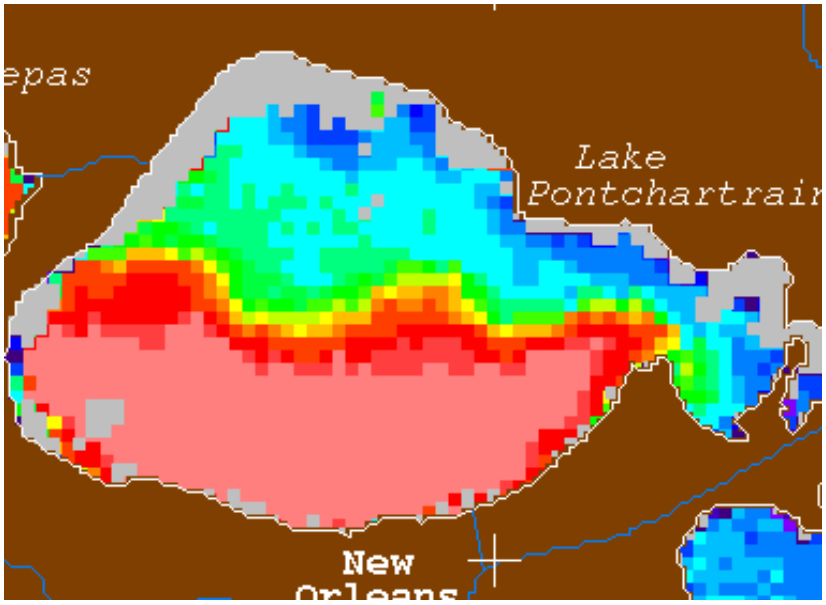

Figure 7.1 Satellite reflectance image of the Lake Pontchartrain during the1997 Bonnet Carré spillway opening on 26th March, 1997

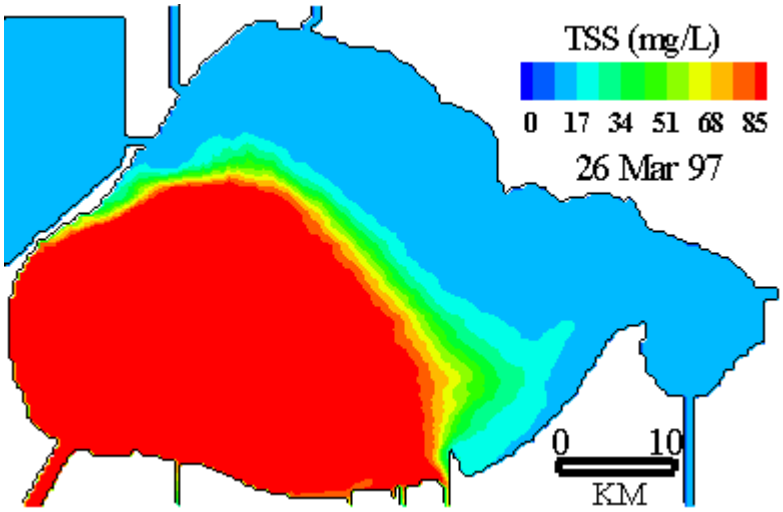

Figure 7.2 Modeled turbidity plume in the Lake Pontchartrain during the1997 Bonnet Carré spillway opening simulation with spatially constant wind for 26th March, 1997

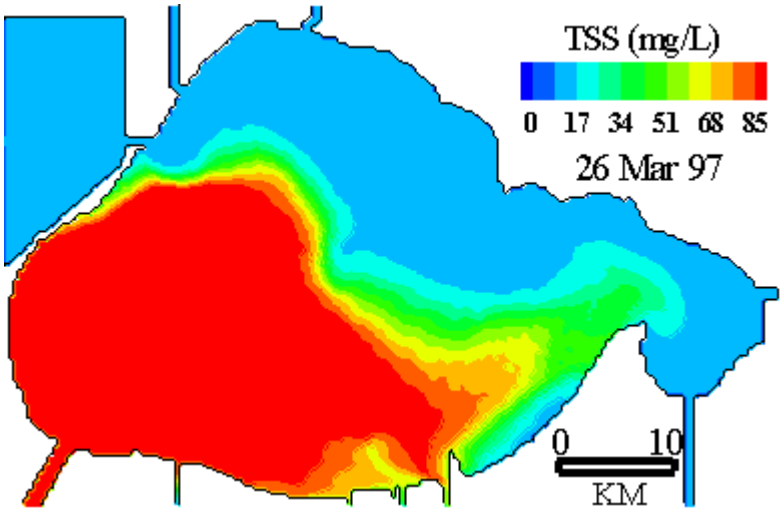

Figure 7.3 Modeled turbidity plume in the Lake Pontchartrain during the1997 Bonnet Carré spillway opening simulation with spatially variable wind for 26th March, 1997

It can be noticed from the reflectance image in the Figure 7.1, the turbid water from the Mississippi River reached the eastern embayment of the Lake Pontchartrain on the 26th March. The model result showed in the Figure 7.2 although indicates an eastward movement of the turbidity plume, it does not reach the eastern embayment as observed in the satellite image. However, when synoptic wind was used the plume indeed reached the eastern embayment of the

Lake Pontchartrain, as shown in the Figure 7.3. This occurred due to a counter clockwise circulation in the wind field near the middle of the lake which pushed the plume migrating northward to eastward. This circulation was absent when a spatially constant wind field was used.

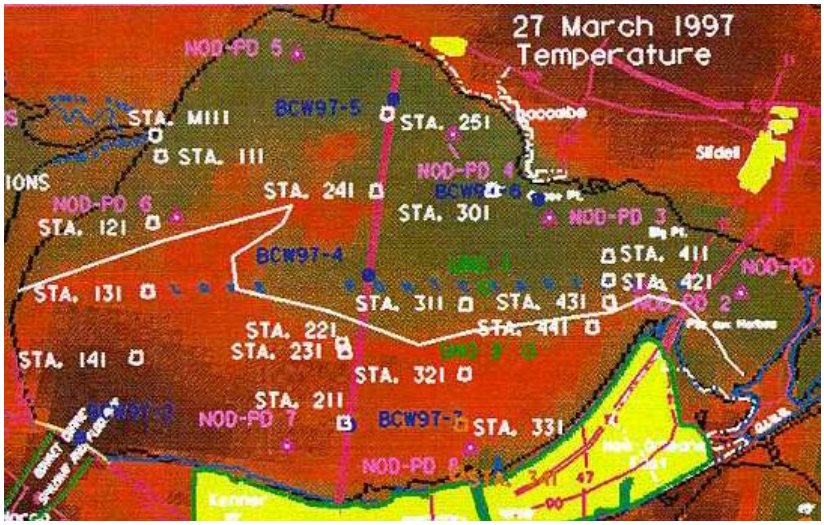

Figure 7.4 Water surface temperature image of the Lake Pontchartrain during the1997 Bonnet Carré spillway opening on 27th March, 1997

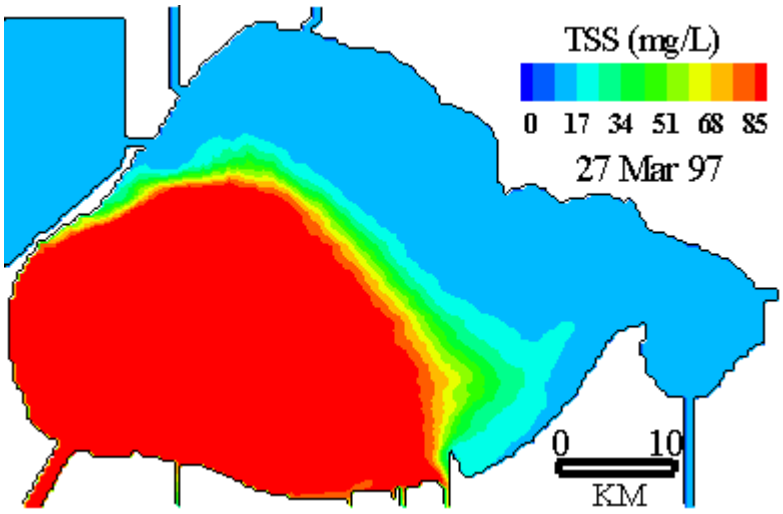

Figure 7.5 Modeled turbidity plume in the Lake Pontchartrain during the1997 Bonnet Carré spillway opening simulation with spatially constant wind for 27th March, 1997

In a similar observation on the 27th March, 1997, a satellite image of the temperature field in Lake Pontchartrain (Figure 7.4) indicated the northward migration of the fresh water plume from the Mississippi River. This feature was again captured by the model only when a spatially variable wind (Figure 7.6) was forced as opposed to a spatially constant wind (Figure 7.5). Over all, the residence times of the Mississippi River plume in the lake were predicted by the model equally well immaterial of a spatially constant or a variable wind field, except for these circulation features.

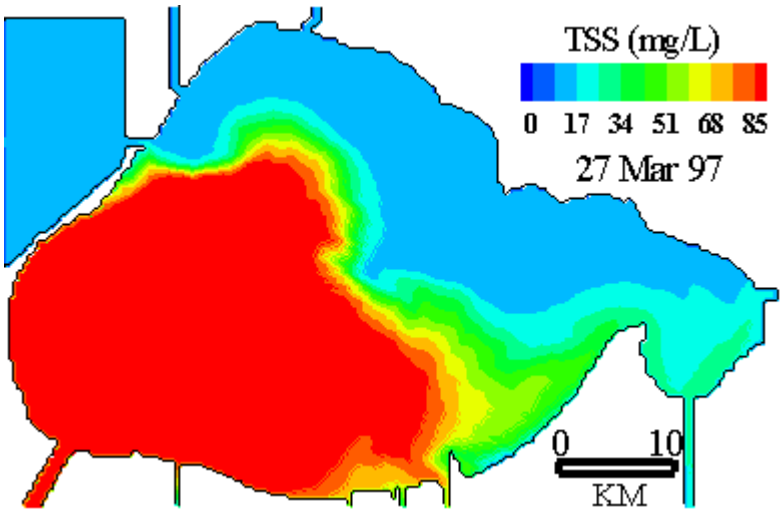

Figure 7.6 Modeled turbidity plume in the Lake Pontchartrain during the1997 Bonnet Carré spillway opening simulation with spatially variable wind for 27th March, 1997

7.4 Wave Model

The wave model used in the ECOMSED was based on the SMB (Sverdrup, Munk and Bretschneider) hindcasting method (USACE, 1984). Traditionally, this method was mainly used in the designing areas in the marine field, thus modeling waves during less frequent – high intensity events. The model was found to successfully predict the wave periods and height

observations taken during Tropical Storm Isidore in Lake Pontchartrain on September 27th 2002. The wave heights of ~1 m at periods of ~4.5 s for northerly winds of 18 m s^{-1} were consistent with observations made during the Tropical Storm Isidore at the London Canal on the south shore of Lake Pontchartrain (McCorquodale, 2002).

In addition, the model has performed reasonably well when compared to the calibrated wave model results by Signell and List (1997) for smaller and more frequent everyday conditions. However, the model does not include the effects of the radiation stresses due to the wave breaking, which can be critical for the resuspension of the sediments in shallow water environments such as Lake Pontchartrain. Moreover, it does not account for any non-linear wave transformations such as shoaling, refraction, diffraction etc. The latter may not be as critical as the former. ECOMSED allows user to supply the wave data from a more comprehensive external wave model such as WAM or SWAN.

It was found that the mean wave height of the highest one-tenth waves (H_{10}) would produce better results for the resuspension of the sediments rather than the significant wave heights (H_S) generated using the SMB model, during the calibration of the sediment transport model. On an average, a 27 % increment was found in the amount of resuspended sediment when H_{10} was used instead of H_S in the computation of waves induced bed shear in the sediment transport model. The idea behind using H_{10} was that there is a higher probability for a sediment particle to be resuspended initially by the wave with maximum height instead of the H_S. This argument is in line with the findings by Clarke et al. (1982) which indicated that the sediment

particles are primarily suspended by the bursts of turbulence related to peak values of the envelope of surface waves.

7.5 Sediment Transport Model

Lake Pontchartrain is dominated by cohesive bed sediments except for a small number of isolated areas near the mouths of the rivers, spillway and the shoals near the eastern embayment. For this reason, only the cohesive sediment transport was implemented in the present study. The resuspension potential is dependent on the bed shear stress due to the combined effect of currents and waves. When this bed shear stress exceeds a critical value the resuspension of the sediments would initiate. It was observed that wind speeds of 6 knots, with maximum wave heights of ~ 20 cm and periods of about 1.75 s, would initiate the resuspension in Lake Pontchartrain very close to the shore where the lake is shallow. However, wind speeds reaching 8 knots producing wave heights of ~ 25 to 30 cm and periods of about 2.1 s would induce significant resuspension starting along the shoreline extending slowly into middle of the lake over the time. When the wind speeds were below 6 knots, there is negligible resuspension in the lake except for the areas near the tidal passes. A very small amount of sediment was found to be resuspended at the tidal passes when the wind speeds were smaller. The resuspended sediments were found to settle very quickly after the cessation of the wind.

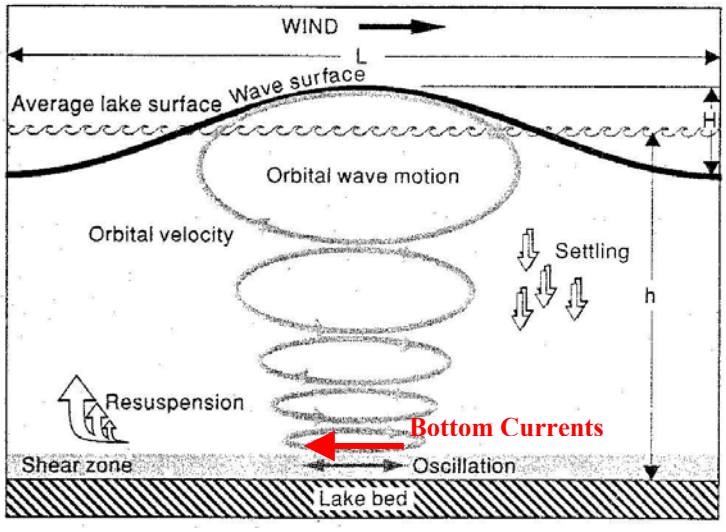

Figure 7.7 Forces induced by wind that cause resuspension of bed sediment (Laenen and LeTourneau, 1996)

The computation of the bed shear due to the combined effect of waves and currents (τ_{CW}) was based on the methodology developed by Grant and Madsen (1979) and Glenn and Grant (1987). In the process of calibration of the sediment transport model, an improvisation over this method was used. In the default method, τ_{CW} was computed by finding the magnitude of the resultant of the friction velocities due to waves and currents. However, the stresses induced due to waves and currents can be either additive or subtractive as shown in the Figure 7.7. Hence τ_{CW} estimated by the default method may be under-predicted. To assure that maximum possible bed shear was computed, a vector addition of the friction velocities due to waves and currents was performed for the two possible cases. Then τ_{CW} was estimated by using the magnitude of the maximum resultant of the friction velocities.

8. CONCLUSIONS

The major results of this study include:

- A Lake-wide model capable of simulating water surface elevations, currents, transport of contaminants, and waves was developed, calibrated and validated for Lake Pontchartrain.
- The Lake-wide model successfully predicts the presence of two gyre circulation patterns in Lake Pontchartrain.
- The results from the 1997 Bonnet Carré spillway opening simulation indicated that forcing spatially variable wind was necessary in order to capture certain circulations patterns.
- A statistical analysis performed on the water surface elevation data from the USGS gage at the Rigolets and the USACE gage at Seabrook Bridge on the IHNC for the year 1997 showed that the tide was similar at both the locations.
- It was found that the bed roughness had little effect on quality of the water surface elevations predicted by the Lake-wide model. However, there was considerable effect on the currents.
- The Lake-wide model was found to be stable only when the α value in Equation 14 which controls the horizontal diffusivity in the Smolarkewicz's formulation, was in the range of 0.02 and 0.4. In this range the effect of α value on the model results was insignificant. Model was found to be stable when an external mode time step of 2 s was used.

- The wave model successfully predicted the wave heights and the periods observed during the Tropical Storm Isidore near the London canal in the Lake Pontchartrain.
- A Lake-wide sediment transport model for Lake Pontchartrain was developed and calibrated.
- The sediment resuspension was initiated when the wind speeds were over 6 knots. The sediments near the shoreline were resuspended first and then the offshore sediments.
- It was found that the sediment model predicts better results when mean wave height of the highest one-tenth waves (H_{10}) was used in the computation of bed shear stress instead of the significant wave heights (H_S) generated using the SMB model.
- The Near-field model capable to simulate hydrodynamics, sediment transport, and fate and transport of fecal coliform was successfully developed and nested with the Lake-wide model for the north shore of Lake Pontchartrain. The Near-field model was calibrated and validated based on the measured fecal coliform data from the field.
- The Near-field model was found to be stable when the α value was ranging between 0.5 and 0.75. Further, the model was stable when an external mode time step of 0.75 s was used.
- From operational point of view, advection scheme used in the north shore model would have very little effect on the results.
- The north shore model indicated that the fecal coliform plume can be highly dynamic and sporadic depending on the wind and tide conditions. It also showed that the impact of a storm event on the fecal coliform levels in the lake can be anywhere from 1.5 day for a typical summer event to 4 days for an extreme winter event.

- The modeling framework developed for the north shore was successfully applied to the south shore of Lake Pontchartrain to simulate fate and transport of fecal coliforms discharged through the urban stormwater outfalls.

9. RECOMMENDATIONS

When compared to a single model, making a nesting application operational is harder. However, a nested application was developed as it was computationally very expensive to have a Lake-wide Cartesian grid whose horizontal resolution is limited by the canal widths. In the future, numerical models that allow the use of unstructured grids such as FVCOM (Chen et al., 2003a) should be evaluated. Thus a nested application can be avoided since the unstructured grids allow using variable grid size while allowing mass conservation.

A better wave model which includes the important factors such as the radiation stresses and the various wave transformations would be necessary to simulate the wave data more accurately.

The sediment transport model in the current state provides results with reasonable accuracy. However, a comprehensive sediment transport modeling study would be required to further calibrate this model. High frequency suspended data at various locations in the lake would be useful in addition to the satellite reflectance images currently used. Moreover, provisions should be made in model to vary the bed properties such as critical shear stress for resuspension, the time of consolidation etc., spatially. Currently, ECOMSED allows the user to specify a node to be either non-cohesive or cohesive. Modifications are required to allow the presence of both the materials at any given node.

In regards to modeling of the sediment bound fecal coliform, currently it is being assumed that all the sediment bound fecal coliforms are released into the water column as soon as the sediment is resuspended. However, this may not be completely realistic. Hence to better quantify the fraction of bacteria released, further studies are required. Relationship between the applied bottom shear stress and the fecal coliforms released into the water column should be explored.

Although not significant in the current study, future models with the ability to simulate wetting and drying processes should be pursued. This feature can prove to be important while simulating the Lake-wide hydrodynamics in estuarine environments such as Lake Pontchartrain which are surrounded by inter-tidal flats and wetlands.

10. REFERENCES

Babinchak, J.A., Graikoski, J.T., Dudley, S., and Nitkowski, M.F., 1977, Effect of Dredge Spoil Deposition on Fecal Coliform Counts in Sediments at a Disposal Site. Applied and Environmental Microbiology, Vol. 34, No. 1 P. 38-41

Barbé, D.E., Carnelos, S., and McCorquodale, J.A., 2001, Climatic effect on Water Quality Evaluation. Journal of Environmental Science and Health, A36 (10), 1919-1933

Barbé, D.E., Francis J.C., and Gunta M., 1999, Modeling Microbial Levels using Precipitation Data and Seasonal Analysis. Journal of Environmental Science and Health, A34 (3), 507-527

Barbé, D.E., Francis J.C., 1992, A Study of Microbial Levels in the Tchefuncte River. Final US EPA Report

Berntsen, J., 2002, Users guide for a modesplit σ-coordinate numerical model, Version 3.0, University of Bergen, Bergen, Norway

Blumberg, A. F., and Mellor, G. L., 1987, A description of a three-dimensional coastal model. Three Dimensional Coastal Ocean Models, N. S. Heaps, ed., American Geophysical Union, Washington, D.C., 1-16

Blumberg, A.F., R.P. Signell, and H. L. Jenter., 1993, Modeling Transport Processes in the Coastal Ocean. Journal of Marine Environmental Engineering. Vol. 1, pp 31-52

Blumberg, A.F., Z-G Ji, and C.K. Ziegler., 1996, Modeling outfall plume behavior using far field circulation model. Journal of Hydraulic Engineering. Vol. 122, No. 11

Blumberg, Alan F., 1996, An Estuarine and Coastal Ocean Version of POM. Proceedings of the Princeton Ocean Model Users Meeting (POM96), Princeton, NJ

Blumberg, A.F., Ahsan, Q., Li, H., Kaluarachchi, I. D., and Lewis, J.K., 2001, Circulation, Sediment and Water Quality Modeling in the Northern Gulf of Mexico, in: Bridging the Gap: Meeting the World's Water and Environmental Resources Challenges, Proceedings of the World Water and Environmental Resources Congress, Don Phelps, Gerald Sehlke (eds), ASCE

Borgeouis-Calvin A., Rheams A., and Dufrechou C., 2004, Pollution Source Tracking in the Bogue Falaya/Tchefuncte River Watershed. Abstract to the Basics of the Basin, Seventh Biennial Research Symposium

Burton, G.A. Jr, Gunnison, D. and Lanza, G.R., 1987, Survival of pathogenic bacteria in various freshwater sediments. Applied and Environmental Microbiology 53, 633-638

Carnelos, S., 2003, Fate of Pathogen Indicators in the Stormwater Runoff. Ph.D. Dissertation, Dept. of Civil and Environmental Engineering, University of New Orleans, New Orleans, LA

Carnelos, S., 2000, Urban Runoff Drainage to Lake Pontchartrain: Outfall Plume Modeling and Shoreline Water Quality. M.Sc. Eng. Thesis, University of New Orleans, New Orleans, LA

Chen, C. H. Liu, R. C. Beardsley, 2003a, An unstructured, finite-volume, three-dimensional, primitive equation ocean model: application to coastal ocean and estuaries. J. Atm. &Oceanic Tech., 20, 159-186

Clarke, T.L., Lesht, B., Young, R.A., Swift, D.J.P. and Freeland, G.L., 1982, Sediment resuspension by surface-wave action: an examination of possible mechanisms. Marine Geology, 49: 43-59.

Connolly, J.P., Blumberg, A.F., and Quadrini, J.D., 1999, Modeling Fate of Pathogenic Organisms in Coastal Waters of Oahu, Hawaii. Journal of Environmental Engineering, Vol. 125, No. 5

Crabill, C., Donald, R., Snelling, J., Foust, R. and Southam, G., 1999, The impact of sediment fecal coliform reservoirs on seasonal water quality in Oak Creek, Arizona. Water Research 33, 2163-2171

Cruise, J.F., and Arora, K., 1990, A Hydroclimatic Application Strategy for the Poisson Partial Duration Model. Water Resources Bulletin 26(3):431-442

Davies C. M., Bavor H.J., 2000, The fate of stormwater-associated bacteria in constructed wetland and water pollution control pond systems. Applied and Environmental Microbiology 89, 349-360

Davies C. M., Long J. A. H., Donald M. and Ashbolt N. J., 1995, Survival of fecal microorganisms in marine and freshwater sediments. Applied and Environmental Microbiology 61, 1888-1896

Donsel and Geldreich., 1971, Relationships of Salmonellae to Fecal Coliforms in Bottom Sediments. Water Research. 5:1079-1087

Jack d. Doyle, J. D., Tunnicliff, B., Kramer, R., Kuehl, R., and Brickler, S. K., 1992, Instability of fecal coliform populations in Waters and bottom sediments at recreational Beaches in Arizona. Water Resources Vol. 26, no. 7, Pp. 979-988

Englande, A.J., Jin, G., Dufrechou, C., 2002, Microbial contamination in Lake Pontchartrain basin and best management practices on microbial contamination reduction. Journal of Environmental Science and Health, Part A – Toxic/Hazardous Substances & Environmental Engineering, Vol 37, Issue 9

Gael, B.T., 1980, Models for understanding the hydrodynamics of Lake Pontchartrain. Environmental analysis of Lake Pontchartrain, Louisiana, its surrounding wetlands, and selected land uses, Chapter 3, J.H. Stone, ed., Prepared for USACE, New Orleans, Contract # DACW29-77-C-0253

Gailani, J., Lick, W., Ziegler, C.K. and Endicott, D., 1996, Development and Calibration of a Fine-Grained Sediment Transport Model for the Buffalo River. J. Great Lakes Res., 22, 765-778

Gailani, J., C. K. Ziegler, and W. Lick, 1991, The Transport of Sediments in the Fox River, J. Great Lakes Res., 17, 479-494

Galland, J.C., Goutal, N., Hervouet, J.-M., 1991, TELEMAC: A new numerical model for solving shallow water equations. Adv. Water Reources, 14(3), 138-148

Gary and Adams., 1985, Indicator bacteria in water and stream sediments near the snowy range in southern Wyoming. Water, Air, and Soil Pollution. 25:133-144

Geldreich and Kenner., 1969, Microbiology: Water. Journal of Water Pollution Control. 54:931-942

Georgiou, I., 2002, Three dimensional hydrodynamic modeling of saltwater intrusion and circulation in Lake Pontchartrain. Ph.D. Dissertation, Dept. of Civil and Environmental Engineering, University of New Orleans, New Orleans, LA

Georgiou, I.Y., Tittlebaum, E.M., 2001, Sanitary sewer overflows associated with non-NPDES entities. Environ Engg and Policy, Springer & Verlag, Germany, Vol. 2, No.3, 121-130

Gerba and McLeod, 1976, Effect of sediments on the survival of Escheria Coli in marine waters. Applied Environmental Microbiology. 32:114-120

Glenn, S.M. and Grant, W.D., 1987, A suspended sediment stratification correction for combined waves and current flows. J. Geophys. Res., 92(C8):8244-8264

Gonzalez, J., Iriberri, J.M., Egea, J. and Barcina, I., 1990, Differential rates of digestion of bacteria by freshwater and marine phagotrophic protozoa. Applied and Environmental Microbiology 56, 1851-1857

Goyal, S. M., Gerba, C. P., and Melnick, J. L., 1977, Occurrence and distribution of bacterial indicators and pathogens in canal communities along the Texas coast. Applied and Environmental Microbiology 34:139-149

Grant, W.D. and Madsen, O.S., 1979, Combined Wave and Current Interaction with a Rough Bottom. J. Geophys. Res., 84(C4):1797-1808

Grimes, D.J., 1975, Release of Sediment-Bound Fecal Coliforms by Dredging. Appl. Microbiol., 29, 109

Hamilton, G. D., Soileau C. W., and Stroud A. D., 1982, Numerical modeling study of Lake Pontchartrain. Journal of the Waterways, Port, Coastal and Ocean Division, ASCE, 108, 49-64

Haralampides, K., 2000, A study of the hydrodynamics and salinity regimes of the Lake Pontchartrain system. Ph.D. Dissertation, Dept. of Civil and Environmental Engineering, University of New Orleans, New Orleans, LA

Howell, Coyne, Cornelius., 1996, Effect of Sediment Particle Size and Temperature on Fecal Bacteria Mortality Rates and the Fecal Coliform/Fecal Streptococci Ratio. Journal of Environmental Quality. 25:1216-1220

HydroQual, Inc., 2002, A primer for ECOMSED. Users Manual, Ver. 1.3, HydroQual, Inc., Mahwah, NJ, USA, 188pp.

Jamieson, R. C., Joy, D. M., Lee, H., Kostaschuk, R., and Gordon, R. J., 2005, Resuspension of Sediment-Associated Escherichia coli in a Natural Stream. Journal of Environmental Quality 34:581-589

Janin, J.-M., Marcos, F., Denot, T., 1997, Code TELEMAC-3D-Version 2.2. Note the'oritique. Tech. Rep. HE-42/97/049/B, Electricite' de France (EDF-DER), Laboratoire National d'Hydraulique

Jin, G. Englande, A.J., Bradford, H., Jeng, H., 2004, Comparison of E. coli, Enterococci, and Fecal Coliform as Indicators for Brackish Water Quality Assessment. Water Environmental Research, 76, 245

Jin, G., Englande, A.J., Liu, A., 2003, A Preliminary Study on Coastal Water Quality Monitoring and Modeling. Journal of Environmental Science and Health, Part A—Toxic/Hazardous Substances & Environmental Engineering, Vol 38, Issue 3

Karim, M.F and Holly, F.M., 1986, Armoring and Sorting Simulation in Alluvial Rivers. ASCE J. Hydr. Engr., 112(8):705-715

Krone, R.B., 1962, Flume Studies of the Transport of Sediment in Estuarial Processes. Final Report, Hydraulic Engineering Laboratory and Sanitary Engineering Research Laboratory, University of California, Berkeley

LaBelle, R. L., and Gerba, C.P., Goyal, S.M., Melnick, J. L., Cech, I., Bogdan, G.F., 1980, Relationships between Environmental Factors, Bacterial Indicators, and the Occurrence of Enteric Viruses in Estuarine Sediments. Applied and Environmental Microbiology Vol. 39, No. 3 p. 588-596

LaBelle, R. L., and C. P. Gerba, 1979, Influence of pH, salinity, and organic matter on the adsorption of enteric viruses to estuarine sediment. Applied and Environmental Microbiology 38:93-101

Laenen, A. and LeTourneau, A.P., 1996, Upper Klamath Basin Nutrient-Loading Study – Estimate of Wind-Induced Resuspension of Bed Sediment during Periods of Low Lake Elevation, U.S. Geological Survey Open-File Report 95-414. Portland, Oregon.

Le Fevre, N.M. and G.D. Lewis, G.D., 2003, The role of resuspension in enterococci distribution in water at an urban beach. Water Science and Technology Vol 47 No 3 pp 205–210

Leal, J.C., 2004, Water Quality Study and Plume Behavior Modeling for Lake Pontchartrain at the Mouth of the Tchefuncte River. M.S. Thesis, Dept. of Civil and Environmental Engineering, University of New Orleans, New Orleans, LA

Lick, W., Lick, J. and Ziegler, C.K., 1994, The Resuspension and Transport of Fine-Grained Sediments in Lake Erie. J. Great Lakes Res., 20(4), 599-612

List, J.H., Signell, R.P., 2001, Pontchartrain Basin Land Loss – Long-Term Near-Bottom Velocity in Lake Pontchartrain in S. Penland, A. Beall and J. Waters (editors), Environmental Atlas of Lake Pontchartrain Basin. Lake Pontchartrain Basin Foundation, New Orleans, LA, p.65

Louisiana Department of Environmental Quality, 2004, Louisiana Water Quality Inventory: Integrated Report, Baton Rouge, Louisiana

Luyten, P.J., Jones, J.E., Proctor, R., Tabor, A., Tett, P., and Wild-Allen, K., 1998, COHERENS: A Coupled Hydrodynamical-Ecological Model for Regional and Shelf Seas: User Documentation. MUMM Report, Management Unit of the Mathematical Models of the North Sea, 914pp

Luyten, P.J., Deleersnijder, E., Ozer, J. and Ruddick, K.G., 1996, Presentation of a family of turbulence closure models for stratified shallow water flows and preliminary application to the Rhine outflow region. Continental Shelf Research, 16, 101-130

McAnally, W. H., Berger, R.C., Bonnet C W.C., Isphording, F.D., Imsand, G.C. Flowers., 1996, Bonnet Carré freshwater diversion, numerical model investigation of pontchartrain basin estuary salinity changes. Hydraulics Laboratory, USACE, Waterways Experiment Station, Vicksburg, MS

McCorquodale, J.A., Georgiou, I., Carnelos, S., and Englande, A.J., 2004, Modeling Pathogens in Storm Water Plumes, Special Issue of the Journal of Environmental Engineering and Science, National Research Council of Canada, Ottawa, ON p. 419

McCorquodale, J.A., Englande, A.J., Carnelos, S., Georgiou, I., Wang, Y., 2003, Fate of Pathogen Indicators in Stormwater Runoff (Final Project Report for the U.S. Environmental

Protection Agency), Urban Waste Management and Research Center, University of New Orleans, New Orleans, LA

McCorquodale, J. A., 2002, Personal communication about wave heights near the mouth of London canal in the south shore of Lake Pontchartrain during the Tropical storm Isidore, New Orleans, LA

McCorquodale, Barbé,Wang, Carnelos,S., 2001, Pontchartrain Basin Land Loss – Freshwater inflows into Lake Pontchartrain system in S. Penland, A. Beall and J. Waters (editors), Environmental Atlas of Lake Pontchartrain Basin. Lake Pontchartrain Basin Foundation, New Orleans, LA, p.65

McCorquodale, J. A., Barbé, D. E., Wang, Y. and Carnelos, S., 2001, Freshwater Inflows to the Lake Pontchartrain System. Environmental Atlas of Lake Pontchartrain Basin." in S. Penland, A. Ball and J. Waters, eds., Lake Pontchartrain Basin Foundation, New Orleans, LA, 65

Mellor, G. L., 1998, A Three-dimensional, primitive equation, numerical ocean model. A users guide, Atmospheric and Oceanic Sciences, Princeton University, Princeton, NJ

Mellor, G. L., 1996, Introduction to physical oceanography, American Institute of Physics, Woodbury, NY

Mellor, G.L. and Yamada, T., 1982, Development of a turbulence closure model for geo-physical fluid problems. Reviews of Geophysics and Space Physics, 20, 851-875

Miller, R.L., and McKee, B.A., 2004, Using MODIS Terra 250 m imagery to map concentrations of total suspended matter in coastal waters. Remote Sensing of Environment 93 (2004) 259-266

Oey, L.-Y., G.L. Mellor, and R. I. Hires., 1985a, A three-dimensional simulation of the Hudson-Raritan estuary. Part I: Description of the model and model simulations, J. Phys. Oceanogr, 15, 1676-1692

Oey, L.-Y., G. L. Mellor, and R. I. Hires., 1985b, A three-dimensional simulation of the Hudson-Raritan estuary. Part II: Comparison with observation, J. Phys. Oceanogr., 15, 1693-1709

Partheniades, E., 1992, Estuarine Sediment Dynamics and Shoaling Processes. in Handbook of Coastal and Ocean Engineering, Vol. 3, J. Herbick, ed., pp. 985- 1071

Pettibone, G.W., Irvine, K.N. and Monahan, K.M., 1996, Impact Of A Ship Passage On Bacteria Levels And Suspended Sediment Characteristics In The Buffalo River, New York. Water Research 30, 2517-2521

Reid, R.O., Bodine, B. R., 1968, Numerical Model for Storm Surges in Galveston Bay. ASCE Journal of Waterways and Harbors Division, Vol. 94, No. WW1

Rodi W., 1984, Turbulence models and their application in hydraulics. International Association for Hydraulic Research, 2nd edition, Delft, Netherlands, 104 pp

Roper M M & Marshall K C., 1974, Modification of the interaction between Escherichia coli and bacteriophage in saline sediments. Microbial Ecol. 1:1 -13, 1974

Shrestha, P.L., A.F. Blumberg, D.M. Di Toro and F. Hellweger , 2000, A three-dimensional model for cohesive sediment transport in shallow bays. Invited Paper, ASCE Joint Conference on Water Resources Engineering and Water Resources Planning and Management, July 30-august 2, 2000, Minneapolis, MN

Shulman, I., and J.K. Lewis, 1995, Optimization approach to the treatment of open boundary conditions. J. Phys. Oceanogr., 25, 1006-1011

Signell, R.P., List, J.H., Stumpf, R.P., Evans, J., 2001, U.S. Geological Survey, Wind Driven Circulation and Sediment Resuspension Processes in Lake Pontchartrain, Louisiana. URL: http://pubs.usgs.gov/of/of98-805/html/signell.htm

Signell, R. P. and Harris, C.K., 1999, Modeling surface trapped river plumes: a sensitivity study. Estuarine and Coastal Modeling, M. L. Spaulding, and H.L. Buttler, eds., ASCE, 209-222

Signell, R.P. and J.H. List., 1997, Modeling Waves and Circulation in Lake Pontchartrain." Gulf Coast Association of Geological Societies Transactions, 47, 529-532

Smolarkiewicz, P.K., 1984, A fully Multidimensional Positive Definite Advection Transport Algoritym with Small Implicit Diffusion. J. Comp. Phys., 54:325-362

Stone, J. S., Subra,W. A., and Minvielle, P. J., 1972, Surface circulation of Lake Pontchartrain: A wind dominated system. Final Report, Gulf South Research Institute, Proj. NS-255, 122 pp

Stronach, J.A., Backhaus, J.O. and Murty T.S., 1993, An update on the numerical simulation of oceanographic processes in the waters between Vancouver Island and the mainland: The GF8 Model. in: Oceanogr. Mar.Biol. Annu. Rev., 1-86, A. D. Ansell, R. N. Gibson and Margaret Barnes (eds)

Stumpf, R.P., 2001, Satellite Imagery: Lake Pontchartrain Basin and Gulf of Mexico, URL: http://pubs.usgs.gov/of/of98-805/html/stumpf.htm

United States Army Corps of Engineers (USACE), Waterways Experiment Station (WES) Hydraulics Laboratory, 1997, User's Guide to RMA2 WES, Version 4.3

United States Army Corps of Engineers (USACE), Waterways Experiment Station (WES) Hydraulics Laboratory, 1997, User's Guide to RMA4 WES

United States Army Corps of Engineers (USACE), Waterways Experiment Station (WES) Hydraulics Laboratory, 1997, User's Guide to RMA10 WES

United States Army Corps of Engineers (USACE), 1984, Shore Protection Manual, Volume I, Coastal Engineering Research Center. Waterways Experiment Station, Vicksburg, Mississippi

United States Geological Survey, Coastal and Marine Geology (CMG), 20041123, Louisiana Marine Geology and Geophysics from Field Activity: P-5-98-LA

Van Donsel, D.J., and Geldreich, E.E., 1971, Relationships of Salmonellae to Fecal Coliforms in Bottom Sediments. Water Resources, 1079

Van Rijn, L.C., 1993, Principles of Sediment Transport in Rivers, Estuaries and Coastal Seas. Aqua Publications, Amsterdam, the Netherlands

Van Rijn, L.C., 1984, Sediment transport, part II: suspended load transport, ASCE J. Hydr. Engr., 110(11):1613-1638

Ziegler, C.K. and Nisbet, B.S., 1995, Long-Term Simulation of Fine-Grained Sediment Transport in Large Reservoir, ASCE J. Hyd. Engr., 121 (11), 773-781

Ziegler, C.K. and Nisbet, B.S., 1994, Fine-Grained Sediment Transport in Pawtuxet River, Rhode Island, ASCE J. Hyd. Engr., 120(5):561-576

APPENDIX A

Table A1 Pump discharges at each canal for the south shore calibration event from April 4th to 9th, 2005

	Flows (m^3/s)							
Simulation Hour	St. Charles Parish Line Canal	Duncan Canal	Elmwood Canal	Suburban Canal	Bonnabel Canal	17th Street Canal	Orleans Outfall Canal	London Canal
54.5	32	0	0	0	0	0	0	2
55.0	32	32	0	0	0	0	0	2
55.5	32	32	0	0	0	0	0	2
56.0	42	32	32	0	0	0	0	2
56.5	42	42	32	0	0	0	0	2
57.0	42	42	32	55	8	0	0	0
57.5	42	42	42	55	8	0	0	0
58.0	13	42	42	55	8	31	0	31
58.5	17	13	42	55	30	31	16	31
59.0	17	17	42	55	30	31	44	31
59.5	17	17	13	55	30	31	44	31
60.0	17	17	17	55	30	31	16	31
60.5	4	17	17	25	0	31	16	31
61.0	0	4	17	25	8	31	16	31
61.5	0	0	17	25	8	31	0	31
62.0	0	0	4	25	8	31	0	31
62.5	0	0	0	25	8	31	16	31
63.0	0	0	0	8	0	31	0	31
63.5	0	0	0	0	0	31	0	0
64.0	0	0	0	0	0	31	0	0
64.5	0	0	0	0	0	31	0	0
65.0	0	0	0	0	0	31	0	0
65.5	0	0	0	0	0	31	0	0
66.0	0	0	0	0	0	31	21	0
66.5	0	0	0	0	0	31	6	0

Table A2 Total coliform levels forced at each canal for the south shore calibration event from April 4th to 9th, 2005

	Total Coliform Levels (MPN/100 mL)							
Simulation Hour	St. Charles Parish Line Canal	Duncan Canal	Elmwood Canal	Suburban Canal	Bonnabel Canal	17th Street Canal	Orleans Outfall Canal	London Canal
54.5	2100	0	0	0	0	0	0	4000
55.0	55972	2100	0	0	0	0	0	4000
55.5	62750	55972	0	0	0	0	0	4000
56.0	80875	62750	2100	0	0	0	0	4000
56.5	78938	80875	55972	0	0	0	0	4000
57.0	90750	78938	62750	800	1250	0	0	0
57.5	111313	90750	80875	160000	3667	0	0	0
58.0	60188	111313	78938	160000	22313	5938	0	2100
58.5	35729	60188	90750	160000	75000	7625	2100	160000
59.0	15133	35729	111313	160000	67500	9313	50000	160000
59.5	15671	15133	60188	160000	101250	11000	160000	160000
60.0	16235	15671	35729	160000	161250	12688	160000	160000
60.5	18197	16235	15133	80000	0	14375	50000	160000
61.0	0	18197	15671	80000	11125	16063	50000	160000
61.5	0	0	16235	16375	11275	17750	0	160000
62.0	0	0	18197	16250	11325	19438	0	160000
62.5	0	0	0	16125	11456	21125	50000	160000
63.0	0	0	0	16074	0	26895	0	160000
63.5	0	0	0	0	0	32665	0	0
64.0	0	0	0	0	0	38435	0	0
64.5	0	0	0	0	0	44205	0	0
65.0	0	0	0	0	0	49974	0	0
65.5	0	0	0	0	0	55744	0	0
66.0	0	0	0	0	0	61514	2100	0
66.5	0	0	0	0	0	67284	2100	0

VITA

The author, elder son of Ramaswamy Chilmakuri and Annapoorna Kodali, was born in Hyderabad, India in 1978. He graduated in June, 2000 with a Bachelors degree in Civil Engineering from Jawaharlal Nehru Technological University, Hyderabad, India. He came to the United States of America in August, 2000 to pursue his graduate studies at University of New Orleans, New Orleans, LA. In May 2002, he earned his Master of Science degree in Civil and Environmental Engineering specializing in Water Resources Engineering from University of New Orleans. He continued to pursue his doctoral degree in Engineering and Applied Sciences with specialization in Hydraulics and Environmental Modeling at the University of New Orleans. He finished all the requirements and would graduate with a doctoral degree in December 2005.